The relationships between neutrino Majorana mass and other physics

Takahiro Ohata

January 21, 2021

Abstract

The standard model (SM) can explain most of the experimental results. However, there are some pieces of evidence that indicate beyond the standard model (BSM) physics. We mainly focus on neutrino oscillation in this thesis. It necessarily indicates BSM couplings to the lepton sector and gives reliable and strong hints of BSM physics.

The neutrino oscillation is explained by neutrino Dirac/Majorana masses. Seesaw models are well-known ones which derive the Majorana masses. Seesaw models generally contain (heavy) BSM particles which couple to the SM lepton sector. On the other hand, the lepton number symmetry is broken in the Majorana mass terms, though it is (classically) unbroken in the SM. In the Majoron models, the origin of the symmetry-breaking scale is explained, and the associated Nambu-Goldstone boson (Majoron) appears. The heavy BSM particles and/or the Majoron may describe other BSM physics. Throughout this thesis, we discuss the relationships between the neutrino Majorana mass and other physics, for example, the muon g-2 anomaly [1], the observed dark matter relic density [2, 3], and the strong CP problem [3].

First, we explain the neutrino oscillation and the muon g-2 anomaly by Type II seesaw model. In order to explain the muon g-2 anomaly, we introduce the double charged scalar to Type II seesaw model. Then the constraints from lepton flavor violation indicate that discrete lepton flavor symmetry exists.

Second, we consider the production mechanism for TeV scale Majoron dark matter. TeV scale Majoron dark matter can explain the anomalous results in the positron fraction detected by the cosmic ray observations. However, its production mechanism is not clear. We show three scenarios in which TeV scale Majoron is produced as much as the observed dark matter relic density.

Third, we construct the minimal model in which the lepton number symmetry breaking in the seesaw model is identified as the Peccei-Quinn one in the axion model. Some radiative seesaw model contains colored heavy particles coupling to the SM lepton sector. This is identified as heavy colored fermions in the KSVZ axion scenario.

Contents

Part I
Introduction

The standard model (SM) can explain most of the experimental results. However, there are some evidences which indicate the beyond standard model (BSM). For example, there are the experimental results which can not be explained by SM; dark matter (DM), dark energy, inflation (the horizon problem), neutrino oscillation, anomalous results in flavor experiments, baryon asymmetry and etc. Furthermore, SM has the theoretical problems; the strong CP problem, hierarchy problem and etc.

We mainly focus on the BSM physics which explain the neutrino oscillation. The existence of neutrino oscillation is very reliable. It will not be denied by the future experiments. Furthermore, The neutrino oscillation indicates the BSM particles which couples to the SM lepton sector. It is the very strong hint of BSM.

Neutrino oscillation is the transition from one weak eigenstates $|\nu_\alpha\rangle$ to the other one $|\nu_\beta\rangle$. In order to explain it, the weak eigenstates and the mass eigenstates of neutrinos must be different:

$$|\nu_\alpha\rangle = \sum_i U^*_{\alpha i} |\nu_i\rangle. \tag{0.1}$$

Here, $U_{\alpha i}$ is Pontecorvo-Maki-Nakagawa-Sakata (PMNS) matrix [4,5], and it is parametrized as follows:

$$\begin{aligned} U_{\alpha i} = &\begin{pmatrix} c_{12}c_{13} & s_{12}c_{13} & s_{13}e^{-i\delta_{\rm CP}} \\ -s_{12}c_{23} - c_{12}s_{23}s_{13}e^{i\delta_{\rm CP}} & c_{12}c_{23} - s_{12}s_{23}s_{13}e^{i\delta_{\rm CP}} & s_{23}c_{13} \\ s_{12}s_{23} - c_{12}c_{23}s_{13}e^{i\delta_{\rm CP}} & -c_{12}s_{23} - s_{12}c_{23}s_{13}e^{i\delta_{\rm CP}} & c_{23}c_{13} \end{pmatrix} \\ &\times \mathrm{diag}(1,\, e^{i\alpha_{21}/2},\, e^{i\alpha_{31}/2}), \end{aligned} \tag{0.2}$$

$$\theta_{ij} \in [0,\, \pi/2),\, \delta_{\rm CP} = [0,\, 2\pi),\, c_{ij} = \cos\theta_{ij},\, s_{ij} = \sin\theta_{ij}. \tag{0.3}$$

The parameters in the PMNS matrix are measured by experiments using solar, atmospheric, reactor and accelerator neutrinos.

NuFIT [6] shows the global fits of these parameters: [1]

$$\sin^2\theta_{12} = 0.304^{+0.012}_{-0.012},\ \sin^2\theta_{23} = 0.573^{+0.016}_{-0.020},\ \sin^2\theta_{13} = 0.02219^{+0.00062}_{-0.00063},$$
$$\delta_{\rm CP} = \frac{197^{+27}_{-24}}{180}\pi,\ \Delta m^2_{21} = 7.42^{+0.21}_{-0.20}\times 10^{-5}{\rm eV}^2,\ \Delta m^2_{3\ell} = 2.517^{+0.026}_{-0.028}\times 10^{-3}{\rm eV}^2$$
(Normal Ordering /with SK atmospheric data) (0.4)

$$\sin^2\theta_{12} = 0.304^{+0.013}_{-0.012},\ \sin^2\theta_{23} = 0.575^{+0.016}_{-0.019},\ \sin^2\theta_{13} = 0.02238^{+0.00063}_{-0.00062},$$
$$\delta_{\rm CP} = \frac{282^{+26}_{-30}}{180}\pi,\ \Delta m^2_{21} = 7.42^{+0.21}_{-0.20}\times 10^{-5}{\rm eV}^2,\ \Delta m^2_{3\ell} = -2.498^{+0.028}_{-0.028}\times 10^{-3}{\rm eV}^2$$
(Inverted Ordering /with SK atmospheric data) (0.5)

This global fits is based on the following experiments:

- Solar experiments (Homestake [7], Gallex & GNO [8], SAGE [9], SK [10–13], SNO [14], Borexino [15–17], Standard Solar Model (external information) [18])
- Atmospheric experiments (IceCube [19, 20], SK [21], Atmospheric neutrino fluxes (external information) [22])
- Reactor experiments (KamLAND [23], Daya Bay [24], Double-Chooz [25, 26], Daya-Bay 2 [27], Reno [28, 29])
- Accelerator experiments (MINOS [30, 31], T2K [32, 33], NOvA [34, 35])

Next, we review the BSM physics which explain the neutrino oscillation. There are two well-known methods to explain neutrino oscillation: Dirac mass and Majorana mass.

In Dirac mass method, massless right-handed neutrinos ν_R are introduced:

$$\mathcal{L} \supset -y\overline{L}\tilde{H}\nu_R + {\rm H.c.} \tag{0.6}$$

Here, L is the doublet SM lepton, H is the SM Higgs particle and $\tilde{H} = (i\sigma_2)H^*$. After electroweak symmetry breaking, the neutrinos obtain nonzero Dirac masses.

Another method is Majorana mass method. The dimension-5 higher dimensional operator is allowed by SM gauge symmetry:

$$\mathcal{L}_{\rm eff} \supset -\frac{1}{\Lambda}\overline{L^c}H\tilde{H}^\dagger L + {\rm H.c.} \tag{0.7}$$

After electroweak symmetry breaking, the neutrinos obtain nonzero Majorana masses. The simplest UV completions for this operator are known as "seesaw models": Type I

[1] Here, $\Delta m^2_{3\ell} := \Delta m^2_{31} > 0$ for NO, $\Delta m^2_{3\ell} := \Delta m^2_{32} < 0$ for IO.

seesaw (right-handed fermion $N_R \in (\mathbf{1}, \mathbf{1}, 0)$ [2]) [36–40], Type II seesaw (complex scalar $\Delta \in (\mathbf{1}, \mathbf{3}, +1)$) [41–43] and Type III seesaw (right-handed fermion $\Sigma_R \in (\mathbf{1}, \mathbf{3}, 0)$) [44]. The coefficient of the effective operator is suppressed by heavy BSM scale, it explains the smallness of neutrino masses.

There are models which give the neutrino masses at loop level. They are called as "radiative seesaw models". Zee model [45, 46] and Zee-Babu model [47, 48] are well-known radiative seesaw models. Furthermore, there are radiative seesaw models with dark matters; KNT model [49], the scotogenic model [50] and etc. In these models, dark matter is stabilized by extra $\mathbb{Z}_2$ symmetry.

The important feature of the neutrino Majorana masses is that they break the lepton number symmetry. This symmetry is classically and accidentally conserved in SM. Therefore, we want to know the origin of the breaking. Majoron models [51, 52] is well known models which explain the origin of lepton number symmetry breaking. In Majoron models, this breaking is identified as the vacuum expectation value (VEV) of complex scalar. Majoron is the pseudo Nambu-Goldstone (NG) boson of the lepton symmetry breaking.

In this thesis, we show the relationships between the neutrino Majorana masses and the other BSM physics. Seesaw models contain the heavy particles coupling to SM lepton sector. Therefore, they may explain the problems relating to lepton; such as muon g-2 anomaly ([1], Part II). Furthermore, the origin of the lepton number symmetry breaking also relates other physics. Majorons have no electromagnetic charge, therefore, it can become dark matter ([2], Part III). On the other hand, the lepton number symmetry breaking can be identified as the other symmetry breaking ([3], Part IV).

In Part II, we show the relationship between the neutrino oscillation and the muon g-2 anomaly. We briefly review the muon g-2 anomaly in §1. In §2, we show the methods explaining both muon g-2 anomaly and neutrino oscillation. In §2.1, we show that Type II seesaw model cannot explain the muon g-2 anomaly, because the contribution from Type II seesaw has the opposite sign to $\Delta a_\mu = a_\mu^{\rm exp} - a_\mu^{\rm SM}$, which is the known facts shown in [53]. In §2.2 and §2.3, we explain our idea to solve it. In §2.2, it can be solved by a double charged complex scalar $k^{++} \in (\mathbf{1}, \mathbf{1}, +2)$. In this extended model, the discrete lepton flavor symmetry must be imposed, in order to avoid LFV constraints (§2.3). In §3 and §4, we concretely construct two models, and show that they can explain both the muon g-2 anomaly and the neutrino oscillation, and avoid all LFV constraints.

In Part III, we show the relationship between the neutrino oscillation and the existence of dark matter. In this part, we identify the (TeV scale) Majoron as dark matter. In §6, we review the Majoron dark matter. There are a lot of researches on Majoron dark matter with GeV scale or lighter masses (§6.1). In §6.2, we show that TeV scale Ma-

[2] $X \in (\mathbf{m}, \mathbf{n}, p)$ means that X are in $SU(3)_C$ **m**-plet and $SU(2)_L$ **n**-plet, and its $U(1)_Y$ charge is p.

joron dark matter is interesting, because it can explain the anomalous results in positron fraction detected by cosmic ray experiments. However, it is not obvious that the TeV scale Majoron can be produced as much as the DM relic density. In §7, we illustrates the difficulty and our solutions of it. In §8, 9 and 10, we explain three scenarios in which TeV Majoron is produced as much as the observed dark matter relic density. In these sections, we show the Lagrangian of Majoron models, Boltzmann equations, the approximation formulae and numerical results for the Majoron dark matter density.

In Part IV, we show that the lepton number symmetry can be identified as Peccei Quinn (PQ) symmetry in axion model. First, we review the strong CP problem (§12.1), axion models (§12.2) and their experimental constraints (§12.3). In §13, we show previous works in which the PQ symmetry in the QCD axion model is identified as the lepton number symmetry in the Majoron model (L=PQ models). In §14.1, we construct the minimal L=PQ models, by identifying the heavy quark in KSVZ axion model with the heavy fermion in (radiative) seesaw model. We call this as "Ma-xion" model. In §14.2, we show the particle contents and their Lagrangian in Ma-xion model. In §14.3, we derive the axion-SM-SM coupling by the redefinition of fields, and the experimental constraints on them. In §14.4, we show that Ma-xion models can explain the dark matter relic density and the neutrino oscillation.

Part II
The muon g-2 anomaly and the neutrino oscillation

1 The review of the muon g-2 anomaly

1.1 The muon g-2 anomaly

Recent results about muon $g-2$ anomaly are summarized in [54]. This section is based on this.

The lepton ℓ^- has the magnetic dipole moment (MDM):

$$\boldsymbol{\mu} = g\frac{e}{2m_\ell}\mathbf{s}. \tag{1.1}$$

This g is called as Lande g-factor. $g = 2$ in tree-level, and differ from 2 in loop-level. It is useful to define the parameter a as $a = \frac{g-2}{2}$. It was precisely measured by BNL experiment [55] [3]:

$$a_\mu(\text{exp}) = 116\ 592\ 089(63) \times 10^{-11}. \tag{1.2}$$

The Standard Model prediction of a contains the contributions from QED, electro-weak, hadron vaccum porlarization (HVP) and hadron light by light (HLbL). The latest results of QED are calculated by [57, 58]:

$$a_\mu^{\text{QED}}(\alpha(\text{Cs})) = 116\ 584\ 718.931(104) \times 10^{-11}. \tag{1.3}$$

The contribution from electro-weak is calculated by [59, 60]:

$$a_\mu^{\text{EW}} = 153.6(1.0) \times 10^{-11}. \tag{1.4}$$

There are two methods to calculate HVP contribution: data-driven (or phenomenological) evaluation and lattice QED-QCD calculation. First, we show data-driven results. The leading order contribution from HVP is calculated by [61–66]:

$$a_\mu^{\text{HVP, LO}} = 6931(40) \times 10^{-11}. \tag{1.5}$$

The NLO contribution [66] and NNLO contribution [67] are shown as follows:

$$a_\mu^{\text{HVP, NLO}} = -\,98.3(7) \times 10^{-11},\ a_\mu^{\text{HVP, NNLO}} = 12.4(1) \times 10^{-11}. \tag{1.6}$$

[3] Here, we used the latest value of $\lambda = \mu_\mu/\mu_p = 3.183345142(71)$ [56].

Therefore, the HVP contribution calculated by the data-driven evaluation are:

$$a_\mu^{\mathrm{HVP}} = a_\mu^{\mathrm{HVP,\,LO}} + a_\mu^{\mathrm{HVP,\,NLO}} + a_\mu^{\mathrm{HVP,\,NNLO}} = 6845(40) \times 10^{-11}. \tag{1.7}$$

The HVP contribution calculated by lattice QED-QED are shown follows [68–76]:

$$a_\mu^{\mathrm{HVP,\,LO}} = 7116(184) \times 10^{-11}. \tag{1.8}$$

This has large uncertainty, therefore, we do not use in this thesis. In the last year, BMW-2020 [77] calculates the HVP contribution by lattice, with small uncertainty:

$$a_\mu^{\mathrm{HVP,\,LO}} = 7087(28)(45) \times 10^{-11}. \tag{1.9}$$

This result consists with no new physics. In this thesis, we do not use this results, and we wait other lattice HVP results with small uncertainty.

The HLbL contribution are calculated by the data-driven evaluation and the lattice calculation. The data-driven result [78–90] and next to leading order result [91] are shown as follows:

$$a_\mu^{\mathrm{HLbL}} = (69.3(4.1) + 20(19) + 3(1)) \times 10^{-11} = 92(19) \times 10^{-11}, \tag{1.10}$$

$$a_\mu^{\mathrm{HLbL,\,NLO}} = 2(1) \times 10^{-11}. \tag{1.11}$$

Lattice results of HLbL [92] are shown as follows:

$$a_\mu^{\mathrm{HLbL}} = 78.7(30.6)_{\mathrm{stat}}(17.7)_{\mathrm{sys}} \times 10^{-11}. \tag{1.12}$$

Then, HLbL results are shown as follows [54]: [4]

$$a_\mu^{\mathrm{HLbL}}(\mathrm{phenomenology} + \mathrm{Lattice}) = 90(17) \times 10^{-11}, \tag{1.13}$$

$$a_\mu^{\mathrm{HLbL}}(\mathrm{phenomenology} + \mathrm{Lattice}) + a_\mu^{\mathrm{HLbL,\,NLO}} = 92(18) \times 10^{-11}. \tag{1.14}$$

Total SM contribution is given by QED + EW + HVP + HLbL, therefore,

$$a_\mu^{\mathrm{SM}} = a_\mu^{\mathrm{QED}} + a_\mu^{\mathrm{EW}} + a_\mu^{\mathrm{HVP,\,LO}} + a_\mu^{\mathrm{HVP,\,NLO}} + a_\mu^{\mathrm{HVP,\,NNLO}} + a_\mu^{\mathrm{HLbL}} + a_\mu^{\mathrm{HLbL,\,NLO}} \tag{1.15}$$

$$= 116\,591\,810(43) \times 10^{-11}. \tag{1.16}$$

Here, we used HVP results given by data-driven evaluation, it is because the uncertainties of lattice results are large. Then, the difference between SM prediction and experiment results are shown as follows:

$$\Delta a_\mu = a_\mu^{\mathrm{exp}} - a_\mu^{\mathrm{SM}} = 279(76) \times 10^{-11}. \tag{1.17}$$

This suggests that there is 3.7σ discrepancy. This is called as "muon g-2 anomaly".

[4] Here, we take into account that c-quark contributions are not contained in lattice results.

1.2 The contribution from the BSM dipole effective action to the muon g-2 anomaly

The muon g-2 anomaly can be explained by BSM physics. In this section, we evaluate the contribution from effective Hamiltonian (generated by heavy BSM particles) to lepton g-2 and electric dipole moment (EDM). We assume that the effective Hamiltonian is given as follows:

$$H = -\int d^3x F_{\mu\nu}\bar{\ell}\sigma^{\mu\nu}(A_L P_L + A_R P_R)\ell,\ (A_R = A_L^*). \tag{1.18}$$

Here, ℓ is SM charged lepton field, $F_{\mu\nu}$ is the electro-magnetic field strength and $\sigma^{\mu\nu}$ is defined as $\sigma^{\mu\nu} = i[\gamma^\mu, \gamma^\nu]/2$. We evaluate this effective Hamiltonian by lepton state vectors $|\ell(p, s)\rangle$ and background electro-magnetic fields, then, we can get the BSM contributions to lepton g-2 and electric dipole moment (EDM).

First, we evaluate the dipole operator as follows [5] (assuming $F_{\mu\nu}$ does not depend on $\mathbf{x}$):

$$\int d^3x \langle \ell(p', r')|\bar{\ell}\sigma^{\mu\nu}(A_L P_L + A_R P_R)\ell|\ell(p, r)\rangle \tag{1.19}$$

$$= \int d^3x \frac{d^3k}{(2\pi)^3\sqrt{2E_k}}\frac{d^3k'}{(2\pi)^3\sqrt{2E_{k'}}}\sum_{s,\,s'}\sqrt{2E_p}\sqrt{2E_{p'}} \tag{1.20}$$

$$\times \Big[\overline{u}^{s'}(k')\sigma^{\mu\nu}(A_L P_L + A_R P_R)u^s(k)e^{-i(k-k')x}\langle 0|a_{p'}^{r'}(a_{k'}^{s'})^\dagger a_k^s(a_p^r)^\dagger|0\rangle$$

$$+ \overline{v}^{s'}(k')\sigma^{\mu\nu}(A_L P_L + A_R P_R)v^s(k)e^{+i(k-k')x}\langle 0|a_{p'}^{r'}b_{k'}^{s'}(b_k^s)^\dagger(a_p^r)^\dagger|0\rangle\Big] \tag{1.21}$$

$$= \int d^3x \frac{d^3k}{\sqrt{2E_k}}\frac{d^3k'}{\sqrt{2E_{k'}}}\sqrt{2E_p}\sqrt{2E_{p'}} \tag{1.22}$$

$$\times \Big[\overline{u}^{r'}(k')\sigma^{\mu\nu}(A_L P_L + A_R P_R)u^r(k)e^{-i(p-p')x}\delta^3(\mathbf{k}-\mathbf{p})\delta^3(\mathbf{k}'-\mathbf{p}')$$

$$+ \overline{v}^{s}(k')\sigma^{\mu\nu}(A_L P_L + A_R P_R)v^s(k)\delta^{r'r}\delta^3(\mathbf{k}-\mathbf{k}')\delta^3(\mathbf{p}-\mathbf{p}')\Big] \tag{1.23}$$

$$\to \overline{u}^{r'}(p')\sigma^{\mu\nu}(A_L P_L + A_R P_R)u^r(p) \times (2\pi)^3\delta^3(\mathbf{p}-\mathbf{p}') \tag{1.24}$$

$$\text{(Here, we ignore 2nd term).} \tag{1.25}$$

[5] Here, we use the following notations: $\Psi(x) = \int \frac{d^3p}{(2\pi)^3}\frac{1}{\sqrt{2E_\mathbf{p}}}\sum_s \left(a_\mathbf{p}^s u^s(p)e^{-ipx} + b_\mathbf{p}^{s\dagger}v^s(p)e^{+ipx}\right)$. The spinors $u(p)$ and $v(p)$ is defined as follows: $u(p) = \Lambda_{\frac{1}{2}}u(m, \mathbf{0})$, $v(p) = \Lambda_{\frac{1}{2}}v(m, \mathbf{0})$, $u^s(m, \mathbf{0}) = \sqrt{m}\begin{pmatrix}\xi_s\\ \xi_s\end{pmatrix}$, $v^s(m, \mathbf{0}) = \sqrt{m}\begin{pmatrix}\eta_s\\ -\eta_s\end{pmatrix}$, $\xi_r^\dagger\xi_s = \delta_{rs}$, $\eta_r^\dagger\eta_s = \delta_{rs}$. Here, $\Lambda_{\frac{1}{2}}$ is Lorentz transformation of spinors defined as follows $\Lambda_{\frac{1}{2}} = \exp(-i\omega_{\mu\nu}S^{\mu\nu}/2)$, $S^{\mu\nu} = i[\gamma^\mu, \gamma^\nu]/4$, $\Lambda_{\frac{1}{2}}^{-1}\gamma^\mu\Lambda_{\frac{1}{2}} = \Lambda^\mu{}_\nu\gamma^\nu$, $p^\mu\Lambda_\mu{}^\nu = (m, \mathbf{0})^\nu$. The one particle state vector of Ψ is defined as $|\Psi(p, s)\rangle = \sqrt{2E_p}a_p^{s\dagger}|0\rangle$

Then, we can evaluate the effective Hamiltonian by lepton state vectors and background electro-magnetic fields [6]:

$$\frac{\langle \ell(p',\, r')|\hat{H}|\ell(p,\, r)\rangle}{\langle \ell(p',\, r')|\ell(p,\, r)\rangle} = -\frac{1}{\delta^{rr'}}\frac{1}{2E_p}F_{\mu\nu}\overline{u}^{r'}(p')\sigma^{\mu\nu}(A_L P_L + A_R P_R)u^r(p) \tag{1.26}$$

$$= -\frac{1}{2}\big[-2i(A_L - A_R)E^i - 2(A_L + A_R)B^i\big](\xi^r)^\dagger\sigma^i\xi^r. \tag{1.27}$$

Therefore, the BSM contributions to EDM and MDM are: [7]

$$\mathbf{d}^{\rm BSM} = -2i(A_L - A_R)\mathbf{s},\ \boldsymbol{\mu}^{\rm BSM} = -2(A_L + A_R)\mathbf{s} = \frac{(\Delta a_\ell)e}{m_\ell}\mathbf{s}, \tag{1.28}$$

therefore, we can get the formulae for BSM contribution to Δa_ℓ and EDM:

$$\Delta a_\ell = -\frac{2m_\ell}{e}(A_L + A_R),\ |d_\ell| = \big|-i(A_L - A_R)\big|. \tag{1.29}$$

There are a lot of BSM models which explain the muon g-2 anomaly; for example the extra gauge boson [93–110], the two Higgs doublet model [111–119] and so on. We explain the muon g-2 anomaly by the Type II seesaw model.

2 The relationship between the neutrino oscillation and the muon g-2 anomaly

In this section, we show the relationship between muon g-2 anomaly and neutrino oscillation.

Type I and III seesaw contain one coupling: $\overline{L}N_R\tilde{\phi}$ and $\overline{L}\Sigma_R\tilde{\phi}$, respectively. On the other hands, type II seesaw contains "two" couplings $y_\Delta\overline{L^c}\Delta L$ and $\mu_1\phi^{\rm T}(i\sigma_2)\Delta^\dagger\phi$. Therefore, type II seesaw can explain neutrino mass with TeV scale BSM particles and $O(1)$ Yukawa couplings, by setting μ_1 as small value. We want to use these TeV particles and $O(1)$ Yukawa couplings to explain muon g-2 anomaly.

In §2.1, we show that Type II seesaw model cannot explain the muon g-2 anomaly, because the contribution from Type II seesaw has the opposite sign to $\Delta a_\mu = a_\mu^{\rm exp} - a_\mu^{\rm SM}$. It is shown in [53].

In §2.2 and §2.3, we explain our idea to solve it. In §2.2, it can be done by a double charged complex scalar $k^{++} \in (\mathbf{1},\, \mathbf{1},\, +2)$. In this extended model, the discrete lepton flavor symmetry must be imposed, in order to avoid LFV constraints (§2.3).

---

[6] $A^\mu = (\phi,\, \mathbf{A})^\mu$, $F_{0i} = E^i$, $\epsilon^{ijk}F_{ij} = -2B^k$, $F_{\mu\nu}\sigma^{\mu\nu} = -2iE^i\begin{pmatrix}\sigma^i & \\ & -\sigma^i\end{pmatrix} - 2B^k\Sigma^k$, $\sigma^{0i} = -i\begin{pmatrix}\sigma^i & \\ & -\sigma^i\end{pmatrix}$, $\sigma^{ij} = \epsilon^{ijk}\Sigma^k$, $\Sigma^k := \begin{pmatrix}\sigma^k & \\ & \sigma^k\end{pmatrix}$.

[7] When EDM is $\mathbf{d}$ and MDM is $\boldsymbol{\mu}$, the Hamiltonian under background electro-magnetic field is given as follows: $H = -\mathbf{d}\cdot\mathbf{E} - \boldsymbol{\mu}\cdot\mathbf{B}$.

2.1 Type II seesaw and muon $g-2$

Type II seesaw model has BSM particle $\Delta \in (\mathbf{1}, \mathbf{3})_{+1}$. Then, the Yukawa coupling of Δ [8] are shown as follows:

$$\mathcal{L}_{\rm Y} = - y_\Delta^{ab} \overline{L_a^c} (i\sigma_2) \Delta L_b + \text{H.c.} \tag{2.1}$$

$$= - \frac{1}{2}(2y_\Delta^{ab}) \frac{v_\Delta + \delta_0 + i\delta_1}{\sqrt{2}} \overline{\nu_a^c} \nu_b + \sqrt{2} y_\Delta^{ab} (U_{\rm PMNS})_{bi} \delta^+ \overline{\ell_{La}^c} \nu_i + \frac{1}{2}(2y_\Delta^{ab}) \delta^{++} \overline{\ell_{La}^c} \ell_{Lb} + \text{H.c.} \tag{2.2}$$

Here, $L_a\,(a = e,\, \mu,\, \tau)$ is the SM doublet lepton field. The first term in (2.2) gives neutrino Majorana masses. The second and third terms in (2.2) give the contribution to the lepton g-2.

The VEV of Δ is given by $\mu \phi^{\rm T} (i\sigma_2) \Delta^\dagger \phi$, after electro-weak symmetry breaking. The ρ parameter depends on v_Δ:

$$\rho = \frac{m_W^2}{m_Z^2 \cos^2\theta_W} = \frac{1 + 2v_\Delta^2/v_\phi^2}{1 + 4v_\Delta^2/v_\phi^2}. \tag{2.3}$$

The experimental value of ρ is 1.00038 ± 0.00020 [120]. Therefore, $v_\Delta \ll O(1)$ GeV.

In appendix §A.1.2, we calculate the lepton g-2, by using the following Lagrangian:

$$\mathcal{L} \supset H_i^{++} \overline{\ell_a^C} (f_{iL}^{ab} P_L + f_{iR}^{ab} P_R) \ell_b + h_i^{aj} H_i^+ \overline{\ell_a^C} \nu_{Lj} + \text{H.c.} \tag{2.4}$$

By comparing this with Type II seesaw model, H_i^{++}, H_i^+, f_{iL}^{ab}, f_{iR}^{ab}, h_i^{aj} are given as follows:

$$f_{iL}^{ab} = y_\Delta^{\alpha\beta},\ f_{iR}^{ab} = 0,\ h_i^{aj} = \sqrt{2} y_\Delta^{ab} (U_{\rm PMNS})_{bj},\ H_i^{++} = \delta^{++},\ H_i^+ = \delta^+. \tag{2.5}$$

Then, lepton g-2 and the coefficient of dipole operators can calculated from the formula

[8] $\Delta^\alpha{}_\beta = \begin{pmatrix} \delta^+/\sqrt{2} & \delta^{++} \\ (v_\Delta + \delta_0 + i\delta_1)/\sqrt{2} & -\delta^+/\sqrt{2} \end{pmatrix}$.

in §A.1.2:

$$\Delta a_{\ell_a} = -\frac{2m_{\ell_a}}{e}(A_L + A_R)^{aa},\ A_{L,R} = A_{L,R}^{H^+} + A_{L,R}^{H^{++}}, \tag{2.6}$$

$$A_L^{H^+aa} = A_R^{H^+aa} = \frac{e}{24(4\pi)^2}\sum_i \frac{[h_i h_i^\dagger]^{aa} m_{\ell_a}}{M_{H_i^+}^2} = \frac{e}{12(4\pi)^2}\frac{[y_\Delta y_\Delta^\dagger]^{aa} m_{\ell_a}}{M_{\delta^+}^2}, \tag{2.7}$$

$$\begin{aligned} A_L^{H^{++}aa} \simeq & \frac{e}{3(4\pi)^2}\sum_i \frac{1}{M_i^{++2}}\Big[2m_{\ell_a} f_{iL}^{\dagger ac} f_{iL}^{ca} + 2m_{\ell_a} f_{iR}^{\dagger ac} f_{iR}^{ca} \\ & + \big\{-3 + 6\ln(M_i^{++2}/m_{\ell_c}^2)\big\} m_{\ell_c} f_{iR}^{\dagger ac} f_{iL}^{ca}\Big] \end{aligned} \tag{2.8}$$

$$= \frac{2e}{3(4\pi)^2}\frac{m_{\ell_a}[y_\Delta^\dagger y_\Delta]^{aa}}{M_{\delta^{++}}^2}, \tag{2.9}$$

$$\begin{aligned} A_R^{H^{++}aa} \simeq & \frac{e}{3(4\pi)^2}\sum_i \frac{1}{M_i^{++2}}\Big[2m_{\ell_a} f_{iR}^{\dagger ac} f_{iR}^{ca} + 2m_{\ell_a} f_{iL}^{\dagger ac} f_{iL}^{ca} \\ & + \big\{-3 + 6\ln(M_i^{++2}/m_{\ell_c}^2)\big\} m_{\ell_c} f_{iL}^{\dagger ac} f_{iR}^{ca}\Big], \end{aligned} \tag{2.10}$$

$$= \frac{2e}{3(4\pi)^2}\frac{m_{\ell_a}[y_\Delta^\dagger y_\Delta]^{aa}}{M_{\delta^{++}}^2}. \tag{2.11}$$

Here, $A_{L,R}^{H^+}$ is the contribution from single charged scalar, $A_{L,R}^{H^{++}}$ is the one from double charged scalar. Therefore, [9]

$$\Delta a_{\ell_a} = -\frac{[y_\Delta y_\Delta^\dagger]^{aa} m_{\ell_a}^2}{3(4\pi)^2}\left(\frac{1}{M_{\delta^+}^2} + \frac{8}{M_{\delta^{++}}^2}\right) \tag{2.12}$$

This implies that the contributions from δ^+ and δ^{++} have minus sign. Therefore, they cannot explain the muon g-2 anomaly, which has plus sign. In Type II seesaw model, δ^{++} couples to only left handed lepton. This is reason why Δa_μ has minus sign.

In next section, we add a douple charged scalar field $k^{++} \in (\mathbf{1}, \mathbf{1}, +2)$ to Type II seesaw model. Then, the Yukawa coupling between double charged scalar and "right"-handed lepton also exists. It will explain the plus sign of the experimental Δa_μ value.

[9] $y_\Delta = y_\Delta^{\mathrm{T}}$, $[y_\Delta y_\Delta^\dagger]^{aa} = [y_\Delta^\dagger y_\Delta]^{aa} = \sum_i |y_\Delta^{ai}|^2$

2.2 Type II seesaw model with k^{++}

Let us consider Type II seesaw model with double charged scalar k^{++}. First, we consider the scalar potential [10] [11]:

$$\begin{aligned} V[\phi,\Delta,k^{++}] =& \mu_\phi^2(\phi^\dagger\phi) + M_\Delta^2\mathrm{Tr}(\Delta^\dagger\Delta) + M_{k^{++}}^2|k^{++}|^2 \\ &+ [\mu_1\phi^{\mathrm{T}}(i\sigma_2)\Delta^\dagger\phi + \mathrm{H.c.}] + [\mu_2 k^{++}\mathrm{Tr}(\Delta^\dagger\Delta^\dagger) + \mathrm{H.c.}] \\ &+ \lambda(\phi^\dagger\phi)^2 + \lambda_1(\phi^\dagger\phi)\mathrm{Tr}(\Delta^\dagger\Delta) + \lambda_2[\mathrm{Tr}(\Delta^\dagger\Delta)]^2 + \lambda_3\mathrm{Tr}[(\Delta^\dagger\Delta)^2] \\ &+ \lambda_4\phi^\dagger\Delta\Delta^\dagger\phi + \lambda_5\phi^\dagger\phi|k^{++}|^2 + \lambda_6\mathrm{Tr}(\Delta^\dagger\Delta)|k^{++}|^2 \\ &+ [\lambda_7\tilde{\phi}^\dagger\Delta\phi k^{--} + \mathrm{H.c.}] + \lambda_8|k^{++}|^4. \end{aligned} \tag{2.13}$$

We assume that the couplings of ϕ are chosen so that ϕ gets nonzero VEV. After electroweak symmetry breaking, ϕ gets VEV as $\langle\phi\rangle = \frac{1}{\sqrt{2}}\begin{pmatrix}0\\ v_\phi\end{pmatrix}$. Then, Δ also get VEV as $\Delta = \begin{pmatrix}\delta^+/\sqrt{2} & \delta^{++}\\ (v_\Delta+\delta_0+i\delta_1)/\sqrt{2} & -\delta^+/\sqrt{2}\end{pmatrix}$. v_Δ is given by the stationary condition:

$$0 = \left.\frac{\partial V}{\partial\delta_0}\right|_{\mathrm{vac}} = -\frac{\mu_1 v_\phi^2}{\sqrt{2}} + \frac{1}{2}\big[2M_\Delta^2 + (\lambda_1+\lambda_4)v_\phi^2\big]v_\Delta + O(v_\Delta^2), \tag{2.14}$$

i.e,

$$v_\Delta \to \frac{\mu_1 v_\phi^2}{\sqrt{2}\big[M_\Delta^2 + (\lambda_1+\lambda_4)v_\phi^2/2\big]} + O(v_\Delta^2). \tag{2.15}$$

When μ_1 is much smaller than weak scale, the mixing between δ_0 and Higgs becomes tiny. We ignore this mixing effect.

[10] $\mathrm{Tr}\Delta\Delta\Delta^\dagger\Delta^\dagger = \frac{1}{2}\mathrm{Tr}\Delta\Delta\mathrm{Tr}\Delta^\dagger\Delta^\dagger$, $\mathrm{Tr}[\Delta\Delta^\dagger\Delta\Delta^\dagger] = (\mathrm{Tr}\Delta\Delta^\dagger)^2 - \frac{1}{2}\mathrm{Tr}\Delta\Delta\mathrm{Tr}\Delta^\dagger\Delta^\dagger$, $\phi^\dagger\Delta\Delta^\dagger\phi + \phi^\dagger\Delta^\dagger\Delta\phi = \phi^\dagger\phi\mathrm{Tr}\Delta^\dagger\Delta$, $\mathrm{Tr}\Delta\Delta^\dagger\Delta^\dagger = 0$

[11] μ_1 and λ_7 can be real value by redefinition of k^{++} and Δ.

Mass terms of scalar particles are given as follows:

$$
\begin{aligned}
V \supset & \frac{1}{2}\left[M_\Delta^2 + (\lambda_1+\lambda_4)v_\phi^2/2\right](\delta_0^2+\delta_1^2) + \left[M_\Delta^2 + (\lambda_1+\lambda_4/2)v_\phi^2/2\right]|\delta^+|^2 \\
& + \begin{pmatrix}\delta^{--} & k^{--}\end{pmatrix}\begin{pmatrix} M_\Delta^2 + \frac{\lambda_1 v_\phi^2}{2} & \frac{\lambda_7 v_\phi^2}{2} \\ \frac{\lambda_7 v_\phi^2}{2} & M_k^2 + \frac{\lambda_5 v_\phi^2}{2}\end{pmatrix}\begin{pmatrix}\delta^{++} \\ k^{++}\end{pmatrix} && (2.16) \\
\supset & + \begin{pmatrix}H_1^{--} & H_2^{--}\end{pmatrix}\begin{pmatrix} c_\theta & -s_\theta \\ s_\theta & c_\theta\end{pmatrix}\begin{pmatrix} M_\Delta^2 + \frac{\lambda_1 v_\phi^2}{2} & \frac{\lambda_7 v_\phi^2}{2} \\ \frac{\lambda_7 v_\phi^2}{2} & M_k^2 + \frac{\lambda_5 v_\phi^2}{2}\end{pmatrix}\begin{pmatrix} c_\theta & s_\theta \\ -s_\theta & c_\theta\end{pmatrix}\begin{pmatrix}H_1^{++} \\ H_2^{++}\end{pmatrix} && (2.17) \\
= & M_{H_1^{++}}^2 |H_1^{++}|^2 + M_{H_2^{++}}^2 |H_2^{++}|^2, && (2.18) \\
& M_{H_1^{++}}^2 = c_\theta^2 A - 2 s_\theta c_\theta C + s_\theta^2 B,\ M_{H_2^{++}}^2 = s_\theta^2 A + 2 s_\theta c_\theta C + c_\theta^2 B, && (2.19) \\
& A = M_\Delta^2 + \frac{\lambda_1 v_\phi^2}{2},\ B = M_k^2 + \frac{\lambda_5 v_\phi^2}{2},\ C = \lambda_7 v_\phi^2/2, && (2.20) \\
& \tan(2\theta) = -\frac{2C}{A-B},\ -\pi/4 \le \theta \le \pi/4. && (2.21)
\end{aligned}
$$

Here, θ is mixing angle between δ^{++} and k^{++}. θ depends on the scalar coupling $\lambda_7 \tilde{\phi}^\dagger \Delta \phi k^{--}$. The BSM contribution of the muon g-2 has a strong dependence on θ (i.e. λ_7). $H_{1,2}^{++}$ are defined as the mass eigenstates.

Next, we consider the Yukawa couplings of the model. These are shown as follows:

$$
\begin{aligned}
\mathcal{L}_{\rm Y} = & - y_\Delta^{ab}\overline{L_a^c}(i\sigma_2)\Delta L_b - y_S^{ab}\overline{\ell_{Ra}^c}\ell_{Rb}k^{++} + \text{H.c.} && (2.22) \\
= & -\frac{1}{2}(2y_\Delta^{ab})\frac{v_\Delta + \delta_0 + i\delta_1}{\sqrt{2}}\overline{\nu_a^c}\nu_b + \sqrt{2}y_\Delta^{ab}(U_{\rm PMNS})_{bi}\delta^+\overline{\ell_{La}^c}\nu_i \\
& + \frac{1}{2}(2y_\Delta^{ab})(c_\theta H_1^{++} + s_\theta H_2^{++})\overline{\ell_{La}^c}\ell_{Lb} - \frac{1}{2}(2y_S^{ab})(-s_\theta H_1^{++} + c_\theta H_2^{++})\overline{\ell_{Ra}^c}\ell_{Rb}, && (2.23) \\
& \delta^{++} = c_\theta H_1^{++} + s_\theta H_2^{++},\ k^{++} = -s_\theta H_1^{++} + c_\theta H_2^{++},\ \nu_a = (U_{\rm PMNS})_{ai}\nu_i. && (2.24)
\end{aligned}
$$

Here, double charged scalars couple to both left-handed leptons (by y_Δ) and right-handed ones (by y_S). Then, Δa can have positive sign.

Next we evaluate the lepton g-2 and the lepton flavor violating (LFV) decay widths in type II seesaw model with k^{++}. When comparing the Yukawa couplings in this model with one in §A.1.2:

$$
\mathcal{L} \supset H_i^{++}\overline{\ell_a^C}(f_{iL}^{ab}P_L + f_{iR}^{ab}P_R)\ell_b + h_i^{aj}H_i^+\overline{\ell_a^C}\nu_{Lj} + \text{H.c.}, \tag{2.25}
$$

H_i^{++}, H_i^+, f_{iL}^{ab}, f_{iR}^{ab}, h_i^{aj} are given as

$$
\begin{aligned}
& H_i^{++} = \begin{pmatrix}H_1^{++} \\ H_2^{++}\end{pmatrix}_i,\ H_i^+ = \delta^+, && (2.26) \\
& h_i^{aj} = \sqrt{2}y_\Delta^{ab}(U_{\rm PMNS})_{bj},\ f_{iL}^{ab} = y_\Delta^{ab}\begin{pmatrix}c_\theta & s_\theta\end{pmatrix}_i,\ f_{iR}^{ab} = y_S^{ab}\begin{pmatrix}s_\theta & -c_\theta\end{pmatrix}_i. && (2.27)
\end{aligned}
$$

Then, the muon g-2 and the decay widths of LFV processes in type II seesaw with k^{++} are evaluated as follows:

$$\Delta a_{\ell_a} = -\frac{2m_{\ell_a}}{e}(A_L + A_R)^{aa}, \tag{2.28}$$

$$\Gamma(\ell_a \to \ell_b \gamma) = \frac{(m_{\ell_a}^2 - m_{\ell_b}^2)^3}{4\pi m_{\ell_a}^3}\left(|A_L^{ba}|^2 + |A_R^{ba}|^2\right), \tag{2.29}$$

$$A_L^{H^+ba} \simeq \frac{e}{24(4\pi)^2}\sum_i \frac{[h_i h_i^\dagger]^{ab} m_{\ell_b}}{M_{H_i^+}^2} = \frac{e}{12(4\pi)^2}\frac{[y_\Delta y_\Delta^\dagger]^{ab} m_{\ell_b}}{M_{\delta^+}^2}, \tag{2.30}$$

$$A_R^{H^+ba} \simeq \frac{e}{24(4\pi)^2}\sum_i \frac{[h_i h_i^\dagger]^{ab} m_{\ell_a}}{M_{H_i^+}^2} = \frac{e}{12(4\pi)^2}\frac{[y_\Delta y_\Delta^\dagger]^{ab} m_{\ell_a}}{M_{\delta^+}^2}, \tag{2.31}$$

$$\begin{aligned} A_L^{H^{++}ba} \simeq & \frac{e}{3(4\pi)^2}\sum_i \frac{1}{M_i^{++2}}\Big[2m_{\ell_b} f_{iL}^{\dagger bc} f_{iL}^{ca} + 2m_{\ell_a} f_{iR}^{\dagger bc} f_{iR}^{ca} \\ & + \{-3 + 6\ln(M_i^{++2}/m_{\ell_c}^2)\} m_{\ell_c} f_{iR}^{\dagger bc} f_{iL}^{ca}\Big] \end{aligned} \tag{2.32}$$

$$\begin{aligned} A_R^{H^{++}ba} \simeq & \frac{e}{3(4\pi)^2}\sum_i \frac{1}{M_i^{++2}}\Big[2m_{\ell_b} f_{iR}^{\dagger bc} f_{iR}^{ca} + 2m_{\ell_a} f_{iL}^{\dagger bc} f_{iL}^{ca} \\ & + \{-3 + 6\ln(M_i^{++2}/m_{\ell_c}^2)\} m_{\ell_c} f_{iL}^{\dagger bc} f_{iR}^{ca}\Big], \end{aligned} \tag{2.33}$$

$$A^{H^{++}aa} = A_L^{H^{++}aa} + A_R^{H^{++}aa} \tag{2.34}$$

$$\begin{aligned} \simeq & \frac{e}{3(4\pi)^2}\sum_i \frac{1}{M_i^{++2}}\Big[4m_{\ell_a} f_{iL}^{\dagger ac} f_{iL}^{ca} + 4m_{\ell_a} f_{iR}^{\dagger ac} f_{iR}^{ca} \\ & + \{-3 + 6\ln(M_i^{++2}/m_{\ell_c}^2)\} m_{\ell_c}(f_{iR}^{\dagger ac} f_{iL}^{ca} + f_{iL}^{\dagger ac} f_{iR}^{ca})\Big] \end{aligned} \tag{2.35}$$

$$\begin{aligned} \simeq & \frac{e}{3(4\pi)^2}\Bigg\{\frac{1}{M_1^{++2}}\Big[4m_{\ell_a} c_\theta^2 y_\Delta^{\dagger ac} y_\Delta^{ca} + 4m_{\ell_a} s_\theta^2 y_S^{\dagger ac} y_S^{ca} \\ & + \{-3 + 6\ln(M_1^{++2}/m_{\ell_c}^2)\} m_{\ell_c} s_\theta c_\theta (y_S^{\dagger ac} y_\Delta^{ca} + y_\Delta^{\dagger ac} y_S^{ca})\Big] \end{aligned} \tag{2.36}$$

$$\begin{aligned} & + \frac{1}{M_2^{++2}}\Big[4m_{\ell_a} s_\theta^2 y_\Delta^{\dagger ac} y_\Delta^{ca} + 4m_{\ell_a} c_\theta^2 y_S^{\dagger ac} y_S^{ca} \\ & - \{-3 + 6\ln(M_2^{++2}/m_{\ell_c}^2)\} m_{\ell_c} s_\theta c_\theta (y_S^{\dagger ac} y_\Delta^{ca} + y_\Delta^{\dagger ac} y_S^{ca})\Big]\Bigg\}. \end{aligned} \tag{2.37}$$

The terms in (2.36) and (2.37) are important for muon g-2 anomaly. These term can have negative value, it is because these contain both y_S and y_Δ. Furthermore, they contain the chirality flip m_{ℓ_c} in internal Fermion line. When $\ell_c = \tau$, they have large value. Therefore, Δa_μ can be large positive value in this model.

However, dangerous LFV processes occur in this model. We show the plot of $\Gamma(\mu \to e\gamma)/\Gamma(\mu \to e\nu_\mu \nu_e^c)$ vs $M_{H_2^{++}}$ in Figure 1. The parameter settings in Figure 1 are shown

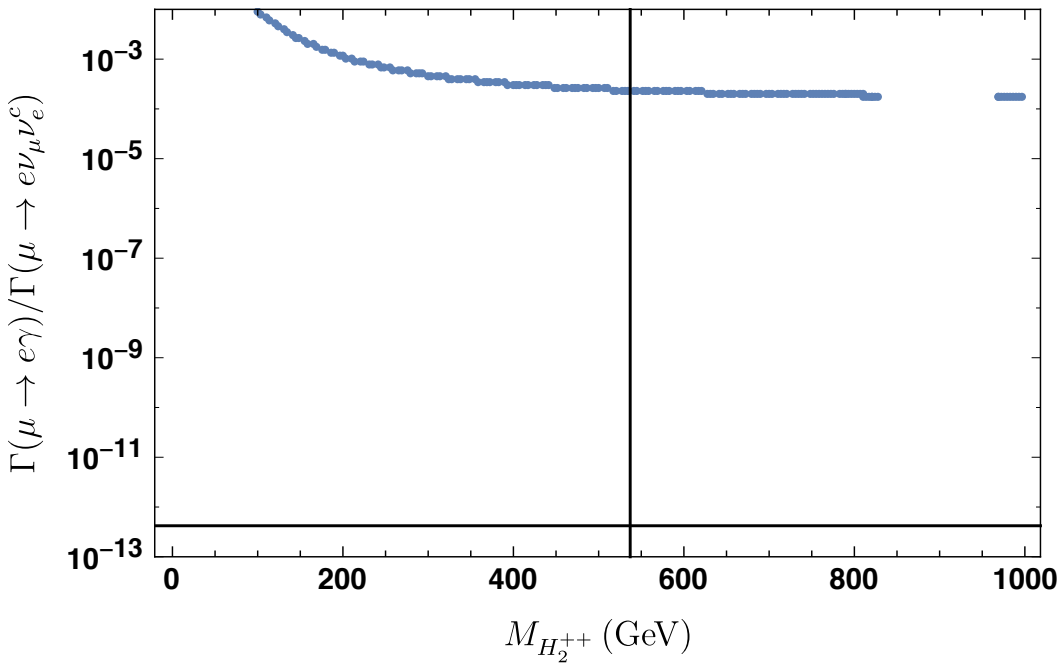

Figure 1: The plane of $\Gamma(\mu \to e\gamma)/\Gamma(\mu \to e\nu_\mu\nu_e^c)$ vs $M_{H_2^{++}}$. Both the muon g-2 anomaly and the neutrino mass matrix are explained at the blue points. The horizontal line is the experimental limit of $\Gamma(\mu \to e\gamma)/\Gamma(\mu \to e\nu_\mu\nu_e^c)$, and the vertical line is the CMS limit of $M_{H_2^{++}}$ (See §A.4).

as follows:

$$v_\Delta = 10^{-10}\text{GeV},\ M_\Delta = 900\text{GeV},\ \lambda_1 = 0,\ \lambda_4 = 0.1,\ \lambda_5 = 0. \tag{2.38}$$

Furthermore, we vary the parameter M_k, and choose λ_7 such that we can explain muon g-2 anomaly. $\Gamma(\mu^- \to e^-\gamma)/\Gamma(\mu^- \to e^-\nu_\mu\nu_e^c)$ is much larger than the experimental limit. Furthermore, other LFV processes ($\mu^- \to e^-e^-e^+$, $\tau^- \to \mu^-\gamma$ and etc.) can also occur. Therefore, we must reduce the LFV process.

In next subsection, we introduce the lepton flavor symmetry to the model.

2.3 The discrete flavor symmetry

LFV processes are shown as follows:

$$\mu^- \to e^-\gamma,\ \mu^- \to e^-e^-e^+,\ \tau^- \to e^-\gamma,\ \tau^- \to \mu^-\gamma, \tag{2.39}$$
$$\tau^- \to e^-e^-e^+,\ \tau^- \to e^-\mu^-e^+,\ \tau^- \to e^-e^-\mu^+, \tag{2.40}$$
$$\tau^- \to \mu^-\mu^-e^+,\ \tau^- \to e^-\mu^-\mu^+,\ \tau^- \to \mu^-\mu^-\mu^+. \tag{2.41}$$

When assigning $\mathbb{Z}_3$ charges on SM leptons:

$$\mathbb{Z}_3 L_e = +L_e,\ \mathbb{Z}_3 L_\mu = +\omega L_\mu,\ \mathbb{Z}_3 L_\tau = +\overline{\omega} L_\tau, \tag{2.42}$$
$$\mathbb{Z}_3 e_R = +e_R,\ \mathbb{Z}_3 \mu_R = +\omega \mu_R,\ \mathbb{Z}_3 \tau_R = +\overline{\omega} \tau_R, \tag{2.43}$$

only $\tau^- \to e^-e^-\mu^+$ and $\tau^- \to \mu^-\mu^-e^+$ are allowed under this symmetry. We impose this symmetry on Type II seesaw model with k^{++}.

We can not explain the neutrino oscillation under the exact $\mathbb{Z}_3$. Therefore, we allow the soft breaking terms of $\mathbb{Z}_3$ which cause the neutrino mass matrices.

In §3 and §4, we concretely construct two models: the model with k_a^+, ($a = e,\ \mu,\ \tau$) (Model I) and the model with Δ_a, ($a = e,\ \mu,\ \tau$) (Model II). Model I has the soft breaking term $\mu_{ab} k_a^+ k_b^+ k^{--}$, and it causes Zee-Babu type neutrino mass matrix [47, 48]. Model II has the soft breaking term $\mu_a \phi^{\mathrm{T}} (i\sigma_2) \Delta_a^\dagger \phi$, and it causes neutrino mass matrix as Type II seesaw.

3 Model I

In this section, we explain Model I. The fields contents of Model I are shown in Table 1. k^{++} and Δ gives the positive contribution to muon g-2. Only with k^{++} and Δ, neutrino oscillation can not be explained due to $\mathbb{Z}_3$ symmetry. We introduce k_a^+ ($a = e,\ \mu,\ \tau$), then, neutrino can gain Zee-Babu type neutrino mass.

	$SU(3)_C$	$SU(2)_L$	$U(1)_Y$	$\mathbb{Z}_3$
k^{++}	**1**	**1**	2	1
Δ	**1**	**3**	1	1
k_e^+	**1**	**1**	1	1
k_μ^+	**1**	**1**	1	ω
k_τ^+	**1**	**1**	1	$\overline{\omega}$

Table 1: Field contents in Model I

Yukawa couplings in Model I are shown as follows:

$$\begin{aligned}
\mathcal{L}_{\rm Y} =& -y_\Delta^{ab}\overline{L_a^c}(i\sigma_2)\Delta L_b - y_S^{ab}\overline{\ell_{Ra}^c}\ell_{Rb}k^{++} - y_A^a\epsilon^{abc}k_a^+\overline{L_b^c}(i\sigma_2)L_c + \text{H.c.} \\
=& -\frac{1}{2}(2y_\Delta^{ab})\frac{v_\Delta+\delta_0+i\delta_1}{\sqrt{2}}\overline{\nu_a^c}\nu_b \\
&+\sqrt{2}y_\Delta^{ab}(U_{\rm PMNS})_{bi}\delta^+\overline{\ell_{La}^c}\nu_i + 2y_A^c\epsilon^{cab}(U_{\rm PMNS})_{bi}\overline{\ell_{La}^c}\nu_i k_c^+ \\
&+\frac{1}{2}(2y_\Delta^{ab})(c_\theta H_1^{++}+s_\theta H_2^{++})\overline{\ell_{La}^c}\ell_{Lb} - \frac{1}{2}(2y_S^{ab})(-s_\theta H_1^{++}+c_\theta H_2^{++})\overline{\ell_{Ra}^c}\ell_{Rb},
\end{aligned} \tag{3.1}$$

$$y_\Delta^{ab} = \begin{pmatrix} y_\Delta^{ee} & 0 & 0 \\ 0 & 0 & y_\Delta^{\mu\tau} \\ 0 & y_\Delta^{\mu\tau} & 0 \end{pmatrix},\ y_S^{ab} = \begin{pmatrix} y_S^{ee} & 0 & 0 \\ 0 & 0 & y_S^{\mu\tau} \\ 0 & y_S^{\mu\tau} & 0 \end{pmatrix},$$

$$\delta^{++} = c_\theta H_1^{++} + s_\theta H_2^{++},\ k^{++} = -s_\theta H_1^{++} + c_\theta H_2^{++},\ \nu_a = (U_{\rm PMNS})_{ai}\nu_i. \tag{3.2}$$

The term in (3.1) contributes neutrino mass as Type II seesaw, however, it can not explain neutrino oscillation data, because y_Δ is restricted by $\mathbb{Z}_3$ symmetry. y_Δ, y_A and y_S cause the neutrino mass as Zee-Babu models.

Scalar potential of ϕ (SM Higgs), Δ, k^{++} is shown as follows: [12]

$$\begin{aligned}
V[\phi,\Delta,k^{++}] =& \mu_\phi^2(\phi^\dagger\phi) + M_\Delta^2{\rm Tr}(\Delta^\dagger\Delta) + M_{k^{++}}^2|k^{++}|^2 + (M_{k^+}^2)_{ab}k_a^+k_b^- \\
&+[\mu_1\phi^{\rm T}(i\sigma_2)\Delta^\dagger\phi + \text{H.c.}] + [\mu_2 k^{++}{\rm Tr}(\Delta^\dagger\Delta^\dagger) + \text{H.c.}] \\
&+[\mu_{ab}k_a^+k_b^+k^{--} + \text{H.c.}] \\
&+\lambda(\phi^\dagger\phi)^2 + \lambda_1(\phi^\dagger\phi){\rm Tr}(\Delta^\dagger\Delta) + \lambda_2[{\rm Tr}(\Delta^\dagger\Delta)]^2 + \lambda_3{\rm Tr}[(\Delta^\dagger\Delta)^2] \\
&+\lambda_4\phi^\dagger\Delta\Delta^\dagger\phi + \lambda_5\phi^\dagger\phi|k^{++}|^2 + \lambda_6{\rm Tr}(\Delta^\dagger\Delta)|k^{++}|^2 \\
&+[\lambda_7\tilde{\phi}^\dagger\Delta\phi k^{--} + \text{H.c.}] + \lambda_8|k^{++}|^4 \\
&+\lambda_{9a}k_a^+k_a^-\phi^\dagger\phi + \lambda_{10a}k_a^+k_a^-{\rm Tr}\Delta^\dagger\Delta \\
&+\lambda_{11a}k_a^+k_a^-k^{++}k^{--} + [\lambda_{12e}k_e^+\phi^\dagger\Delta^\dagger\phi + \text{H.c.}] \\
&+[\lambda_{13abcd}k_a^+k_b^+k_c^-k_d^- + \text{H.c.}]
\end{aligned} \tag{3.3}$$

[12] μ_1 and λ_7 can be real value by redefinition of k^{++} and Δ.

We assume the couplings of scalar potential so that ϕ gets nonzero electro-weak VEV. When $\mu_1 \phi^{\mathrm{T}}(i\sigma_2)\Delta^\dagger \phi$ is nonzero, Δ obtains nonzero VEV. $\mu_{ab} k_a^+ k_b^+ k^{--}$ is $\mathbb{Z}_3$ soft breaking term, and it causes neutrino oscillation by Zee-Babu mass matrix. $\lambda_7 \tilde{\phi}^\dagger \Delta \phi k^{--}$ causes k^{++}-δ^{++} mixing, and it explains muon g-2 anomaly.

For simplicity, we assume the following condition:

$$M^2_{k^+ ab} = M^2_{k_a^+} \delta_{ab},\ \mu_1 = \mu_2 = 0, \tag{3.4}$$

$$\lambda_1 = \lambda_5 = \lambda_{9a} = \lambda_{10a} = \lambda_{11a} = \lambda_{12e} = \lambda_{13abcd} = 0. \tag{3.5}$$

We set $\mu_1 = 0$, therefore, the VEV of Δ becomes zero. Then, the scalar masses are given as follows

$$M^2_{\delta^+} = M^2_\Delta + \frac{\lambda_4 v_\phi^2}{4},\ M^2_{k_a^+} = M^2_{k_a^+}, \tag{3.6}$$

$$M^2_{H_1^{++}} = c_\theta^2 A - 2 s_\theta c_\theta C + s_\theta^2 B \tag{3.7}$$

$$M^2_{H_2^{++}} = s_\theta^2 A + 2 s_\theta c_\theta C + c_\theta^2 B, \tag{3.8}$$

$$A = M^2_\Delta,\ B = M^2_{k^{++}},\ C = \lambda_7 v_\phi^2/2, \tag{3.9}$$

$$\tan(2\theta) = -\frac{2C}{A-B},\ -\pi/4 \le \theta \le \pi/4. \tag{3.10}$$

Here, $H^{++}_{1,2}$ are defined as the mass eigenstates. θ is the mixing angle between δ^{++} and k^{++}. θ depends on the scalar coupling $\lambda_7 \tilde{\phi}^\dagger \Delta \phi k^{--}$. The BSM contribution of the muon g-2 has a strong dependence on θ (i.e. λ_7).

Next we evaluate the lepton g-2 and the lepton flavor violating (LFV) decay widths in type II seesaw model with k^{++}. When comparing the Yukawa couplings in Model I with one in §A.1.2:

$$\mathcal{L} \supset H_i^{++} \overline{\ell_a^C} (f_{iL}^{ab} P_L + f_{iR}^{ab} P_R) \ell_b + h_i^{aj} H_i^+ \overline{\ell_a^C} \nu_{Lj} + \text{H.c.}, \tag{3.11}$$

H_i^{++}, H_i^+, f_{iL}^{ab}, f_{iR}^{ab}, h_i^{aj} are given as follows:

$$H_i^{++} = \begin{pmatrix} H_1^{++} \\ H_2^{++} \end{pmatrix}_i,\ H_i^+ = \begin{pmatrix} H_1^+ \\ H_2^+ \\ H_3^+ \\ H_4^+ \end{pmatrix}_i = \begin{pmatrix} \delta^+ \\ k_e^+ \\ k_\mu^+ \\ k_\tau^+ \end{pmatrix}_i \tag{3.12}$$

$$h_i^{aj} = \begin{pmatrix} \sqrt{2} y_\Delta^{ab} & 2 y_A^e \epsilon^{eab} & 2 y_A^\mu \epsilon^{\mu ab} & 2 y_A^\tau \epsilon^{\tau ab} \end{pmatrix}_i (U_{\text{PMNS}})_{bj} \tag{3.13}$$

$$f_{iL}^{ab} = y_\Delta^{ab} \begin{pmatrix} c_\theta & s_\theta \end{pmatrix}_i,\ f_{iR}^{ab} = y_S^{ab} \begin{pmatrix} s_\theta & -c_\theta \end{pmatrix}_i. \tag{3.14}$$

In §A.1.2, we calculate muon g-2 and LFV processes, by using the Yukawa couplings in

(3.11). When using them, muon g-2 are shown as follows:

$$\Delta a_\mu^{H^+} \simeq -\frac{m_\mu^2}{3(4\pi)^2}\left(\frac{2|y_{A\tau}|^2}{M_{k_\tau^+}^2}+\frac{2|y_{Ae}|^2}{M_{k_e^+}^2}+\frac{|y_{\Delta\mu\tau}|^2}{M_{\delta^+}^2}\right) \quad (m_\ell \ll M_{H^+}),$$

$$\begin{aligned}\Delta a_\mu^{H^{++}} \simeq& -\frac{2m_\mu}{3(4\pi)^2}\left\{\frac{4m_\mu\left(|y_\Delta^{\mu\tau}|^2c_\theta^2+|y_S^{\mu\tau}|^2s_\theta^2\right)+m_\tau(y_\Delta^{\mu\tau}y_S^{\mu\tau *}+y_S^{\mu\tau}y_\Delta^{\mu\tau *})s_\theta c_\theta\left\{6\ln(M_{H_1^{++}}^2/m_\tau^2)-3\right\}}{M_{H_1^{++}}^2}\right.\\ &\left.+\frac{4m_\mu\left(|y_S^{\mu\tau}|^2c_\theta^2+|y_\Delta^{\mu\tau}|^2s_\theta^2\right)-m_\tau(y_\Delta^{\mu\tau}y_S^{\mu\tau *}+y_S^{\mu\tau}y_\Delta^{\mu\tau *})s_\theta c_\theta\left\{6\ln(M_{H_2^{++}}^2/m_\tau^2)-3\right\}}{M_{H_2^{++}}^2}\right\}\end{aligned} \tag{3.15}$$

$$\sim\frac{y_\Delta^{\mu\tau}y_S^{\mu\tau}s_\theta c_\theta m_\mu m_\tau \Delta M}{M_{H_1^{++}}^3\pi^2}\ln\frac{m_\tau^2}{M_{H_1^{++}}^2},\ \left(M_{H_2^{++}}-M_{H_1^{++}}=\Delta M,\text{ when } y_\Delta^{\mu\tau},y_S^{\mu\tau}\in\mathbb{R}\right) \tag{3.16}$$

Here, $\Delta a_\mu^{H^+}$ ($\Delta a_\mu^{H^{++}}$) are the contribution from singly (doubly) charged scalar, respectively. $\Delta a_\mu^{H^{++}}$ contains the large contribution with m_τ chirality flip. It depends on Yukawa couplings $y_\Delta^{\mu\tau}$ and $y_S^{\mu\tau}$, mass difference of doubly charged scalars ΔM, and the mixing angle θ. In order to explain muon g-2 anomaly, these Yukawa couplings, mixing angle (i.e. λ_7) and mass difference must be large. We will discuss these later.

The branching ratios of LFV process conserving $\mathbb{Z}_3$ symmetry ($\tau\to ee\overline{\mu}$, $\tau\to\mu\mu\overline{e}$) are given as follows:

$$\mathrm{Br}(\tau\to ee\overline{\mu})/\mathrm{Br}(\tau\to\mu\nu_\tau\overline{\nu_\mu}) \tag{3.17}$$

$$\begin{aligned}=&\frac{1}{4G_F^2}\left\{|y_S^{ee}|^2|y_S^{\mu\tau}|^2\left(\frac{s_\theta^2}{M_{H_1^{++}}^2}+\frac{c_\theta^2}{M_{H_2^{++}}^2}\right)^2+|y_\Delta^{ee}|^2|y_\Delta^{\mu\tau}|^2\left(\frac{c_\theta^2}{M_{H_1^{++}}^2}+\frac{s_\theta^2}{M_{H_2^{++}}^2}\right)^2\right.\\ &\left.+\left(|y_\Delta^{ee}|^2|y_S^{\mu\tau}|^2+|y_S^{ee}|^2|y_\Delta^{\mu\tau}|^2\right)s_\theta^2c_\theta^2\left(\frac{1}{M_{H_1^{++}}^2}-\frac{1}{M_{H_2^{++}}^2}\right)^2\right\},\end{aligned} \tag{3.18}$$

$$\mathrm{Br}(\tau\to\mu\mu\overline{e})/\mathrm{Br}(\tau\to\mu\nu_\tau\overline{\nu_\mu})=0. \tag{3.19}$$

In order to reduce $\mathrm{Br}(\tau\to ee\overline{\mu})/\mathrm{Br}(\tau\to\mu\nu_\tau\overline{\nu_\mu})$, we choose y_S^{ee} and y_Δ^{ee} as small (we choose these as $y_S^{ee}=0$, $y_\Delta^{ee}=0.001$ later).

Neutrino mass matrices are given as

$$(M_{\mathrm{II},\nu})_{ab}=\sqrt{2}y_S^{ab}v_\Delta \tag{3.20}$$

$$\begin{aligned}(M_{k,\nu})_{ab}=&-16(y_A^m\epsilon^{mca})m_{\ell_c}(y_S^\dagger)^{cd}m_{\ell_d}(y_A^n\epsilon^{ndb})\mu^{*mn}\\ &\times\left\{s_\theta^2I_5(m_m^+,m_{\ell_c},m_n^+,m_{\ell_d},m_1^{++})+c_\theta^2I_5(m_m^+,m_{\ell_c},m_n^+,m_{\ell_d},m_2^{++})\right\}\end{aligned} \tag{3.21}$$

$$\begin{aligned}(M_{\Delta,\nu})_{ab}=&16s_\theta c_\theta(y_A^m\epsilon^{mca})(y_\Delta^\dagger)_{cd}(y_A^n\epsilon^{ndb})\mu_{mn}^*\\ &\times\left\{J_5(m_m^+,m_{\ell_c},m_n^+,m_{\ell_d},m_1^{++})-J_5(m_m^+,m_{\ell_c},m_n^+,m_{\ell_d},m_2^{++})\right\}\end{aligned} \tag{3.22}$$

Here, I_5 and J_5 are defined as follows [13]

$$I_5(m_a, m_b, m_c, m_d, m_e) \tag{3.23}$$

$$\equiv(\tilde{\mathfrak{m}})^{-2\epsilon} \int \frac{d^D p}{(2\pi)^D} \frac{d^D q}{(2\pi)^D} \frac{1}{(p^2 - m_a^2)(p^2 - m_b^2)(q^2 - m_c^2)(q^2 - m_d^2)\{(p+q)^2 - m_e^2\}}, \tag{3.24}$$

$$J_5(m_a, m_b, m_c, m_d, m_e) \tag{3.25}$$

$$\equiv(\tilde{\mathfrak{m}})^{-2\epsilon} \int \frac{d^D p}{(2\pi)^D} \frac{d^D q}{(2\pi)^D} \frac{p \cdot q}{(p^2 - m_a^2)(p^2 - m_b^2)(q^2 - m_c^2)(q^2 - m_d^2)\{(p+q)^2 - m_e^2\}}. \tag{3.26}$$

The diagrams of $(M_{k,\nu})_{ab}$ and $(M_{\Delta,\nu})_{ab}$ are given in Figure 2 and Figure 3, respectively.

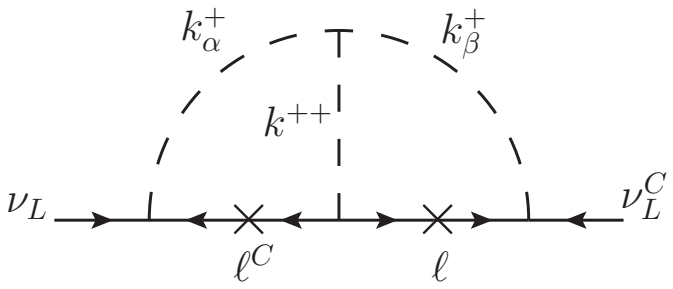

Figure 2: The diagram of neutrino mass $(M_{k,\nu})_{ab}$

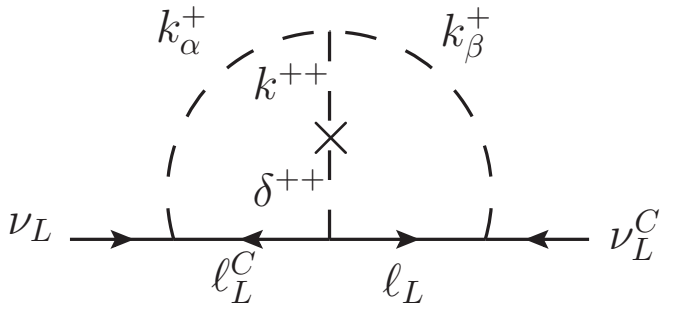

Figure 3: The diagram of neutrino mass $(M_{\Delta,\nu})_{ab}$

[13] Here, $\tilde{\mathfrak{m}}$ is 't Hooft cale. Please see §A.3 for a detail. The physical values do not depend on this.

We show the plots of $\Gamma(\tau \to ee\mu^c)/\Gamma(\tau \to e\nu_e^c\nu_\tau)$ vs $M_{H_2^{++}}$ in Figure 4 [14], λ_7 vs $M_{H_1^{++}}$ in Figure 5, and λ_7 vs $M_{H_2^{++}}$ in Figure 6. Here, we set parameters as:

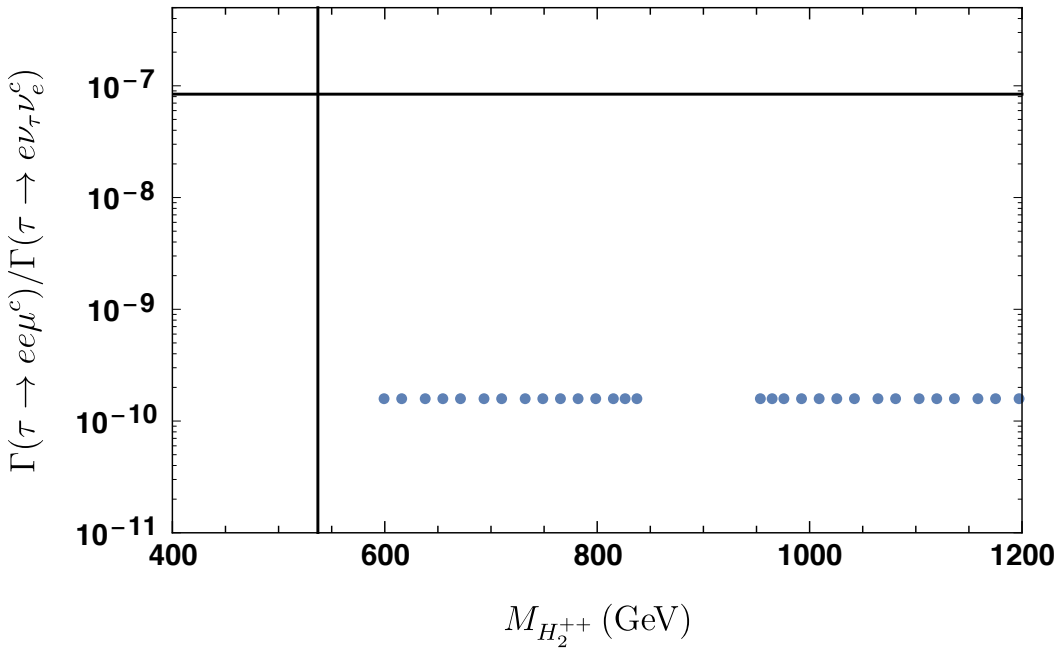

Figure 4: The plane of $\Gamma(\tau \to ee\mu^c)/\Gamma(\tau \to e\nu_e^c\nu_\tau)$ vs $M_{H_2^{++}}$. Both the muon g-2 anomaly and the neutrino mass matrix are explained at the blue points. The horizontal line is the experimental limit of $\Gamma(\tau \to ee\mu^c)/\Gamma(\tau \to e\nu_e^c\nu_\tau)$, and the vertical line is the CMS limit of $M_{H_2^{++}}$ (See §A.4).

$$y_S^{ee} = 0,\ y_S^{\mu\tau} = 1,\ y_\Delta^{ee} = 0.001,\ y_\Delta^{\mu\tau} = 0.2, \tag{3.27}$$

$$y_{Ae} = y_{A\mu} = y_{A\tau} = 0.1,\ \lambda_4 = 0.1,\ M_\Delta = 900\text{GeV}, \tag{3.28}$$

$$M_{k_e^+} = 2000\text{GeV},\ M_{k_\mu^+} = 2200\text{GeV},\ M_{k_\tau^+} = 2400\text{GeV},\ M_{k^{++}} = M_\Delta + \delta M. \tag{3.29}$$

We vary δM from -299 to 281 GeV, and choose λ_7 and μ^{ab} such that we can explain muon g-2 and neutrino mass matrix. Then LFV decay rate, muon g-2, $M_{H_1^{++}}$ and $M_{H_2^{++}}$ vary with δM.

In Figure 4, we can see that LFV constraint of $\Gamma(\tau \to ee\mu^c)$ can be avoided. The reason why we can avoid is we choose y_Δ^{ee} and y_S^{ee} as small.

In Figure 5 and 6, we can see that there is a parameter region where $\lambda_7 \sim O(1)$ and the CMS constraint on $M_{H_{1,2}}$: $M_{H_{1,2}^{++}} \gtrsim 537\text{GeV}$ (Please see §A.4). The constraints on doubly charged scalars is very crucial. In our models, doubly charged scalars mainly decay to $\mu^+\tau^+$ channel. Our model will be tested by this channel in future experiments.

[14] $\tau \to \mu\mu e^c$ does not occur in Model I.

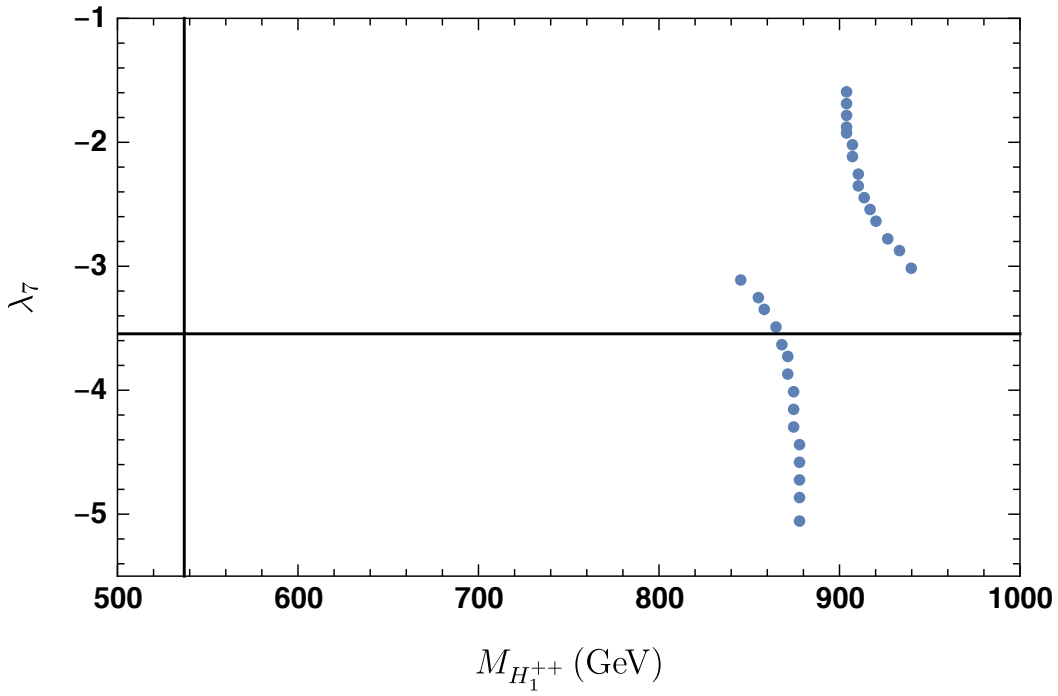

Figure 5: The plane of λ_7 vs $M_{H_1^{++}}$. Both the muon g-2 anomaly and the neutrino mass matrix are explained at the blue points. The horizontal line is $|\lambda_7| < \sqrt{4\pi}$ (perturbativity constraint), and the vertical line is the CMS limit of $M_{H_2^{++}}$ (See §A.4).

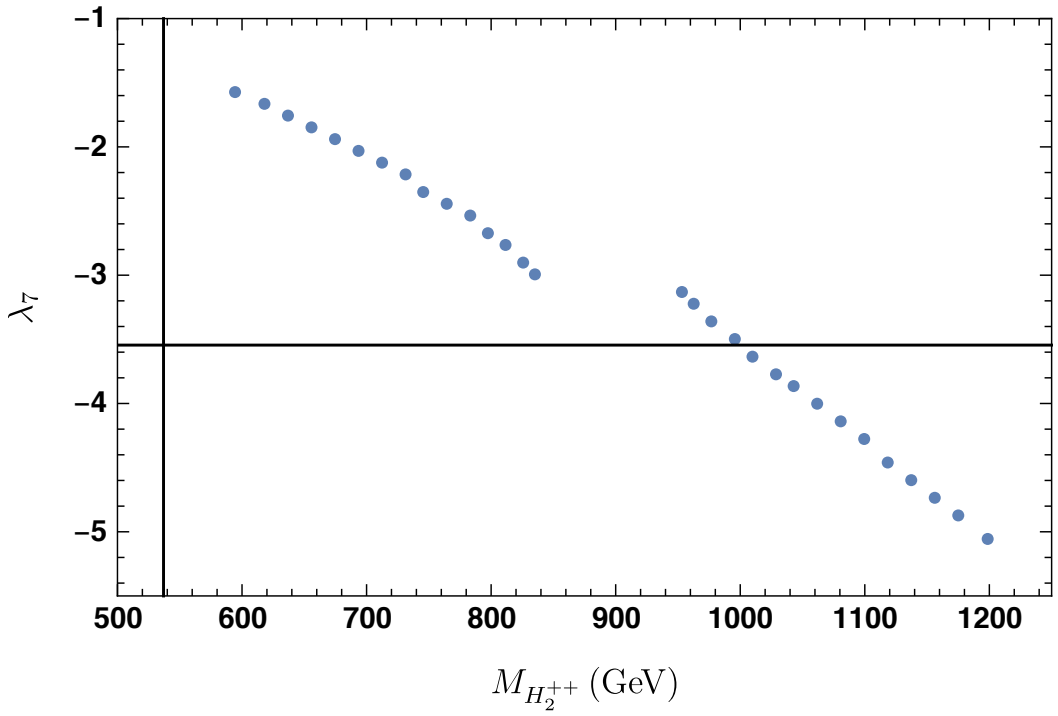

Figure 6: The plane of λ_7 vs $M_{H_2^{++}}$. Both the muon g-2 anomaly and the neutrino mass matrix are explained at the blue points. The horizontal line is $|\lambda_7| < \sqrt{4\pi}$ (perturbativity constraint), and the vertical line is the CMS limit of $M_{H_2^{++}}$ (See §A.4).

4 Model II

In this section, we explain Model II. Model II contains the particles listed in Table 2. k^{++} and Δ_e give the positive contribution to muon g-2. Only with k^{++} and Δ_e, neutrino

	$SU(3)_C$	$SU(2)_L$	$U(1)_Y$	$\mathbb{Z}_3$
k^{++}	**1**	**1**	2	1
Δ_e	**1**	**3**	1	1
Δ_μ	**1**	**3**	1	ω
Δ_τ	**1**	**3**	1	$\overline{\omega}$

Table 2: Field contents in Model II

oscillation can not be explained due to $\mathbb{Z}_3$ symmetry. We introduce Δ_a ($a = \mu, \tau$), then, neutrino oscillation can be done.

The scalar potential of ϕ, Δ_a and k^{++} is given as follows:

$$\begin{aligned} V[\phi, \Delta_a, k^{++}] =& \mu_\phi^2(\phi^\dagger\phi) + (M_{\Delta_a}^2)\mathrm{Tr}(\Delta_a^\dagger\Delta_a) + M_k^2|k^{++}|^2 \\ &+ [\mu_a\phi^{\mathrm{T}}(i\sigma_2)\Delta_a^\dagger\phi + \mathrm{H.c.}] + [\mu_{2a}k^{--}\mathrm{Tr}(\Delta_a\Delta_a) + \mathrm{H.c.}] \\ &+ \lambda(\phi^\dagger\phi)^2 + \lambda_{1a}(\phi^\dagger\phi)\mathrm{Tr}(\Delta_a^\dagger\Delta_a) \\ &+ [\lambda_{2abcd}\mathrm{Tr}(\Delta_a^\dagger\Delta_b)\mathrm{Tr}(\Delta_c^\dagger\Delta_d) + \mathrm{H.c.}] \\ &+ [\lambda_{3abcd}\mathrm{Tr}(\Delta_a^\dagger\Delta_b\Delta_c^\dagger\Delta_d) + \mathrm{H.c.}] \\ &+ \lambda_{4a}\phi^\dagger\Delta_a\Delta_a^\dagger\phi + \lambda_5\phi^\dagger\phi|k^{++}|^2 + \lambda_{6a}\mathrm{Tr}(\Delta_a^\dagger\Delta_a)|k^{++}|^2 \\ &+ \lambda_7[\tilde{\phi}^\dagger\Delta_e\phi k^{--} + \mathrm{H.c.}] + \lambda_8|k^{++}|^4. \end{aligned} \tag{4.1}$$

We assume the couplings of scalar potential so that ϕ gets nonzero electro-weak VEV. Furthermore, $M_{\Delta_a}^2$ and μ_{2a} are assumed to be diagonal. $\mathbb{Z}_3$ is softly broken by μ_a. When $\mu_a\phi^{\mathrm{T}}(i\sigma_2)\Delta_a^\dagger\phi$ is nonzero, Δ_a obtains nonzero VEV. Then, neutrino gains Majorana mass terms as type II seesaw model. By redefinition of k^{++}, λ_7 can be real. $\lambda_7\tilde{\phi}^\dagger\Delta_e\phi k^{--}$ causes k^{++}-δ^{++} mixing, and it explains muon g-2 anomaly.

After EWSB, Δ_a gain nonzero VEV: [15]

$$\delta_a^0 = \frac{1}{\sqrt{2}}(v_{a\Delta} + h_{2a} + i\eta_{2a}),\ v_{a\Delta} = \frac{\mu_a v_\phi^2}{\sqrt{2}M_{\Delta_a}^2} \tag{4.2}$$

We assume $v_\Delta \ll v_\phi$, then, the mixing angle between ϕ and Δ becomes tiny. We ignore this effect.

[15] $\Delta_a = \begin{pmatrix} \delta_a^+/\sqrt{2} & \delta_a^{++} \\ (v_{a\Delta} + \delta_{a0} + i\delta_{a1})/\sqrt{2} & -\delta_a^+/\sqrt{2} \end{pmatrix}$

Masses of scalar fields are

$$M^2_{H^+_1} = \big(M^2_{\Delta_e} + \lambda_{1e}v^2/2 + \lambda_{4e}v^2/4\big), \tag{4.3}$$
$$M^2_{H^+_2} = \big(M^2_{\Delta_\mu} + \lambda_{1\mu}v^2/2 + \lambda_{4\mu}v^2/4\big), \tag{4.4}$$
$$M^2_{H^+_3} = \big(M^2_{\Delta_\tau} + \lambda_{1\tau}v^2/2 + \lambda_{4\tau}v^2/4\big), \tag{4.5}$$
$$M^2_{H^{++}_{11}} = c^2_\theta A - 2s_\theta c_\theta C + s^2_\theta B,\ M^2_{H^{++}_{12}} = M^2_{\Delta_\mu} + \lambda_{1\mu}v^2/2, \tag{4.6}$$
$$M^2_{H^{++}_{13}} = M^2_{\Delta_\tau} + \lambda_{1\tau}v^2/2,\ M^2_{H^{++}_2} = s^2_\theta A + 2s_\theta c_\theta C + c^2_\theta B, \tag{4.7}$$
$$A = M^2_{\Delta_e} + \lambda_{1e}v^2/2,\ B = M^2_k + \lambda_5 v^2/2,\ C = \lambda_7 v^2/2, \tag{4.8}$$
$$\delta^{++}_e = c_\theta H^{++}_{11} + s_\theta H^{++}_2,\ \delta^{++}_\mu = H^{++}_{12},\ \delta^{++}_\tau = H^{++}_{13}, \tag{4.9}$$
$$k^{++} = -s_\theta H^{++}_{11} + c_\theta H^{++}_2, H^+_a = \delta^+_a, \tag{4.10}$$
$$\tan(2\theta) = -\frac{2C}{A-B},\ (-\pi/4 \le \theta \le \pi/4). \tag{4.11}$$

Here, $H^+_{1,2,3}$ are the mass eigenstates of singly charged scalar fields. When $v_{\Delta_a} \ll v_\phi$, these are same as singly charged scalars in Δ_a: $H^+_1 \simeq \delta^+_e$, $H^+_2 \simeq \delta^+_\mu$ and $H^+_3 \simeq \delta^+_\tau$. $H_{11,12,13,2}$ are the mass eigenstates of doubly charged scalar fields. When $v_{\Delta_a} \ll v_\phi$, $H^{++}_{12} \simeq \delta^{++}_\mu$ and $H^{++}_{13} \simeq \delta^{++}_\tau$. δ^{++}_e and k^{++} mix with the mixing angle θ. θ depends on the coupling $\lambda_7 \tilde{\phi}^\dagger \Delta_e \phi k^{--}$.

The Yukawa couplings in Model II are given as follows:

$$\mathcal{L}_{\rm Yuk} = -Y^{ab}_c \overline{L^c_a}(i\sigma_2)\Delta_c L_b - \frac{1}{2}(2y^{ab}_S)\overline{\ell^c_{Ra}}\ell_{Rb}k^{++} + \text{H.c.} \tag{4.12}$$
$$= -\frac{1}{2}(2Y^{ab}_c)\left(\frac{v_{c\Delta} + \delta_{c0} + i\delta_{c1}}{\sqrt{2}}\overline{\nu^c_a}\nu_b - \sqrt{2}\delta^+_c\overline{\ell^c_{La}}\nu_b - \delta^{++}_c\overline{\ell^c_{La}}\ell_{Lb}\right) \tag{4.13}$$
$$- y^{ab}_S\overline{\ell^c_{Ra}}\ell_{Rb}k^{++} + \text{H.c.} \tag{4.14}$$
$$= -\frac{1}{2}(2Y^{ab}_c)\frac{v_{c\Delta} + \delta_{c0} + i\delta_{c1}}{\sqrt{2}}\overline{\nu^c_{La}}\nu_{Lb} + \sqrt{2}Y^{ab}_c\delta_{ic}H^+_i(U_{\rm PMNS})_{bj}\overline{\ell^c_{La}}\nu_{Lj}$$
$$+ Y^{ab}_c \begin{pmatrix} c_\theta & 0 & 0 & s_\theta \\ 0 & 1 & 0 & 0 \\ 0 & 0 & 1 & 0 \end{pmatrix}_{ci} \begin{pmatrix} H^{++}_{11} \\ H^{++}_{12} \\ H^{++}_{13} \\ H^{++}_2 \end{pmatrix}_i \overline{\ell^c_a}P_L\ell_b - y^{ab}_S(-s_\theta H^{++}_{11} + c_\theta H^{++}_2)\overline{\ell^c_a}P_R\ell_b. \tag{4.15}$$

Here, Yukawa couplings are restricted by the discrete lepton flavor symmetry $\mathbb{Z}_3$:

$$y_S^{ab} = \begin{pmatrix} y_S^{ee} & 0 & 0 \\ 0 & 0 & y_S^{\mu\tau} \\ 0 & y_S^{\mu\tau} & 0 \end{pmatrix}_{ab}, \; Y_e^{ab} = \begin{pmatrix} y_\Delta^{ee} & 0 & 0 \\ 0 & 0 & y_\Delta^{\mu\tau} \\ 0 & y_\Delta^{\mu\tau} & 0 \end{pmatrix}_{ab}, \tag{4.16}$$

$$Y_\mu^{ab} = \begin{pmatrix} 0 & 0 & y_\Delta^{e\tau} \\ 0 & y_\Delta^{\mu\mu} & 0 \\ y_\Delta^{e\tau} & 0 & 0 \end{pmatrix}_{ab}, \; Y_\tau^{ab} = \begin{pmatrix} 0 & y_\Delta^{e\mu} & 0 \\ y_\Delta^{e\mu} & 0 & 0 \\ 0 & 0 & y_\Delta^{\tau\tau} \end{pmatrix}_{ab}. \tag{4.17}$$

The first term in (4.15) gives the neutrino Majorana mass. The other terms in (4.15) give the contributions to muon g-2. H_{11}^{++} and H_2^{++} couple both the left-handed leptons and the right-handed ones. Therefore, the contributions from $H_{11,2}^{++}$ to the muon g-2 can be positive.

When comparing the Yukawa couplings in Model II with the ones in §A.1.2:

$$\mathcal{L} \supset H_i^{++}\overline{\ell_a^C}(f_{iL}^{ab}P_L + f_{iR}^{ab}P_R)\ell_b + h_i^{aj}H_i^+\overline{\ell_a^C}\nu_{Lj} + \text{H.c.}, \tag{4.18}$$

H_i^{++}, H_i^+, f_{iL}^{ab}, f_{iR}^{ab}, h_i^{aj} are given as follows:

$$H_i^{++} = \begin{pmatrix} H_{11}^{++} \\ H_{12}^{++} \\ H_{13}^{++} \\ H_2^{++} \end{pmatrix}_i, \; H_i^+ = \begin{pmatrix} H_1^+ \\ H_2^+ \\ H_3^+ \end{pmatrix}_i, \; f_{iL}^{ab} = Y_c^{ab} \begin{pmatrix} c_\theta & 0 & 0 & s_\theta \\ 0 & 1 & 0 & 0 \\ 0 & 0 & 1 & 0 \end{pmatrix}_{ci}, \tag{4.19}$$

$$f_{iR}^{ab} = -\, y_S^{ab} \begin{pmatrix} -s_\theta & 0 & 0 & c_\theta \end{pmatrix}_i, \; h_i^{aj} = \sqrt{2}Y_i^{ab}\delta_{ic}(U_{\text{PMNS}})_{bj}. \tag{4.20}$$

In §A.1.2, we calculate muon g-2 and LFV processes. When using them, Δa_μ, $\Gamma(\tau \to$

$ee\mu^c)/\Gamma(\tau \to e\nu_e^c\nu_\tau)$ and $\Gamma(\tau \to \mu\mu e^c)/\Gamma(\tau \to e\nu_e^c\nu_\tau)$ are shown as follows:

$$\Delta a_\mu = \Delta a_\mu^{H^+} + \Delta a_\mu^{H^{++}}, \tag{4.21}$$

$$\Delta a_\mu^{H^+} = -\frac{m_\mu^2}{3(4\pi)^2}\Big(\frac{|y_\Delta^{e\mu}|^2}{M_{H_3^+}^2} + \frac{|y_\Delta^{\mu\mu}|^2}{M_{H_2^+}^2} + \frac{|y_\Delta^{\mu\tau}|^2}{M_{H_1^+}^2}\Big), \tag{4.22}$$

$$\begin{aligned}\Delta a_\mu^{H^{++}} =& -\frac{m_\mu^2}{24\pi^2}\Bigg\{\frac{1}{M_{11}^2}\Big[4|y_\Delta^{\mu\tau}|^2 c_\theta^2 - 3(y_\Delta^{\mu\tau}y_S^{*\mu\tau} + y_S^{\mu\tau}y_\Delta^{*\mu\tau})s_\theta c_\theta \\ &\times (m_\tau/m_\mu)\big[1 - 2\ln(M_{H_{11}^{++}}^2/m_\tau^2)\big] + 4|y_S^{\mu\nu}|^2 s_\theta^2\Big] + \frac{4|y_\Delta^{e\mu}|^2}{M_{13}^2} + \frac{4|y_\Delta^{\mu\mu}|^2}{M_{12}^2} \\ &+ \frac{1}{M_{H_2^{++}}^2}\Big[4|y_\Delta^{\mu\tau}|^2 s_\theta^2 + 3(y_\Delta^{\mu\tau}y_S^{*\mu\tau} + y_S^{\mu\tau}y_\Delta^{*\mu\tau})s_\theta c_\theta \\ &\times (m_\tau/m_\mu)\big[1 - 2\ln(M_{H_2^{++}}^2/m_\tau^2)\big] + 4|y_S^{\mu\nu}|^2 c_\theta^2\Big]\Bigg\},\end{aligned} \tag{4.23}$$

$$\begin{aligned}\frac{\Gamma(\tau \to ee\mu^c)}{\Gamma(\tau \to e\nu_e^c\nu_\tau)} =& \frac{1}{4G_F^2(M_{H_{11}^{++}})^4(M_{H_2^{++}})^4}\Bigg\{|y_\Delta^{ee}|^2\Big[|y_\Delta^{\mu\tau}|^2(s_\theta^2 M_{H_{11}^{++}}^2 + c_\theta^2 M_{H_2^{++}}^2)^2 \\ &+ |y_S^{\mu\tau}|^2 c_\theta^2 s_\theta^2 (M_{H_{11}^{++}}^2 - M_{H_2^{++}}^2)^2\Big] + |y_S^{ee}|^2\Big[|y_S^{\mu\tau}|^2(c_\theta^2 M_{H_{11}^{++}}^2 + s_\theta^2 M_{H_2^{++}}^2)^2 \\ &+ |y_\Delta^{\mu\tau}|^2 c_\theta^2 s_\theta^2 (M_{H_{11}^{++}}^2 - M_{H_2^{++}}^2)^2\Big]\Bigg\},\end{aligned} \tag{4.24}$$

$$\frac{\Gamma(\tau \to \mu\mu e^c)}{\Gamma(\tau \to e\nu_e^c\nu_\tau)} = \frac{|y_\Delta^{e\tau}|^2|y_\Delta^{\mu\mu}|^2}{4G_F^2 M_{H_{12}^{++}}^4}. \tag{4.25}$$

We can see that $\Delta a_\mu^{H^+}$ has negative values. On the other hands, $\Delta a_\mu^{H^{++}}$ contains the terms proportional to $(m_\tau/m_\mu)(y_\Delta^{\mu\tau}y_S^{*\mu\tau} + y_S^{\mu\tau}y_\Delta^{*\mu\tau})$. They can be large positive value, therefore, the muon g-2 anomaly can be explained.

The decay width of $\Gamma(\tau \to \mu\mu e^c)$ can be much smaller than LFV experimental limit, by choosing $y_\Delta^{\mu\mu}$ and $y_\Delta^{e\tau}$ as small. We will do this later by choosing $v_{\mu\Delta}$ as $O(10^{-6})$ GeV. $\Gamma(\tau \to ee\mu^c)$ depends on $y_{\Delta,S}^{ee}$ and $y_{\Delta,S}^{\mu\tau}$. They can not be chosen as tiny, when explaining both muon g-2 anomaly and neutrino oscillation. Therefore, the constraint on $\Gamma(\tau \to ee\mu^c)$ is important.

We show the planes of $\Gamma(\tau \to ee\mu^c)/\Gamma(\tau \to e\nu_e^c\nu_\tau)$ vs $M_{H_2^{++}}$ in Figure 7, $\Gamma(\tau \to \mu\mu e^c)/\Gamma(\tau \to e\nu_e^c\nu_\tau)$ vs $M_{H_2^{++}}$ in Figure 8, λ_7 vs $M_{H_{11}^{++}}$ in Figure 9, and λ_7 vs $M_{H_2^{++}}$ in Figure 10.

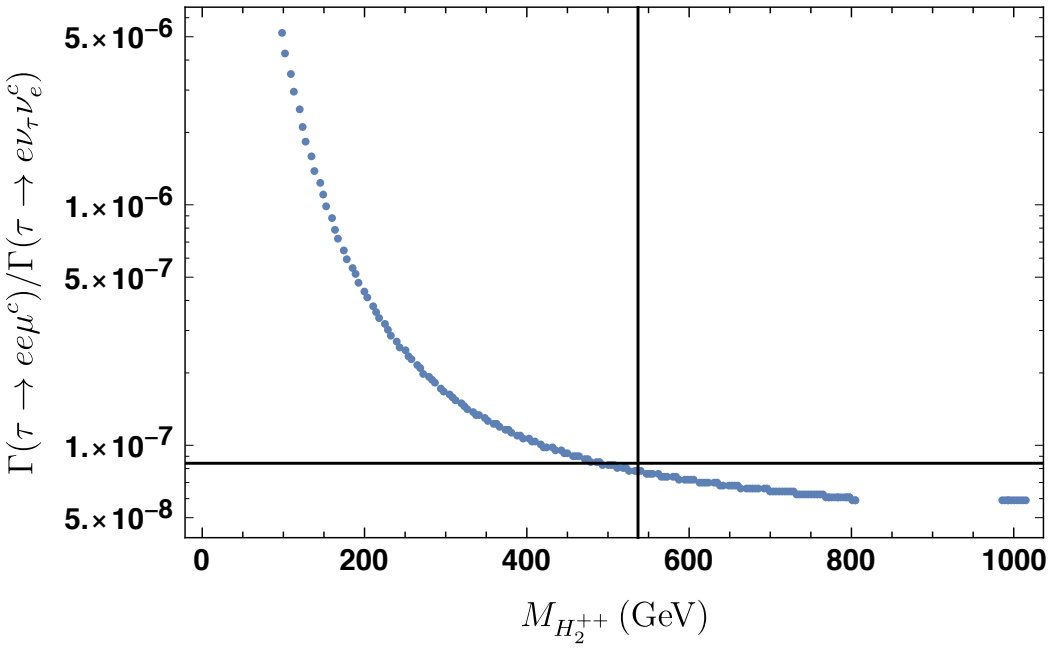

Figure 7: The plane of $\Gamma(\tau \to ee\mu^c)/\Gamma(\tau \to e\nu_e^c\nu_\tau)$ vs $M_{H_2^{++}}$. Both the muon g-2 anomaly and the neutrino mass matrix are explained at the blue points. The horizontal line is the experimental limit of $\Gamma(\tau \to ee\mu^c)/\Gamma(\tau \to e\nu_e^c\nu_\tau)$, and the vertical line is the CMS limit of $M_{H_2^{++}}$ (See §A.4).

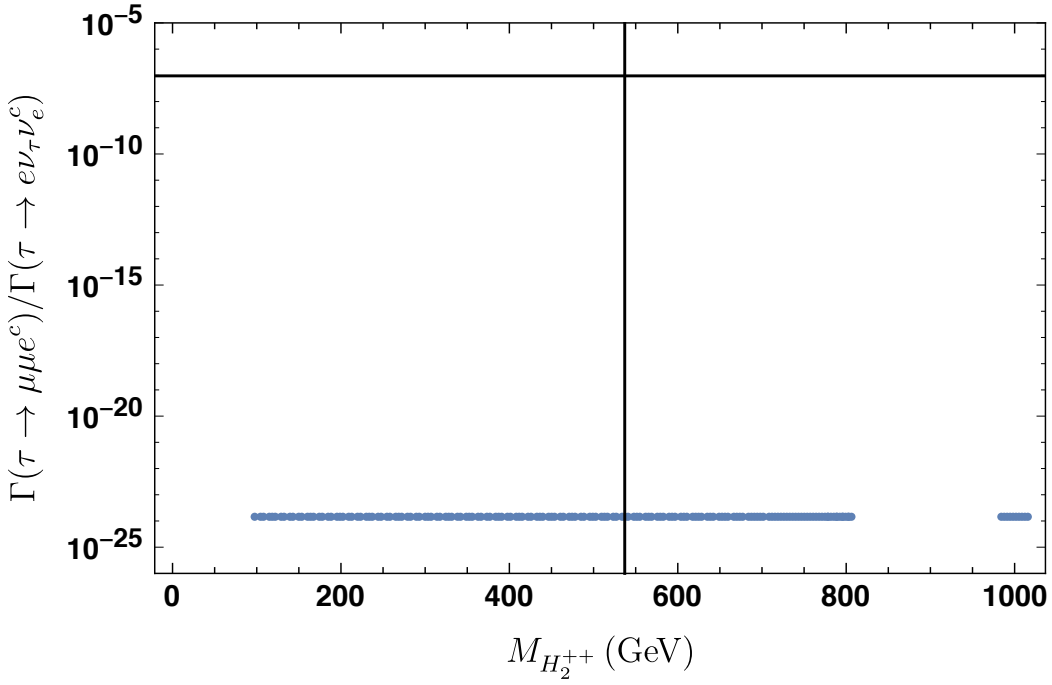

Figure 8: The plane of $\Gamma(\tau \to \mu\mu e^c)/\Gamma(\tau \to e\nu_e^c\nu_\tau)$ vs $M_{H_2^{++}}$. Both the muon g-2 anomaly and the neutrino mass matrix are explained at the blue points. The horizontal line is the experimental limit of $\Gamma(\tau \to \mu\mu e^c)/\Gamma(\tau \to e\nu_e^c\nu_\tau)$, and the vertical line is the CMS limit of $M_{H_2^{++}}$ (See §A.4).

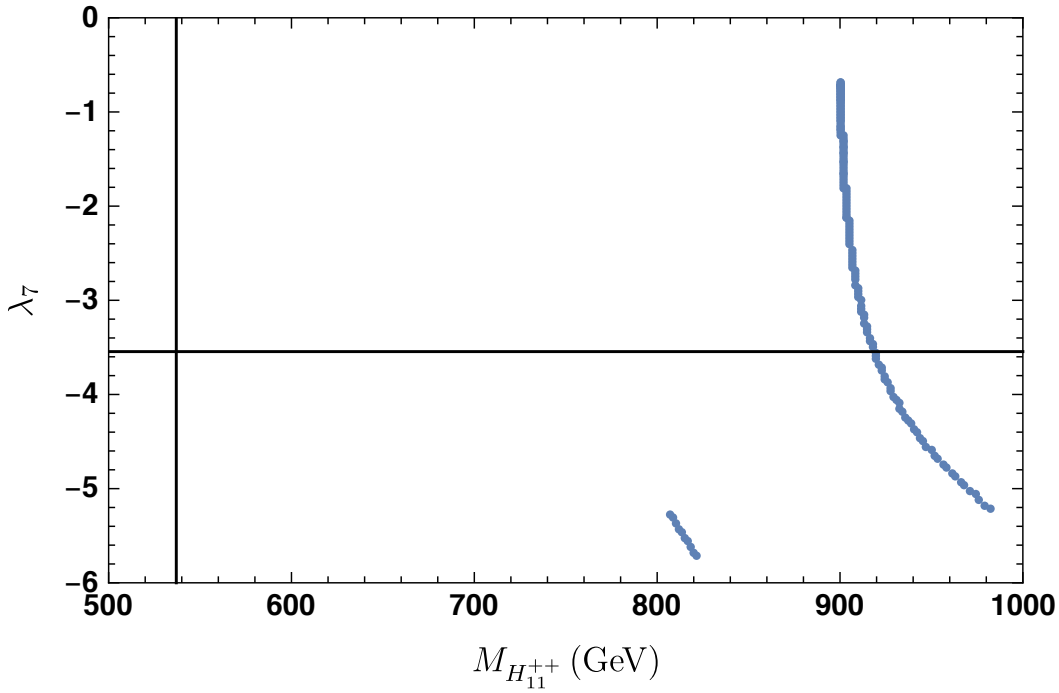

Figure 9: The plane of λ_7 vs $M_{H_{11}^{++}}$. Both the muon g-2 anomaly and the neutrino mass matrix are explained at the blue points. The horizontal line is $|\lambda_7| < \sqrt{4\pi}$ (perturbativity constraint), and the vertical line is the CMS limit of $M_{H_2^{++}}$ (See §A.4).

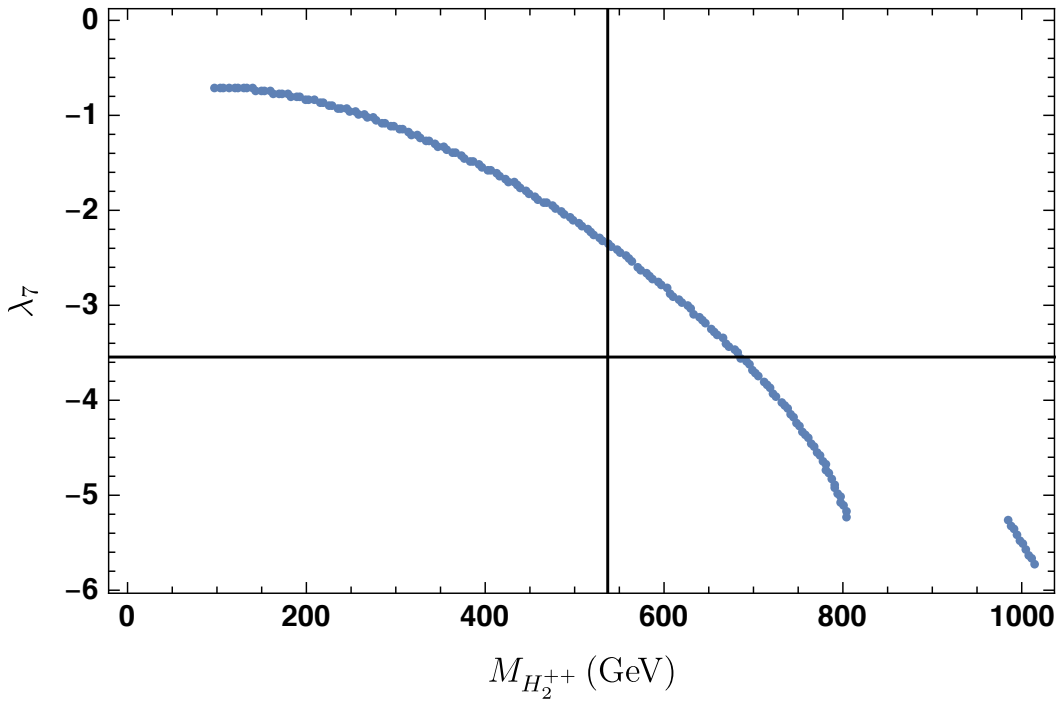

Figure 10: The plane of λ_7 vs $M_{H_2^{++}}$. Both the muon g-2 anomaly and the neutrino mass matrix are explained at the blue points. The horizontal line is $|\lambda_7| < \sqrt{4\pi}$ (perturbativity constraint), and the vertical line is the CMS limit of $M_{H_2^{++}}$ (See §A.4).

Here, we set parameters as:

$$\begin{aligned} y_S^{ee} =& 0,\ y_S^{\mu\tau} = 1, \\ v_{e\Delta} =& 1.3 \times 10^{-10}\text{GeV}, v_{\mu\Delta} = 1.0 \times 10^{-6}\text{GeV},\ v_{\tau\Delta} = 1.0 \times 10^{-6}\text{GeV}, \\ \lambda_{1e} =& 0,\ \lambda_{1\mu} = 0.2,\ \lambda_{1\tau} = 0.4,\ \lambda_{4e} = 0.1,\ \lambda_{4\mu} = 0.3,\ \lambda_{4\tau} = 0.5,\ \lambda_5 = 0, \\ M_{\Delta_e} =& 900\text{GeV},\ M_{\Delta_\mu} = 2000\text{GeV},\ M_{\Delta_\tau} = 2500\text{GeV},\ M_{k^{++}} = M_{\Delta_e} + \delta M. \end{aligned} \tag{4.26}$$

We vary δM from -799 to 46 GeV, and choose λ_7 and y_Δ^{ab} such that we can explain muon g-2 and neutrino mass matrix. Then LFV decay rate, muon g-2, $M_{H_1^{++}}$ and $M_{H_2^{++}}$ vary with δM.

In Figure 7 and 8, we can see that LFV constraint can be avoided. The constraint on $\tau \to ee\mu^c$ is crucial as Figure 7. It is because $y_{\Delta,S}^{ee}$ and $y_{\Delta,S}^{\mu\tau}$ can not be chosen as tiny. The constraint on $\tau \to \mu\mu e^c$ is not crucial as Figure 8, because we can choose $y_\Delta^{e\tau}$ and $y_\Delta^{\mu\mu}$ as small.

In Figure 9 and 10, we can see that there is a parameter region where $\lambda_7 \sim O(1)$ and $M_{H_{11,2}^{++}} \gtrsim 537\text{GeV}$. The constraints on doubly charged scalars are very crucial. In our models, doubly charged scalars mainly decay to $\mu^+\tau^+$ channel. Our model will be tested by this channel in future experiments.

5 Summary of Part II

We can construct the models which can explain both the neutrino oscillation and the muon g-2 anomaly. In these models, we introduce double charged scalar k^{++} into Type II seesaw model, to explain the muon g-2 anomaly. Furthermore, we must impose the discrete lepton flavor symmetry Z_3 to avoid LFV constraints. Then, there are parametric regions, in which the LFV constraints and the CMS constraints on double charged scalars can be avoided and $\lambda_7 \sim O(1)$. Our model will be tested by muon g-2 experiments, LFV constraints and the decays from doubly charged scalars to $\mu^+ + \tau^+$.

Part III
The TeV scale Majoron dark matter

6 The relationship between the neutrino oscillation and the dark matter

In this part, we consider the relationship between neutrino oscillation and the dark matter. There are radiative seesaw models with dark matters; KNT model [49], the scotogenic model [50] and etc. In these models, dark matter is stabilized by extra $\mathbb{Z}_2$ symmetry. Majoron models can also explain both neutrino oscillation and the observed dark matter relic density. We focus on the Majoron dark matter in this Part.

We review the previous works about Majoron dark matter lighter than TeV scale in §6.1. In §6.2, we show that TeV scale Majoron dark matter is interesting, because it can be detected by the cosmic ray experiments.

6.1 The Majoron dark matter lighter than TeV scale

Neutrino oscillations are detected by experiments using solar [7–17], atmospheric [19–21], reactor [23–29] and accelerator [30–35] neutrinos. There are two methods to explain them. One is Dirac mass method, and the other is Majorana mass method. In the Majorana mass method, the following dimension-5 operator is generated by integrating out heavy particles

$$\mathcal{L}_{\text{eff}} \supset -\frac{1}{\Lambda}\overline{L^c}H\tilde{H}^\dagger L + \text{H.c.} \tag{6.1}$$

This term breaks the lepton number symmetry. Majoron models [51, 52] is well known models which explain the origin of lepton number symmetry breaking. In Majoron models, this breaking is identified as the VEV of complex scalar. Majoron is the pseudo NG boson of the lepton symmetry breaking.

Particle contents of the Majoron model are shown in Table 3. Yukawa couplings of

field	$SU(2)_L$	$U(1)_Y$	$U(1)_{B-L}$
L_α (SM doublet lepton)	**2**	$-\frac{1}{2}$	-1
$e^c_{R\alpha}$ (SM singlet lepton)	**1**	$+1$	$+1$
H (SM Higgs)	**2**	$\frac{1}{2}$	0
ν^c_{Ri}	**1**	0	-1
Φ	**1**	0	$+2$

Table 3: field contents

the Majoron models are given as:

$$\mathcal{L} \supset -\frac{f_{ij}}{2}\Phi\overline{\nu^c_{Ri}}\nu_{Rj} - y^\nu_{\alpha i}\overline{L_\alpha}\tilde{H}\nu_{Ri} + \text{H.c.} \tag{6.2}$$

Here, f_{ij} can be real diagonal by redefinition of ν_{iR}. After $\langle\Phi\rangle = \frac{v_\phi}{\sqrt{2}}$, the Lagrangian becomes as: [16]

$$\mathcal{L} = -\frac{M_{N_i}}{2}\overline{N_i}N_i - \frac{f_i}{2\sqrt{2}}\left(\phi\overline{N_i}N_i + i\chi\overline{N_i}\gamma_5 N_i\right) \tag{6.3}$$

$$-\left(y^\nu_{\alpha i}\overline{L_\alpha}\tilde{H}P_R N_i + \text{H.c.}\right) \tag{6.4}$$

$$N_i = \nu_{Ri} + \nu^c_{Ri},\ \Phi = \frac{1}{\sqrt{2}}(v_\phi + \phi + i\chi),\ M_{N_i} = \frac{f_{ij}v_\phi}{\sqrt{2}}. \tag{6.5}$$

Then, N gets Majorana masses, therefore, after integrating out N, we can explain neutrino oscillation. χ is a pseudo NG boson of the lepton number symmetry breaking, and it is called as Majoron.

There are a lot of papers which identify "GeV scale or lighter" Majoron as dark matter. When Majoron is dark matter, Majoron must have non-zero mass. We can give the explicit Majoron mass [121, 122] or the one from quantum gravity [123–125]. In [121, 122, 126–131], the phenomenology of Majoron DM is discussed. The recent constraints on Majoron DM are given in [132,133]. The constraints by indirect detections are given in [132] (see Figure 11 and 12), and the ones by Majoron emission processes in [133] (see Figure 13). The production of Majoron dark matter is discussed in [122]. In [122], Freeze-in mechanism [134] is used for the production.

As above, a lot of papers of "GeV scale or lighter" Majoron dark matter exist. On the other hand, there are anomalous results in the positron fraction (flux of e^+/flux of $e^+ + e^-$) detected by the cosmic ray experiments. This can be explained by "TeV" scale Majoron dark matter. We explain them in next section.

[16] Φ's VEV can be real by redefinition of Φ. Then, $f_{ij}v_\phi$ becomes real diagonal matrix.

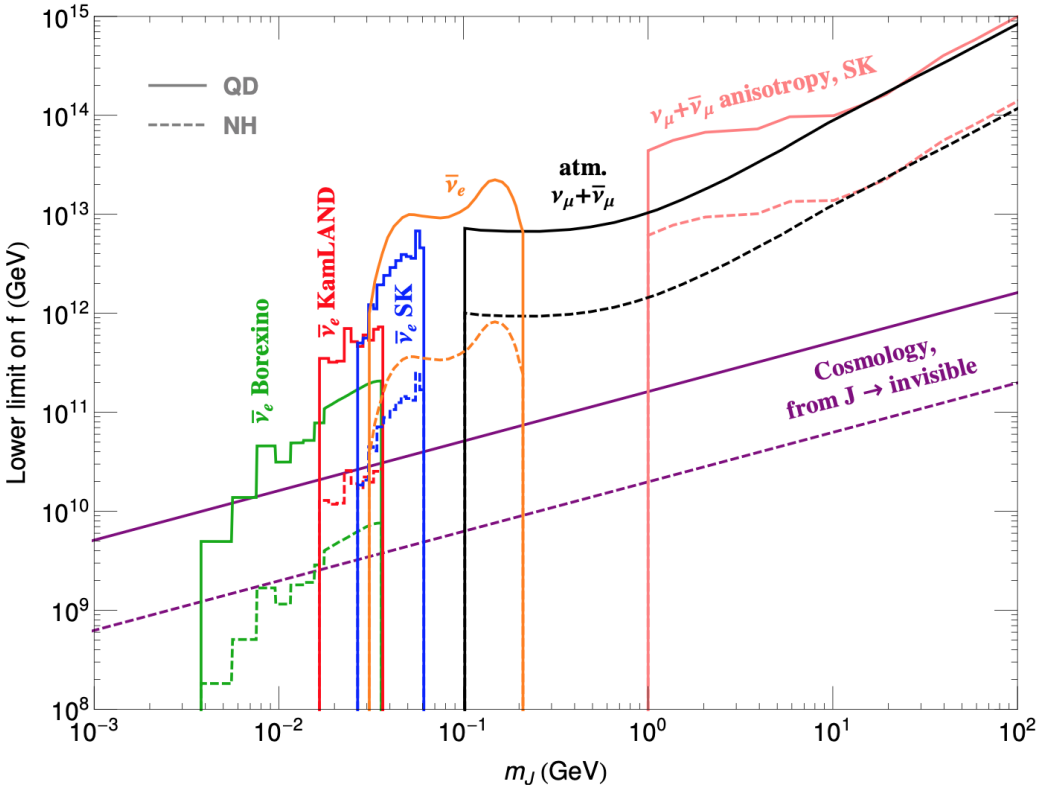

Figure 11: The experimental bounds from the $J \to \nu\nu$ processes [132]. Here, J is Majoron, and f is lepton number breaking scale (it is the same as v_ϕ).

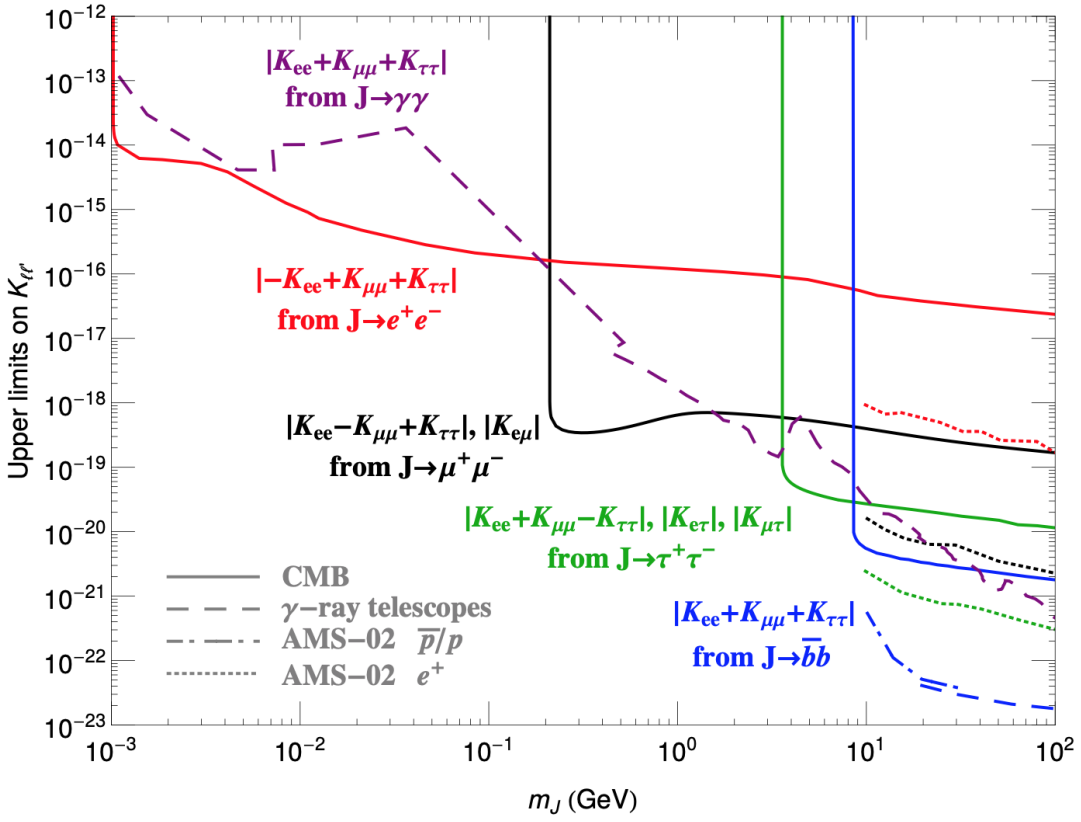

Figure 12: The experimental bounds from DM indirect detections [132]. Here, K is defined as $K_{ab} = y_{ai}y^*_{bi}v_h/(2v_\phi)$, $\langle H\rangle = (0,\, v_h/\sqrt{2})^{\rm T}$.

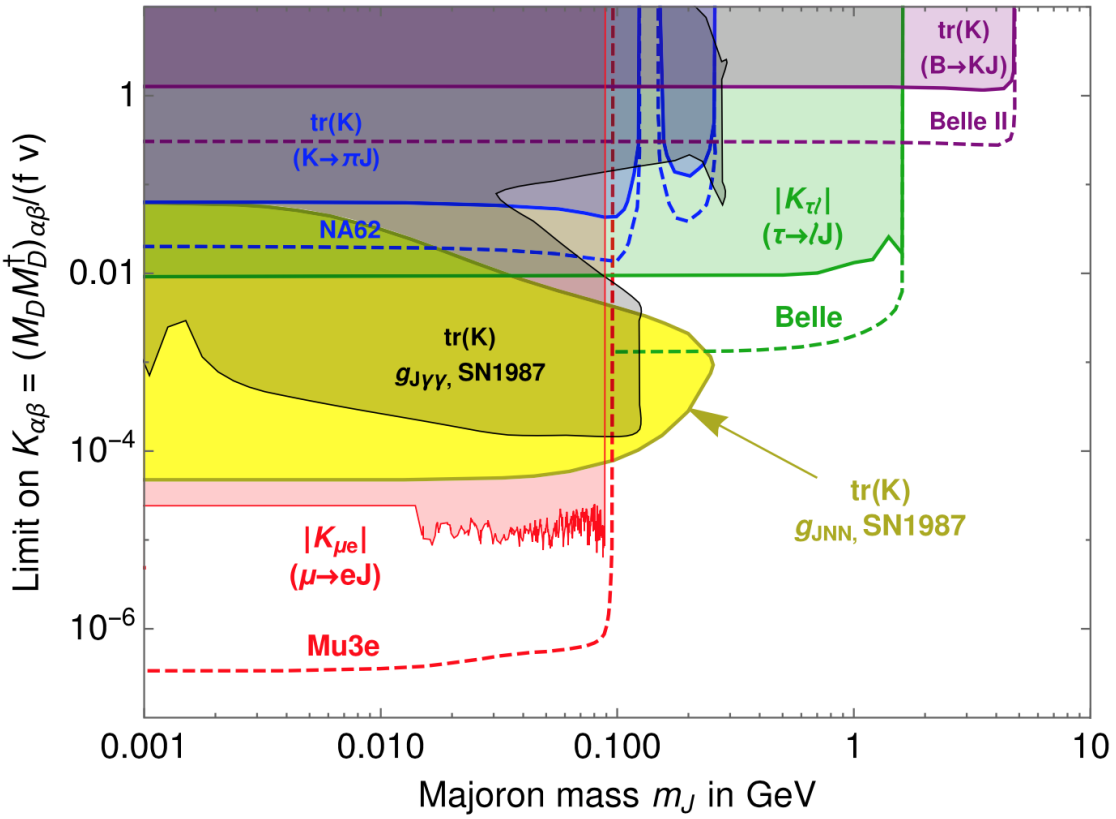

Figure 13: The experimental limit on K_{ab} (by Majoron emission processes and etc.) [133]. Here, K is defined as $K_{ab} = y_{ai} y^*_{bi} v_h/(2v_\phi)$, $\langle H \rangle = (0,\, v_h/\sqrt{2})^{\rm T}$.

6.2 The cosmic ray observation and the TeV scale Majoron dark matter

Recent days, there are anomalous results in positron fraction (flux of e^+/flux of $e^+ + e^-$) detected by the cosmic ray experiments. In Figure 14, [135] shows the observed positron fraction by AMS02 [136–138], HEAT [139], PAMELA [140, 141]. The black line is pure secondary production [142].

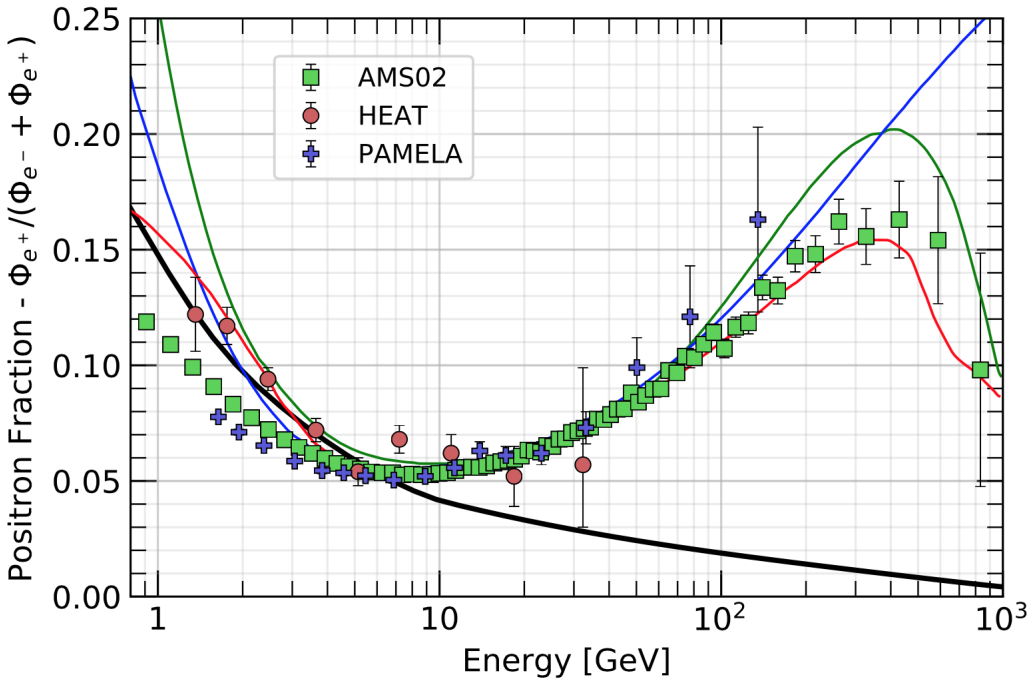

Figure 14: The plot of the energy of cosmic ray vs positron fraction [135]. The black line is pure secondary production [142]. The excess of the positron fraction can be explained by dark matter decay [143] (green line), propagation physics [144] (blue line) and production in pulsers [145] (red line).

We can see the tension between the observed results and the one predicted by pure secondary production. There are some solutions to explain this tension; dark matter decay [143], propagation physics [144] and production in pulsers [145]. We explain this tension by TeV scale Majoron dark matter decay, as [143].

When Majoron is GeV scale or lighter, the main process which contributes to DM indirect detections is $\chi \to b\bar{b}$ (χ: Majoron) as Figure 12. However, when Majoron is TeV scale, other processes of Majoron decay are opened, such as $\chi \to W^+W^-$, ZZ, h^0h^0, Zh^0, $t\bar{t}$. The decay widthes of $\chi \to W^+W^-$, ZZ, h^0h^0, Zh^0 are $\frac{f^2}{16\pi^2} \times O(m_\nu^2 m_\chi^3 / m_{N_R}^4)$, and much

smaller than $\chi \to b\bar{b}$. The decay width of $\chi \to t\bar{t}$ is shown as follows (please see §B.2):

$$\Gamma_{\chi\to t\bar{t}} = \frac{3M_\chi}{4096\pi^3}\frac{\alpha_W^2(v/\sqrt{2})^4 M_t^2}{M_W^4}\Big[\sum_{i,\alpha}|y^\nu_{\alpha i}|^2 f_i M_{N_i}^{-1}\Big]^2. \tag{6.6}$$

$\Gamma_{\chi\to b\bar{b}}$ is suppressed by factor M_b^2/M_t^2. Therefore, when the TeV scale Majoron is DM, the main process which contributes to DM indirect detections is $\chi \to t\bar{t}$.

Furthermore, $\chi \to \nu\nu$ processes are also important. The decay width of $\chi \to \nu\nu$ is given by:

$$\Gamma_{\chi\to\nu\nu} = \frac{m_\chi}{8\pi}\frac{m_{\nu_i}^2}{v_\phi^2}(1-4m_{\nu_i}^2/m_\chi^2)^{3/2}. \tag{6.7}$$

This decay rate is constraited by IceCube experiment $\Gamma_{\chi\to\nu\nu} \lesssim 1/(O(10^{25-26})\text{sec})$ [146, 147]. When $m_\nu \sim 0.1$eV, this constraint can be rewrite as:

$$v_\phi \gtrsim O(10^{15-16})\text{GeV}. \tag{6.8}$$

In Figure 15 and 17, we show the plot of positron fraction vs positron energy and antiproton E_k^2 flux. [17] Here, we use the PPPC4DMID package [148,149] and the formulae for the primary and secondary flux of e^- and the secondary one of e^+ [150]. Furthermore, we show the antiproton E_k^2 flux detected by AMS-02 [151] in Figure 16.

Comparing Figure 15 with Figure 14 (positron fraction), we can explain the excess of positron fraction by the TeV scale Majoron dark matter with $v_\phi = O(10^{15})$ GeV, $m_\chi = O(1)$ TeV and $m_N = 3m_\chi$. In the Majoron model, the mass of N is given as $M_{N_i} = \frac{f_i v_\phi}{\sqrt{2}}$. Therefore, $f \sim O(10^{-(11-12)})$ when the excess is explained. Comparing Figure 17 with Figure 16 (antiproton E_k^2 flux), we can obtain the upper limit of f_i: $|f_i| \lesssim O(10^{11} - 10^{12})$. Please see [152, 153] for details of the constraints of f_i and v_ϕ.

Combining the above results, the TeV scale Majoron dark matter with $f \sim O(10^{-(11-12)})$ and $v_\phi \sim O(10^{15-16})$ GeV may be observed in future cosmic-ray experiments. In this thesis, we consider the production mechanism of TeV scale Majoron dark matter in the early universe.

[17] E_k: antiproton kinetic energy.

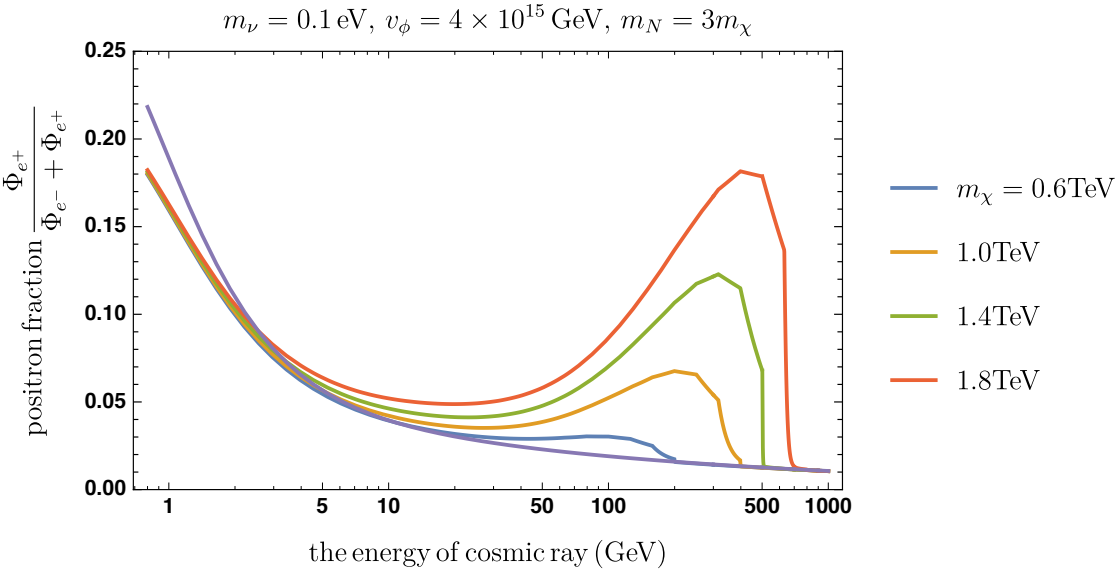

Figure 15: The plot of the energy of cosmic ray vs positron fraction. Here we assumed that DM is the TeV scale Majoron.

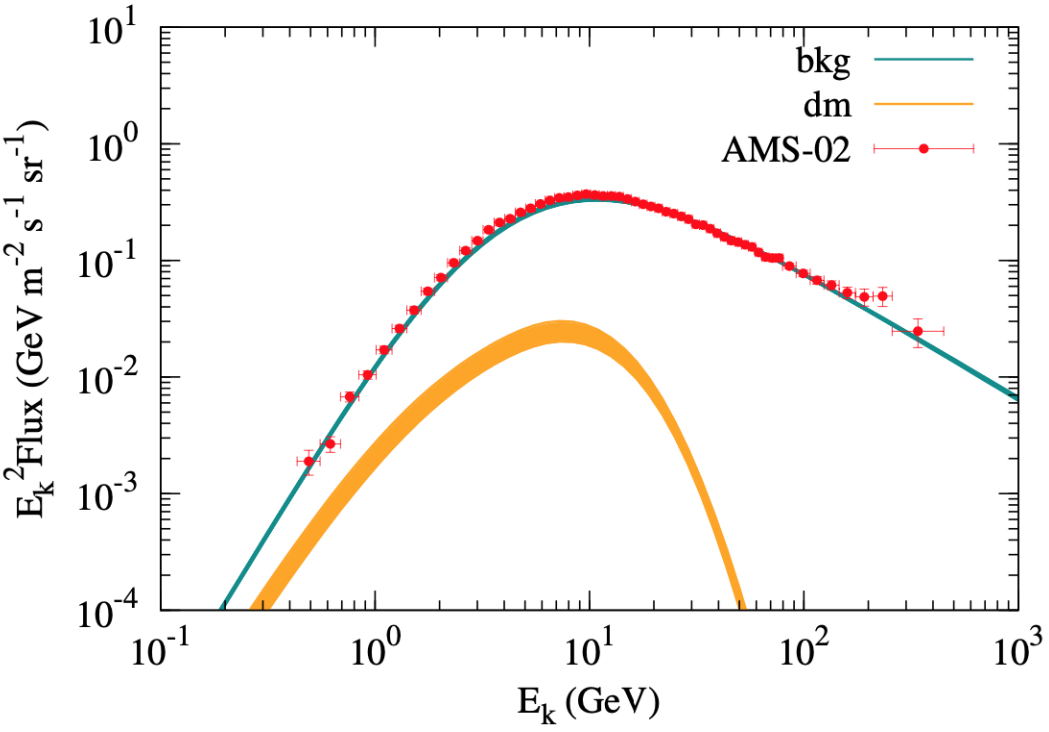

Figure 16: the observed E_k^2 flux of anti-proton [154]

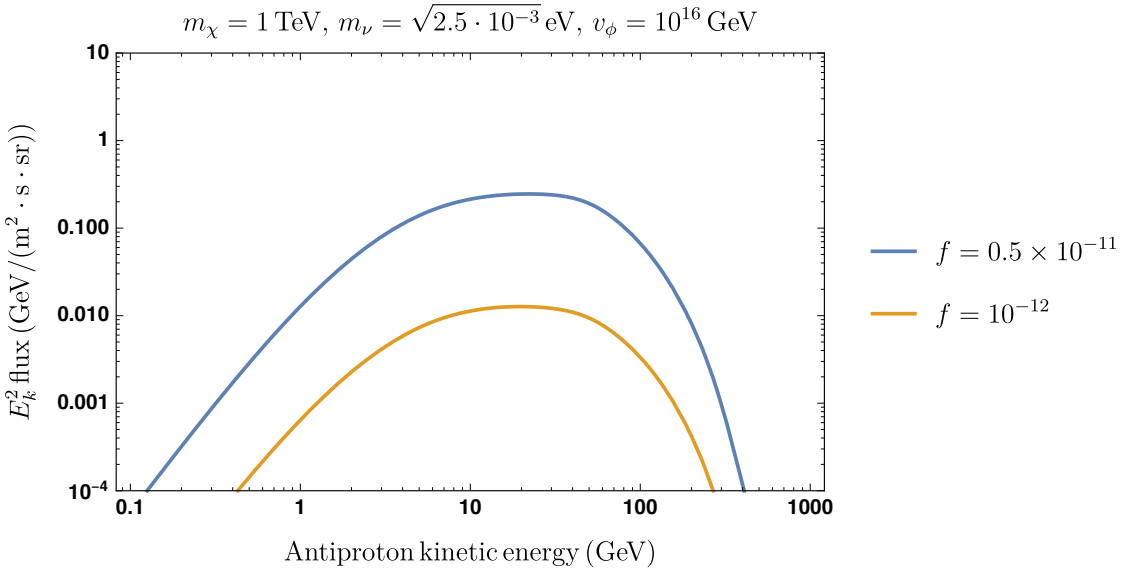

Figure 17: The prot of the antiproton kinetic energy vs E_k^2 flux from TeV Majoron DM decay

7 An introduction to the production of the TeV scale Majoron dark matter

In §6.2, we show that TeV scale Majoron dark matter is interesting, because it can be detected by the cosmic ray experiments. However, it is not obvious that the TeV scale Majoron can be produced as much as the DM relic density. In this section, we illustrate the difficulty and our solutions of it.

First, we show the Lagrangian of Majorana models. The Yukawa couplings of Majoron models are

$$\mathcal{L} \supset -\frac{f_{ij}}{2}\Phi\overline{\nu^c_{Ri}}\nu_{Rj} - y^\nu_{\alpha i}\overline{L_\alpha}\tilde{H}\nu_{Ri} + \text{H.c.} \tag{7.1}$$

$$= -\frac{M_{N_i}}{2}\overline{N_i}N_i - \frac{f_i}{2\sqrt{2}}\left(\phi\overline{N_i}N_i + i\chi\overline{N_i}\gamma_5 N_i\right) - \left(y^\nu_{\alpha i}\overline{L_\alpha}\tilde{H}P_R N_i + \text{H.c.}\right) \tag{7.2}$$

$$N_i = \nu_{Ri} + \nu^c_{Ri},\ \Phi = \frac{1}{\sqrt{2}}(v_\phi + \phi + i\chi),\ M_i = \frac{f_{ij}v_\phi}{\sqrt{2}}. \tag{7.3}$$

The lepton number symmetry is broken by the VEV of Φ. This breaking gives the Majorana masses of N_i. Then, SM neutrino gains the Majorana mass as type I seesaw model. The generation of N_i cannot be changed by the couplings $\phi\overline{N_i}N_i$ and $\chi\overline{N}_i\gamma_5 N_i$. The VEV of Φ is given by the following scalar potential:

$$V = -\frac{\mu_H^2}{2}\left|H\right|^2 - \frac{\mu_\Phi^2}{2}\left|\Phi\right|^2 + \frac{\lambda_H}{2}\left|H\right|^4 + \lambda_{H\Phi}|H|^2|\Phi|^2 + \frac{\lambda_\Phi}{2}\left|\Phi\right|^4 - \frac{m^2}{4}\left[\Phi^2 + (\Phi^*)^2\right]. \tag{7.4}$$

The stationary conditions (before EWSB) of ϕ is

$$\left.\frac{\partial V}{\partial\phi}\right|_{\text{vac}} = 0 \ \rightarrow\ \mu_\Phi^2 = \lambda_\Phi v_\phi^2 - m^2. \tag{7.5}$$

Using this condition, we replace μ_Φ by other parameter. After Φ gets nonzero VEV, potential becomes as follows:

$$V = m_H^2|H|^2 + \frac{m_\chi^2}{2}\chi^2 + \frac{m_\phi^2}{2}\phi^2 + \frac{m_\phi^2}{2v_\phi}\chi^2\phi + \frac{m_\phi^2}{2v_\phi}\phi^3 + \lambda_{H\Phi}v_\phi\phi|H|^2 \tag{7.6}$$

$$+ \frac{m_\phi^2}{8v_\phi^2}\chi^4 + \frac{m_\phi^2}{4v_\phi^2}\chi^2\phi^2 + \frac{m_\phi^2}{8v_\phi^2}\phi^4 + \frac{\lambda_{H\Phi}}{2}(\chi^2+\phi^2)|H|^2 + \frac{\lambda_H}{2}|H|^4, \tag{7.7}$$

$$m_\chi^2 = m^2,\ \lambda_\Phi = \frac{m_\phi^2}{v_\phi^2},\ \mu_H^2 = -2m_H^2 + \lambda_{H\Phi}v_\phi^2. \tag{7.8}$$

We assume $f_i \sim O(10^{-11})$ and $v_\Phi \sim O(10^{15-16})$ GeV, $m_\chi \sim O(10^3)$ GeV. These conditions are imposed by DM indirect detection, shown as §6.2. Furthermore, we must impose $m_\chi < 2m_N$, in order to avoid $\chi \to NN$ channel.

Next, we show the difficulty of Majoron dark matter production.

When $\lambda_{H\Phi} = 0$, Majoron is produced from N or ϕ. The interaction $\chi\overline{N_i}\gamma_5 N_i$ cannot cause $N_2 \to N_1\chi$ process. χ can be produced by $NN \to \phi \to \chi\chi$ (s-channnel) process. This process has a resonance at $s \sim m_\phi$, therefore, Y_N must be somehow large at $T \sim m_\phi$.

When $\lambda_{H\Phi} \neq 0$, χ can be created by $HH \to \chi\chi$. This process is suppressed because χ is (pseudo) NG boson. Therefore, we cannot produce χ by freeze-"out" mechanism.

Last, we show three scenarios in which TeV scale Majoron can be produced as much as the observed DM relic density:

- Scenario A: We introduce Lepton number soft breaking term $-\frac{1}{2}m_{ij}\overline{\nu^c_{Ri}}\nu_{Rj}$, then $N_2 \to N_1\chi$ occurs. We can produce χ via this process by freeze-in mechanism [134].
- Scenario B: χ can be produced via $HH \to \chi\chi$ process, by UV freeze-in mechanism [134, 155].
- Scenario C: χ is produced from N at $T \sim m_\phi$, by freeze-in mechanism [134]. Y_N must be somehow large at $T \sim m_\phi$.

8 Scenario A

8.1 The Lagrangian

In Scenario A, we introduce lepton number soft breaking term $-\frac{1}{2}m_{ij}\overline{\nu^c_{Ri}}\nu_{Rj}$. Then, $N_2 \to N_1\chi$ is happen, therefore, χ can be generated by this process. We assume $M_{N_2} > (M_\chi + M_{N_1}) > M_{N_1} > M_\chi/2$. [18] The Lagrangian in Scenario A is shown as follows:

$$\mathcal{L} = -\frac{1}{2}\left(f_{ij}\Phi + m_{ij}\right)\overline{\nu^c_{Ri}}\nu_{Rj} - y^\nu_{\alpha i}\overline{L_\alpha}\tilde{H}\nu_{Ri} + \text{H.c.} \tag{8.1}$$

[18] If $2M_{N_1} < M_\chi$, $\chi \to 2N_1$ can occur. Then, we cannot avoid cosmic-ray constraints.

Here, f_{ij} can be real and diagonal ($f_{ij} = f_i\delta_{ij}$) by redefining ν_{Ri}. When denoting ν'_{Ri} as mass eigenstate ($\nu_{Ri} = U_{ij}\nu'_{Rj}$), the Lagrangian becomes as follows:

$$\mathcal{L} = -\frac{1}{2}U_{ik}\big(f_{ij}\Phi + m_{ij}\big)U_{jl}\overline{\nu'^{c}_{Rk}}\nu'_{Rl} - y^{\nu}_{\alpha i}U_{ik}\overline{L_\alpha}\tilde{H}\nu'_{Rk} + \text{H.c.} \tag{8.2}$$

$$= -\frac{1}{2}M_{N_i}\overline{N_i}P_R N_i - \frac{1}{2}\frac{F_{kl}}{\sqrt{2}}(\phi + i\chi)\overline{N_k}P_R N_l - Y^{\nu}_{\alpha i}\overline{L_\alpha}\tilde{H}P_R N_k + \text{H.c.} \tag{8.3}$$

$$\left(N_k = \nu'_{Rk} + \nu'^{c}_{Rk},\ F_{kl} = U_{ik}f_{ij}U_{jl},\ M_{N_k}\delta_{kl} = U_{ik}\left(\frac{f_{ij}v_\phi}{\sqrt{2}} + m_{ij}\right)U_{jl}\right) \tag{8.4}$$

$$= -\frac{1}{2}M_{N_i}\overline{N_i}N_i - \frac{1}{2\sqrt{2}}\phi\overline{N_k}\Big(F_{kl}P_R + F^*_{kl}P_L\Big)N_l \tag{8.5}$$

$$-\frac{i}{2\sqrt{2}}\chi\overline{N_k}\Big(F_{kl}P_R - F^*_{kl}P_L\Big)N_l - \Big(Y^{\nu}_{\alpha i}\overline{L_\alpha}\tilde{H}P_R N_k + \text{H.c.}\Big), \tag{8.6}$$

$$Y^{\nu}_{\alpha i} = \frac{\sqrt{2}i}{v_{\text{EW}}}\big[U_{\text{PMNS}}\sqrt{m_\nu^{\text{diag}}}O\sqrt{M_N^{\text{diag}}}\big]_{\alpha i},\ (OO^{\text{T}} = I). \tag{8.7}$$

Here, N_k is Majorana particle with Majorana mass M_{N_k}. $\chi\overline{N_k}(F_{kl}P_R - F^*_{kl}P_L)N_l$ can have off-diagonal part. It is due to lepton number soft breaking term $-\frac{1}{2}m_{ij}\overline{\nu^c_{Ri}}\nu_{Rj}$. This off-diagonal part causes $N_2 \to N_1\chi$. In Scenario A, Majoron is produced via this process. In (8.7), we write $Y^{\nu}_{\alpha i}$ by other parameters (the Casas-Ibarra parametrization [156]). It is useful for numerical estimation.

8.2 The Boltzmann equation

The evolution of the number density of particles is described by Boltzmann equations. The Boltzmann equations in Scenario A are shown as follows:

$$\frac{H(m_\chi)s(m_\chi)}{x^4}\frac{dY_{N_2}}{dx} = -\big[N_2 \leftrightarrow N_1\chi\big] - \sum_a \big[N_2 \leftrightarrow L_aH,\ \overline{L}_a\overline{H}\big], \tag{8.8}$$

$$\frac{H(m_\chi)s(m_\chi)}{x^4}\frac{dY_{N_1}}{dx} = \big[N_2 \leftrightarrow N_1\chi\big] - \sum_a \big[N_1 \leftrightarrow L_aH,\ \overline{L}_a\overline{H}\big], \tag{8.9}$$

$$\frac{H(m_\chi)s(m_\chi)}{x^4}\frac{dY_\chi}{dx} = \big[N_2 \leftrightarrow N_1\chi\big]. \tag{8.10}$$

Here, we define the following quantities:

$$x = \frac{m_\chi}{T},\ r_X = \frac{m_X}{m_\chi},\ Y_a = \frac{n_a}{s},\ y_a = \frac{Y_a}{Y_a^{(\mathrm{eq})}}, \tag{8.11}$$

$$[a\cdots \leftrightarrow b\cdots] = y_a \cdots \gamma^{a\cdots}{}_{b\cdots} - y_b \gamma^{b\cdots}{}_{a\cdots}, \tag{8.12}$$

$$\begin{aligned}\gamma^{a\cdots}{}_{b\cdots} =& \int d\Pi_a \cdots d\Pi_b \cdots \times (2\pi)^4 \delta^4(p_a + \cdots - p_b - \cdots) \\ & \times \left| i\mathcal{M}(a + \cdots \to b + \cdots) \right|^2 f_a^{\mathrm{eq}} \cdots , \\ & (\text{degree of freedom are summed in } |\mathcal{M}|^2.)\end{aligned} \tag{8.13}$$

$$d\Pi_a = \frac{d^3 p_a}{(2\pi)^3 2E}, \quad (\text{degree of freedom } g_a \text{ is contained in } |\mathcal{M}|^2). \tag{8.14}$$

s is entropy density, n_a is number density of a, f_a is the distribution function of a, (eq) means equilibrium, and $H(m_\chi)$ and $s(m_\chi)$ are Hubble parameter and entropy density at $T = m_\chi$, respectively. Y_a is called as the "yield" of a.

In Scenario A, $N_{1,2}$ are produced from thermal bath (SM lepton and Higgs) by the term $[N_{1,2} \leftrightarrow L_a H, \overline{L}_a \overline{H}]$. χ is produced via the decay process $N_2 \to N_1 \chi$. In next section, we evaluate $[a\cdots \leftrightarrow b\cdots]$.

8.3 The evaluation of $[a\cdots \leftrightarrow b\cdots]$

In this subsection, we evaluate $[a\cdots \leftrightarrow b\cdots]$. First, $\left[N_2 \leftrightarrow N_1\chi\right]$ is written by the decay width $\Gamma_{N_2 \to N_1 \chi}$:

$$\left[N_2 \leftrightarrow N_1\chi\right] \simeq \frac{Y_{N_2}}{Y_{N_2}^{\mathrm{eq}}} \gamma^{N_2}{}_{N_1\chi} \, (y_\chi \ll 1) \tag{8.15}$$

$$= \frac{2\pi^2 s(m_{N_2})}{g_{N_2} m_{N_2}^3 (r_{N_2} x)^2 K_2(r_{N_2} x)} \frac{g_{N_2} m_{N_2}^3 \Gamma_{N_2 \to N_1 \chi}}{2\pi^2} (r_{N_2} x)^{-1} K_1(r_{N_2} x) Y_{N_2} \tag{8.16}$$

$$= \frac{s(m_\chi)\Gamma_{N_2 \to N_1 \chi}}{x^3} \frac{K_1(r_{N_2} x)}{K_2(r_{N_2} x)} Y_{N_2}. \tag{8.17}$$

Here, we assume $y_\chi \ll 1$. It is natural assumption in freeze-in mechanism. χ is produced by this process.

Next we evaluate $\left[N_i \leftrightarrow L_a H\right] + \left[N_i \leftrightarrow \overline{L}_a \overline{H}\right]$. It is written by the decay width

$\Gamma_{N_i\to L_aH,\overline{L}_a\overline{H}}$:

$$\begin{aligned}
&\big[N_i \leftrightarrow L_aH\big]+\big[N_i \leftrightarrow \overline{L}_a\overline{H}\big] && (8.18)\\
&=y_{N_i}\gamma^{N_i}{}_{L_aH} - y_{L_a}y_H\gamma^{L_aH}{}_{N_i} + y_{N_i}\gamma^{N_i}{}_{\overline{L}_a\overline{H}} - y_{\overline{L}_a}y_{\overline{H}}\gamma^{\overline{L}_a\overline{H}}{}_{N_i} && (8.19)\\
&=(y_{N_i}-y_{\overline{L}_a}y_{\overline{H}})\gamma^{N_i}{}_{L_aH} + (y_{N_i}-y_{L_a}y_H)\gamma^{N_i}{}_{\overline{L}_a\overline{H}} \quad (CPT) && (8.20)\\
&\simeq(y_{N_i}-1)\gamma^{N_i}{}_{L_aH,\overline{L}_a\overline{H}}, \quad (y_{L_a}\sim y_H\sim 1) && (8.21)\\
&=\frac{s(m_\chi)\Gamma_{N_i\to L_aH,\overline{L}_a\overline{H}}}{x^3}\frac{K_1(r_{N_i}x)}{K_2(r_{N_i}x)}(Y_{N_i}-Y_{N_i}^{\rm eq}). && (8.22)
\end{aligned}$$

N_i is produced from SM thermal bath via this process.

Next, we evaluate the decay widths $\Gamma_{N_2\to N_1\chi}$ and $\Gamma_{N_i\to L_aH,\,\overline{L}_a\overline{H}}$ as follows:

$$\begin{aligned}
|i\mathcal{M}_{N_2\to N_1\chi}|^2 =&\sum_{\rm spin}\left|\overline{u(p_{N_1})}\left[\frac{1}{\sqrt{2}}(F_{12}P_R - F_{12}^*P_L)\right]u(p_{N_2})\right|^2 && (8.23)\\
=&2m_{N_2}E_{N_1}|F_{12}|^2 - m_{N_2}m_{N_1}\big[F_{12}^2+(F_{12}^*)^2\big], && (8.24)\\
\Gamma_{N_2\to N_1\chi} =&\frac{1}{2g_{N_2}m_{N_2}}\frac{1}{8\pi}\sqrt{\lambda(1,\,m_{N_1}^2/m_{N_2}^2,\,m_\chi^2/m_{N_2}^2)} && (8.25)\\
&\times\Big\{(m_{N_2}^2+m_{N_1}^2-m_\chi^2)|F_{12}|^2 - m_{N_2}m_{N_1}\big[F_{12}^2+(F_{12}^*)^2\big]\Big\}, && (8.26)\\
&\big(\lambda(a,\,b,\,c)=(a-b-c)^2-4bc\big), && (8.27)
\end{aligned}$$

$$\begin{aligned}
\Gamma_{N_i\to L_aH} =&\frac{1}{g_{N_i}}\frac{1}{2m_{N_i}}\int\frac{dp_\ell^3}{2E_\ell(2\pi)^3}\int\frac{dp_\Phi^3}{2E_\Phi(2\pi)^3}(2\pi)^4\delta(M_{N_i}-E_\ell-E_\phi) && (8.28)\\
&\times\delta^3(\mathbf{p}_\ell+\mathbf{p}_\phi)\times 2|Y_{\alpha i}^\nu|^2\sum_{\rm spin}\left|\overline{u(p_\ell)}P_Ru(p_N)\right|^2 && (8.29)\\
=&\frac{|Y_{\alpha i}^\nu|^2 m_{N_i}}{16\pi}, && (8.30)\\
\Gamma_{N_i\to L_aH,\,\overline{L}_a\overline{H}} =&\frac{|Y_{\alpha i}^\nu|^2 m_{N_i}}{8\pi}. && (8.31)
\end{aligned}$$

F_{12} in $\Gamma_{N_2\to N_1\chi}$ are chosen as $O(10^{-11})$ so that freeze-in mechanism occurs. $Y_{N_{1,\,2}}$ reach thermal equilibrium at $T\sim m_{N_{1,\,2}}$ via $N_i\leftrightarrow L_aH$, $\overline{L}_a\overline{H}$.

8.4 The approximation formula of dark matter relic

It is useful to derive an approximation formula of the dark matter relic density. First, we integral the Boltzmann equations of Y_χ:

$$Y_\chi(\infty) = \int_{x_R}^{\infty} dx \frac{x^4}{H(m_\chi)s(m_\chi)} \frac{s(m_\chi)\Gamma_{N_2\to N_1\chi}}{x^3} \frac{K_1(r_{N_2}x)}{K_2(r_{N_2}x)} Y_{N_2} \tag{8.32}$$

$$= \frac{\Gamma_{N_2\to N_1\chi}}{H(m_\chi)} \int_{x_R}^{\infty} dx \frac{xK_1(r_{N_2}x)}{K_2(r_{N_2}x)} Y_{N_2}. \tag{8.33}$$

In order to evaluate this integral, we must rewrite Y_{N_2} by the equilibrium yield ($Y^{\rm eq}$). The term $K_1(r_{N_2}x)Y_{N_2}/K_2(r_{N_2}x)$ also appears in the Boltzmann equation of Y_{N_2}. When it is integrated with the boundary condition $Y_{N_2}(\infty) = Y_{N_2}(x_R) = 0$, we can get the following formula:

$$0 = -\int_{x_R}^{\infty} \frac{x^4}{H(m_\chi)s(m_\chi)} \frac{s(m_\chi)K_1(r_{N_2}x)}{K_2(r_{N_2}x)x^3} \tag{8.34}$$

$$\times \left[(\Gamma_{N_2\to N_1\chi} + \Gamma_{N_2\to L_aH,\overline{L}_a\overline{H}})Y_{N_2} - \Gamma_{N_2\to L_aH,\overline{L}_a\overline{H}} Y_{N_2}^{\rm eq}\right], \tag{8.35}$$

i.e,

$$\int_{x_R}^{\infty} dx \frac{xK_1(r_{N_2}x)}{K_2(r_{N_2}x)} Y_{N_2} = \frac{\Gamma_{N_2\to L_aH,\overline{L}_a\overline{H}}}{\Gamma_{N_2\to N_1\chi} + \Gamma_{N_2\to L_aH,\overline{L}_a\overline{H}}} \int_{x_R}^{\infty} dx \frac{xK_1(r_{N_2}x)}{K_2(r_{N_2}x)} Y_{N_2}^{\rm eq}. \tag{8.36}$$

Therefore, the approximation of $Y_\chi(\infty)$ can be evaluated as follows:

$$Y_\chi(\infty) = \frac{\Gamma_{N_2\to N_1\chi}\Gamma_{N_2\to L_aH,\overline{L}_a\overline{H}}}{\Gamma_{N_2\to N_1\chi} + \Gamma_{N_2\to L_aH,\overline{L}_a\overline{H}}} \frac{1}{H(m_\chi)} \int_{x_R}^{\infty} dx \frac{xK_1(r_{N_2}x)}{K_2(r_{N_2}x)} Y_{N_2}^{\rm eq} \tag{8.37}$$

$$= \frac{\Gamma_{N_2\to N_1\chi}\Gamma_{N_2\to L_aH,\overline{L}_a\overline{H}}}{\Gamma_{N_2\to N_1\chi} + \Gamma_{N_2\to L_aH,\overline{L}_a\overline{H}}} \frac{1}{H(m_\chi)} \int_{x_R}^{\infty} dx \frac{xK_1(r_{N_2}x)}{K_2(r_{N_2}x)} \frac{g_{N_2}m_\chi^3(r_{N_2}x)^2K_2(r_{N_2}x)}{2\pi^2 s(m_\chi)} \tag{8.38}$$

$$= \frac{\Gamma_{N_2\to N_1\chi}\Gamma_{N_2\to L_aH,\overline{L}_a\overline{H}}}{\Gamma_{N_2\to N_1\chi} + \Gamma_{N_2\to L_aH,\overline{L}_a\overline{H}}} \frac{r_{N_2}^{-2}g_{N_2}m_\chi^3}{2\pi^2 s(m_\chi)H(m_\chi)} \int_{r_{N_2}x_R}^{\infty} d(r_{N_2}x)K_1(r_{N_2}x)(r_{N_2}x)^3 \tag{8.39}$$

$$\sim \frac{\Gamma_{N_2\to N_1\chi}\Gamma_{N_2\to L_aH,\overline{L}_a\overline{H}}}{\Gamma_{N_2\to N_1\chi} + \Gamma_{N_2\to L_aH,\overline{L}_a\overline{H}}} \frac{3r_{N_2}^{-2}g_{N_2}m_\chi^3}{4\pi s(m_\chi)H(m_\chi)} \ (x_R \to 0) \tag{8.40}$$

$$\sim \frac{405\sqrt{5}g_{N_2}\Gamma_{N_2\to N_1\chi}}{16\pi^{9/2}g_{*S}g_*^{1/2}G^{1/2}m_{N_2}^2}, \ (\Gamma_{N_2\to L_aH,\overline{L}_a\overline{H}} \gg \Gamma_{N_2\to N_1\chi}). \tag{8.41}$$

Using this formula, we show the parametric region where the χ density is equal to the dark matter relic density, in Figure 18 and 19.

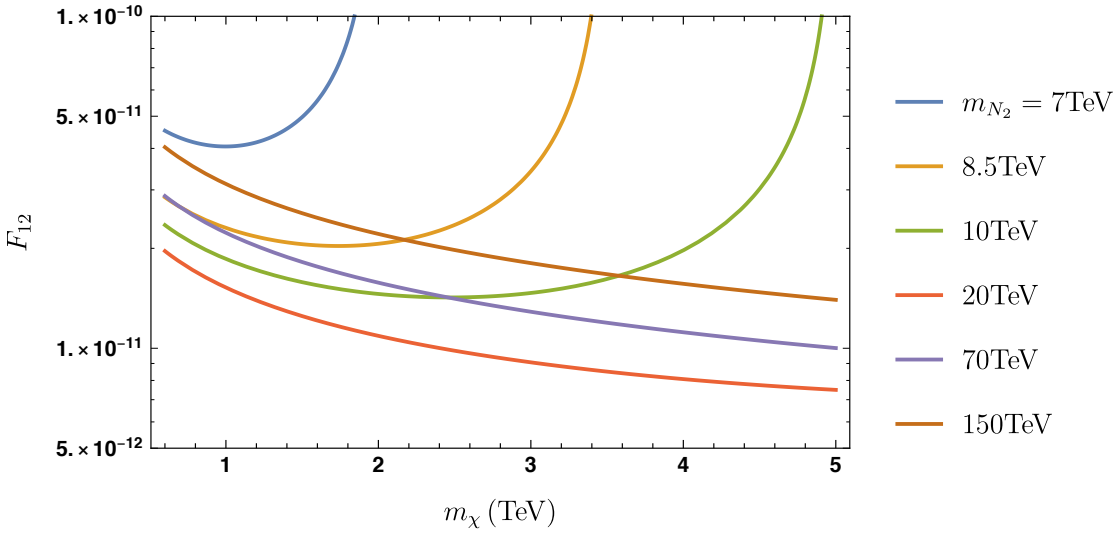

Figure 18: The plot of F_{12} vs m_χ when $m_{N_1} = 5$TeV and the present density of χ is equal to DM relic density

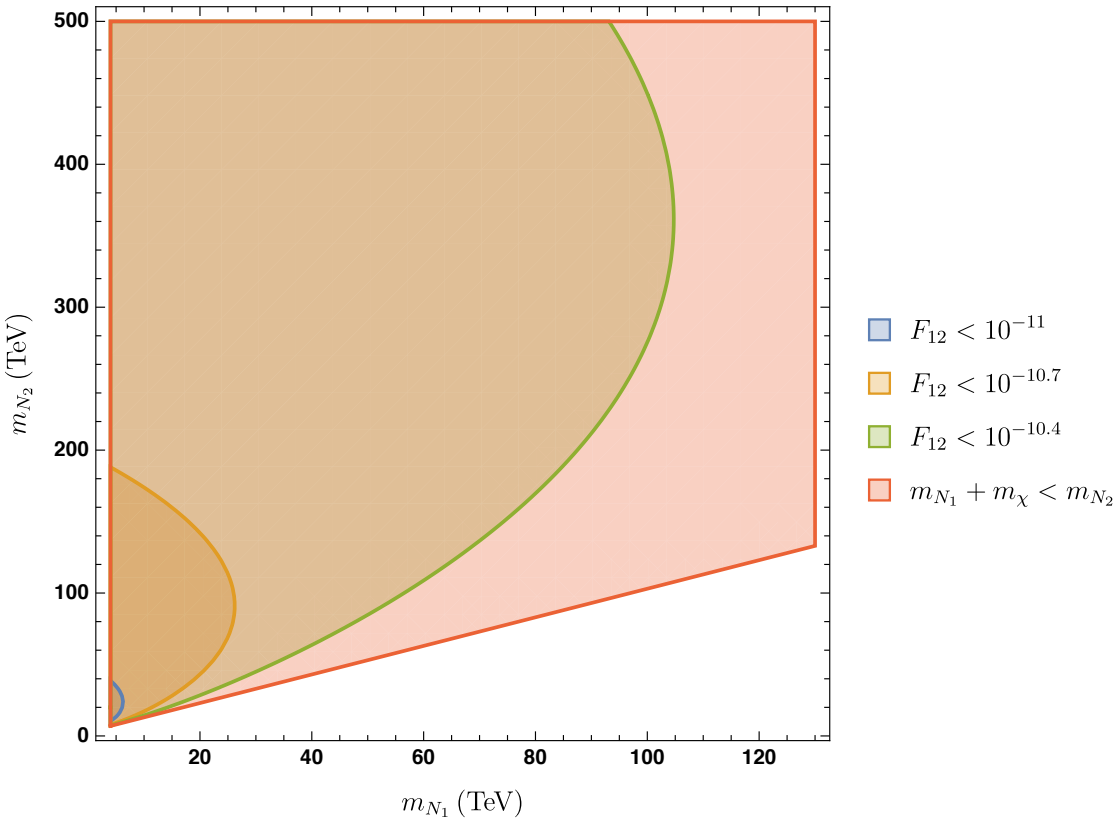

Figure 19: The region of m_{N_1} vs m_{N_2} when the present density of χ is equal to DM relic density.

In Figure 18, we set $m_{N_1} = 5\text{TeV}$ and vary m_{N_2}. We can see that F_{12} has lower limit as $F_{12} \gtrsim O(10^{-11})$.

In Figure 19, we show the region where Majoron DM is sufficiently produced and $F_{12} < 10^{-11}$, $10^{-10.7}$, $10^{-10.4}$. We can see m_{N_1} and m_{N_2} have upper limit.

8.5 The numerical simulation of the production of χ

We show the numerical results for the Boltzmann equation in Figure 20. In this Figure,

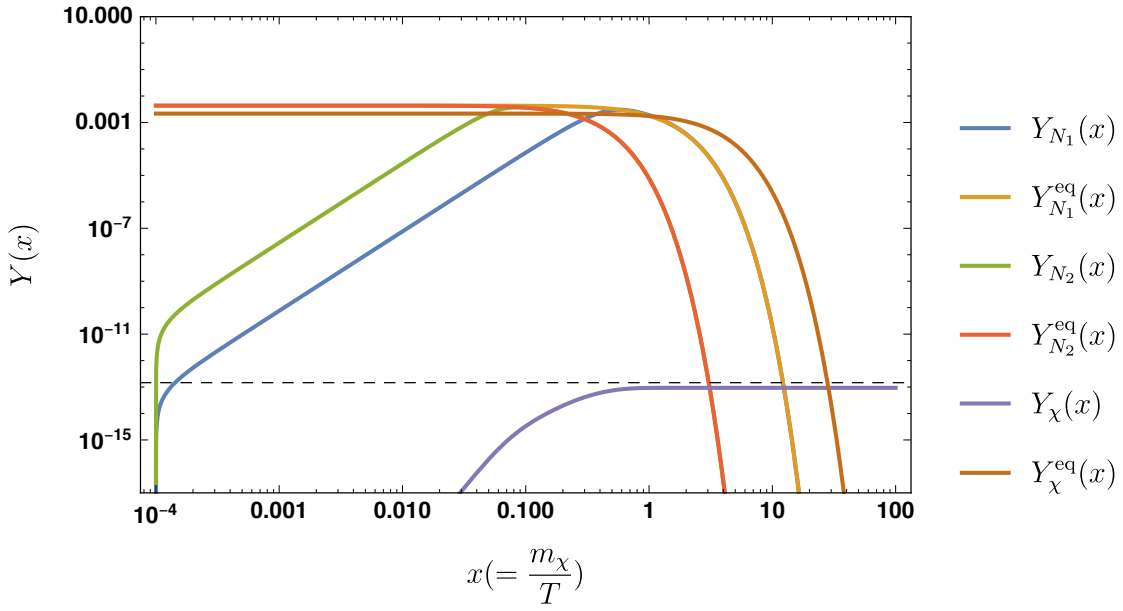

Figure 20: The solution for the Boltzmann equations. Dashed line is the observed DM relic density.

we set parameters as follows:

$$O = \begin{pmatrix} 0 & 0 \\ 1 & 0 \\ 0 & 1 \end{pmatrix} \text{ (Cassas} - \text{Ibarra)}, \tag{8.42}$$

$$U = \begin{pmatrix} \cos 0.3 & -\sin 0.3 \\ \sin 0.3 & \cos 0.3 \end{pmatrix} \text{ (diagonization matrix for mass of } N\text{)}, \tag{8.43}$$

$$m_\chi = 3\text{TeV},\ f_1 = 10^{-11},\ f_2 = 4 \times 10^{-11},\ v_\phi = 10^{15}\text{GeV}, \tag{8.44}$$

$$m_{ij} = U^*_{ik} M^{\rm diag}_{N_k} U^*_{jk} - \frac{f_{ij} v_\phi}{\sqrt{2}},\ m_{\nu_1} = 0,\ \text{neutrino parameter is normal hierarchy}. \tag{8.45}$$

We choose f_i and v_ϕ in order to avoid the constraints from cosmic ray experiments. U is chosen as rotating matrix, then the lepton number soft-breaking term $m_{ij}\overline{\nu^c_{Ri}}\nu_{Rj}$ becomes non-diagonal. Then, $N_2 \to N_1\chi$ can occur.

In Figure 20, we can see that χ is produced at $T \sim m_{N_2}$. At this temperature, Y_{N_2} is sufficiently large. Therefore, χ can be produced as much as the observed DM relic density. Combining above results, Scenario A is possible.

9 ScenarioB

9.1 The Lagrangian

In Scenario B, χ is produced from Higgs: $HH^\dagger \to \chi\chi$. This process occurs due to $\lambda_{H\Phi}|H|^2|\Phi|^2$ coupling. However, this process is highly suppressed by v_ϕ, because χ is pseudo NG boson. Therefore, we use the UV freeze-in mechanism for the dark matter production. In Scenario B, we assume that the reheating temperature T_R is smaller than m_ϕ.

In Scenaro B, the Yukawa couplings are shown as follows:

$$\mathcal{L} \supset -\frac{f_{ij}}{2}\Phi\overline{\nu^c_{Ri}}\nu_{Rj} - y^\nu_{\alpha i}\overline{L_\alpha}\tilde{H}\nu_{Ri} + \text{H.c.} \tag{9.1}$$

Here, f_{ij} can be real diagonal by redefinition of ν_{iR} ($f_{ij} = f_i\delta_{ij}$). After $\langle\Phi\rangle = \frac{v_\phi}{\sqrt{2}}$, the Lagrangian becomes as: [19]

$$\mathcal{L} = -\frac{M_{N_i}}{2}\overline{N_i}N_i - \frac{f_i}{2\sqrt{2}}\left(\phi\overline{N_i}N_i + i\chi\overline{N_i}\gamma_5 N_i\right) \tag{9.2}$$

$$-\left(Y^\nu_{\alpha i}\overline{L_\alpha}\tilde{H}P_R N_i + \text{H.c.}\right) \tag{9.3}$$

$$N_i = \nu_{Ri} + \nu^c_{Ri},\ \Phi = \frac{1}{\sqrt{2}}(v_\phi + \phi + i\chi),\ M_i = \frac{f_{ij}v_\phi}{\sqrt{2}}. \tag{9.4}$$

N gets Majorana masses by the VEV of Φ. Then, we can explain the neutrino oscillation as type I seesaw model.

Scalar potential is given as follows:

$$V = -\frac{\mu_H^2}{2}\left|H\right|^2 - \frac{\mu_\Phi^2}{2}\left|\Phi\right|^2 + \frac{\lambda_H}{2}\left|H\right|^4 + \lambda_{H\Phi}|H|^2|\Phi|^2 + \frac{\lambda_\Phi}{2}\left|\Phi\right|^4 - \frac{m^2}{4}\left[\Phi^2 + (\Phi^*)^2\right]. \tag{9.5}$$

The couplings in the potential is chosen so that Φ gains nonzero VEV. The stationary condition of ϕ (before EWSB) is

$$\left.\frac{\partial V}{\partial\phi}\right|_{\text{vac}} = 0 \ \to\ \mu_\Phi^2 = \lambda_\Phi v_\phi^2 - m^2. \tag{9.6}$$

[19] Φ's VEV can be real by redefinition of Φ. Then, $f_{ij}v_\phi$ becomes real diagonal matrix.

Using them, we replace μ_Φ by other parameter. After Φ gets nonzero VEV, potential becomes as follows:

$$V = m_H^2|H|^2 + \frac{m_\chi^2}{2}\chi^2 + \frac{m_\phi^2}{2}\phi^2 + \frac{m_\phi^2}{2v_\phi}\chi^2\phi + \frac{m_\phi^2}{2v_\phi}\phi^3 + \lambda_{H\Phi}v_\phi\phi|H|^2 \tag{9.7}$$

$$+ \frac{m_\phi^2}{8v_\phi^2}\chi^4 + \frac{m_\phi^2}{4v_\phi^2}\chi^2\phi^2 + \frac{m_\phi^2}{8v_\phi^2}\phi^4 + \frac{\lambda_{H\Phi}}{2}(\chi^2+\phi^2)|H|^2 + \frac{\lambda_H}{2}|H|^4, \tag{9.8}$$

$$m_\chi^2 = m^2,\ \lambda_\Phi = \frac{m_\phi^2}{v_\phi^2},\ \mu_H^2 = -2m_H^2 + \lambda_{H\Phi}v_\phi^2. \tag{9.9}$$

The couplings $\lambda_{H\Phi}\chi^2|H|^2/2!$, $\lambda_{H\Phi}v_\phi\phi|H|^2$ and $(m_\phi^2/v_\phi)\chi^2\phi/2!$ occur the production process of χ ($HH^\dagger \to \chi\chi$).

9.2 The Boltzmann equation

The Boltzmann equation of χ is given as follows:

$$\frac{H(m_\chi)s(m_\chi)}{x^4}\frac{dY_\chi}{dx} = -2\left[2\chi \leftrightarrow HH^\dagger\right] \tag{9.10}$$

$$= -2\left(\frac{Y_\chi^2}{(Y_\chi^{\rm eq})^2} - 1\right)\gamma^{2\chi}{}_{HH^\dagger}, \tag{9.11}$$

$$\gamma^{2\chi}{}_{HH^\dagger} = \frac{1}{2!}\frac{g_\chi^2 T}{32\pi^4}\int_{4m_\chi^2} ds\sigma_{2\chi\to HH^\dagger}(s)s^{\frac{3}{2}}K_1(s^{1/2}/T)\lambda(1,\, m_\chi^2/s,\, m_\chi^2/s), \tag{9.12}$$

$$\big(\lambda(a,\, b,\, c) = (a-b-c)^2 - 4bc\big). \tag{9.13}$$

At the temperature T, the main contribution comes from $s \lesssim T$. It is because the integral contains the modified Bessel function $K_1(s^{1/2}/T)$.

χ is produced via $HH^\dagger \to 2\chi$. The cross-section of $\chi\chi \to HH^\dagger$ is given as follows:

$$i\mathcal{M}_{\chi\chi\to H^\dagger H} = \frac{-im_\phi^2}{v_\phi} \times \frac{i}{s-m_\phi^2} \times (-i\lambda_{H\Phi}v_\phi)\delta_{ab}^{\rm SU(2)} - i\lambda_{H\Phi}\delta_{ab}^{\rm SU(2)} \tag{9.14}$$

$$= i\lambda_{H\Phi}\delta_{ab}^{\rm SU(2)}\frac{s}{m_\phi^2 - s}, \tag{9.15}$$

$$\sigma_{2\chi\to HH^\dagger}(s) = \frac{1}{g_\chi^2}\frac{1}{2^5\pi s}\frac{1}{\sqrt{\lambda(1,\, m_\chi^2/s,\, m_\chi^2/s)}}\int d(\cos\theta)|\mathcal{M}(s,\, \cos\theta)|^2 \tag{9.16}$$

$$\simeq \frac{1}{8\pi s^{1/2}}\frac{1}{\sqrt{s-4m_\chi^2}}|\lambda_{H\Phi}|^2\frac{s^2}{m_\phi^4},\ (s \lesssim T < T_R < m_\phi). \tag{9.17}$$

We assume that m_ϕ is larger than reheating temperature T_R. Therefore, s in propagator of ϕ is negligible.

On the other hands, the cross section increases with s. It is because χ is (pseudo) NG boson. Therefore, this process is the most dominant at $T \sim T_R$. It is the feature of UV freeze-in. Using the above results, we can get the formula of $\gamma^{2\chi}_{HH^\dagger}$:

$$\gamma^{2\chi}{}_{HH^\dagger} \simeq \frac{m_\chi^8 |\lambda_{H\Phi}|^2}{16\pi^{9/2} m_\phi^4} x^{-1} \text{MeijerG}\left[\{\{\}, \{-2\}\}, \{\{-7/2, -1/2, 1/2\}, \{\}\}, x^2\right] \tag{9.18}$$

$$= \frac{3 m_\chi^8 |\lambda_{H\Phi}|^2}{2\pi^5 m_\phi^4 x^8} + O(x^{-6}). \tag{9.19}$$

The production of χ occurs at $T \sim T_R$. At this temperature, $\gamma^{2\chi}_{HH^\dagger} \simeq \frac{3 m_\chi^8 |\lambda_{H\Phi}|^2}{2\pi^5 m_\phi^4 x^8}$. We can get the approximation formula for the dark matter relic density by integrating the Boltzmann equation:

$$Y_\chi(x) \simeq 2 \int_{x_R}^{x} \frac{x^4}{H(m_\chi) s(m_\chi)} \frac{3 m_\chi^8 |\lambda_{H\Phi}|^2}{2\pi^5 m_\phi^4 x^8} \tag{9.20}$$

$$= \frac{m_\chi^8 |\lambda_{H\Phi}|^2}{\pi^5 H(m_\chi) s(m_\chi) m_\phi^4} (x_R^{-3} - x^{-3}), \ (x_R = m_\chi / T_R). \tag{9.21}$$

Using this formula, we show the parametric region where the present χ density is equal to the DM relic density (Figure 21).

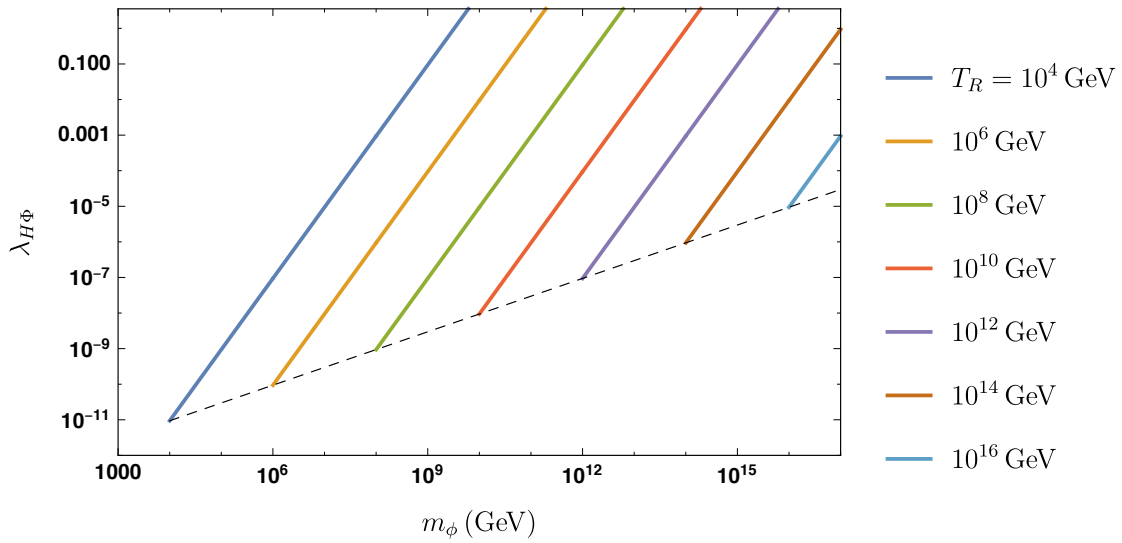

Figure 21: The parametric region where the density of χ is equal to DM relic density and $m_\chi = 10^3$GeV. Here, we vary T_R from 10^4GeV to 10^{15}GeV. Dashed line is $m_\phi = T_R$.

For example, when $m_\chi = 10^3$ GeV, $m_\phi = 10^9$ GeV, $\lambda_{H\Phi} = 10^{-4}$ and $T_R = 10^6$ GeV, χ will be sufficiently produced. Using these parameters, we estimate the numerical solution for Boltzmann equation in Figure 22.

χ is mainly produced at $T \sim T_R$. It is the feature of UV freeze-in mechanism. We can see that the present density of χ is equal to the observed DM relic density, therefore, Scenario B is possible.

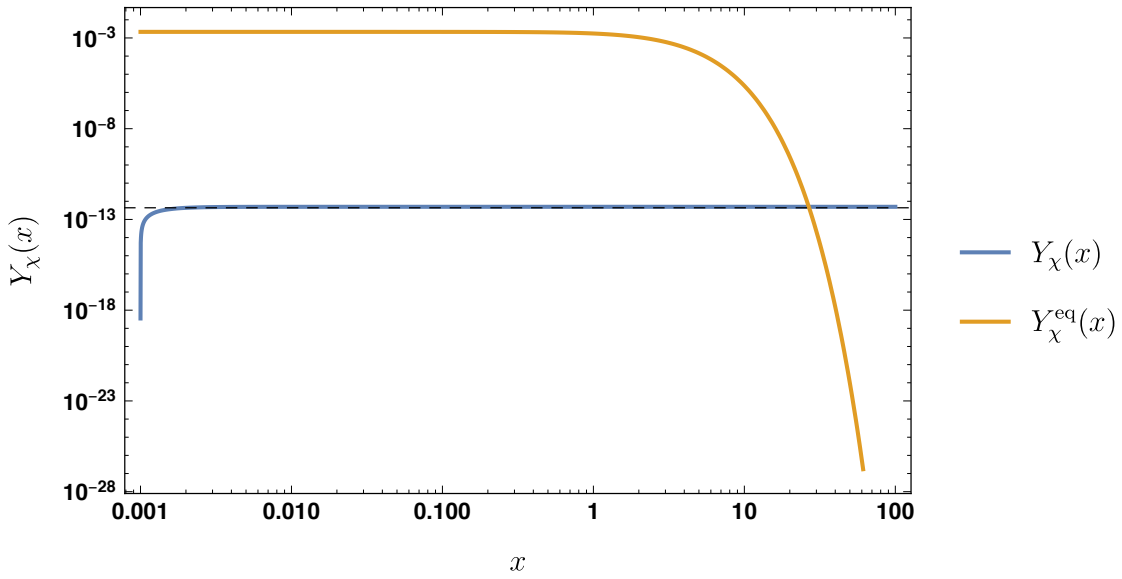

Figure 22: The solution for the Boltzmann equations. Dashed line is the observed DM relic density.

10 Scenario C

In Scenario C, we produce χ by the processes $NN(\to \phi) \to \chi\chi$ (s-channel) and $NN \to \phi$ (real particle) $\to 2\chi$. Both $NN \to \chi\chi$ (s-channel) and $NN \to \phi$ mainly occur at $T \sim m_\phi$. We choose T_R as $T_R \gg m_\phi$ in order to use this processes. Furthermore, Y_{N_i} must be large at $T \sim m_\phi$. In order to realize it, we assume that N_i is non-thermally produced from inflaton or m_ϕ is light ($O(10^5)$ GeV). We denote the former as "Scenario C-nt" (non-thermal) and the latter as "Scenario C-t" (thermal). We assume the mass hierarchy as $m_\phi > m_{N_i} > m_\chi$.

In Scenario C, we assume the following Yukawa couplings:

$$\mathcal{L}_N = -\frac{f_{ij}}{2}\Phi\overline{\nu_{Ri}^c}\nu_{Rj} - y_{\alpha i}^\nu \overline{L_\alpha}\tilde{H}\nu_{Ri} + \text{H.c.} \tag{10.1}$$

f_{ij} can be real diagonal by redefinition of ν_{iR} ($f_{ij} = f_i\delta_{ij}$). After $\langle\Phi\rangle = \frac{v_\phi}{\sqrt{2}}$, the Yukawa couplings become as follows: [20]

$$\mathcal{L} = -\frac{M_{N_i}}{2}\overline{N_i}N_i - \frac{f_i}{2\sqrt{2}}\Big(\phi\overline{N_i}N_i + i\chi\overline{N_i}\gamma_5 N_i\Big) \tag{10.2}$$

$$-\Big(y^\nu_{\alpha i}\overline{L_\alpha}\tilde{H}P_R N_i + \text{H.c.}\Big) \tag{10.3}$$

$$N_i = \nu_{Ri} + \nu^c_{Ri},\ \Phi = \frac{1}{\sqrt{2}}(v_\phi + \phi + i\chi),\ M_i = \frac{f_{ij}v_\phi}{\sqrt{2}}. \tag{10.4}$$

The couplings of $\chi\overline{N_i}\gamma_5 N_i$ and $\phi\overline{N_i}N_i$ are diagonal. Therefore, $N_2 \to N_1\chi$ process cannot occur. These couplings occur the processes $2N_i \to 2\chi$ and $2N_i \to \phi$. The left-handed neutrino gains Majorana mass as type I seesaw model.

Scalar potential (before electro-weak symmetry breaking) is given as follows

$$V = -\frac{\mu_H^2}{2}\big|H\big|^2 - \frac{\mu_\Phi^2}{2}\big|\Phi\big|^2 + \frac{\lambda_H}{2}\big|H\big|^4 + \frac{\lambda_\Phi}{2}\big|\Phi\big|^4 - \frac{m^2}{4}\big[\Phi^2 + (\Phi^*)^2\big] \tag{10.5}$$

$$= m_H^2|H|^2 + \frac{m_\chi^2}{2}\chi^2 + \frac{m_\phi^2}{2}\phi^2 + \frac{m_\phi^2}{2v_\phi}\chi^2\phi + \frac{m_\phi^2}{2v_\phi}\phi^3 \tag{10.6}$$

$$+ \frac{m_\phi^2}{8v_\phi^2}\chi^4 + \frac{m_\phi^2}{4v_\phi^2}\chi^2\phi^2 + \frac{m_\phi^2}{8v_\phi^2}\phi^4 + \frac{\lambda_H}{2}|H|^4, \tag{10.7}$$

$$m_\chi^2 = m^2,\ \lambda_\Phi = \frac{m_\phi^2}{v_\phi^2},\ \mu_H^2 = -2m_H^2. \tag{10.8}$$

Here, the couplings of Φ are chosen so that Φ gains nonzero VEV. The processes of $\phi \to 2\chi$ and $2N_i \leftrightarrow 2\chi$ are occurred by the coupling $(m_\phi^2/v_\phi)\chi^2\phi/2!$.

10.1 The Boltzmann equation

In Scenario C, Boltzmann equation becomes as follows:

$$\frac{H(m_\chi)s(m_\chi)}{x^4}\frac{dY_\phi}{dx} = -\big[\phi \leftrightarrow 2\chi\big] - \sum_i \big[\phi \leftrightarrow 2N_i\big] \tag{10.9}$$

$$\frac{H(m_\chi)s(m_\chi)}{x^4}\frac{dY_{N_i}}{dx} = 2\big[\phi \leftrightarrow 2N_i\big] - 2\big[2N_i \leftrightarrow 2\chi\big] \tag{10.10}$$

$$-\big[N_i \leftrightarrow LH\big] - \big[N_i \leftrightarrow \overline{LH}\big] \tag{10.11}$$

$$\frac{H(m_\chi)s(m_\chi)}{x^4}\frac{dY_\chi}{dx} = 2\big[\phi \leftrightarrow 2\chi\big] + 2\sum_i \big[2N_i \leftrightarrow 2\chi\big]. \tag{10.12}$$

[20] Φ's VEV can be real by redefinition of Φ. Then, $f_{ij}v_\phi$ becomes real diagonal matrix.

N_i is produced from doublet lepton and Higgs in thermal bath. It is also done from inflaton in Scenario C-nt. ϕ and χ are produced from N_i by freeze-in mechanism ($2N_i \to \phi$ and $2N_i \to 2\chi$, respectively) at $T \sim m_\phi$. χ is also produced by the decay of ϕ produced by freeze-in mechanism ($\phi \to 2\chi$).

Next we consider the right-hand side of Boltzmann equations. First, ${\gamma^{N_i}}_{LH,\overline{LH}}$ is given as follows:

$$\gamma^{N_i}{}_{LH,\overline{LH}} = \frac{g_{N_i}}{2\pi^2} m_{N_i}^3 \Gamma_{N_i \to LH,\overline{LH}} (r_{N_i} x)^{-1} K_1(r_{N_i} x), \tag{10.13}$$

$$\Gamma_{N_i \to LH,\overline{LH}} = \sum_a \frac{|y^\nu_{ai}|^2 m_{N_i}}{8\pi}. \tag{10.14}$$

N_i is produced from SM thermal bath via this process.

Second, ${\gamma^\phi}_{2N_i}$ is given as follows:

$$\gamma^\phi{}_{2N_i} = \frac{g_\phi}{2\pi^2} m_\phi^3 \Gamma_{\phi \to 2N_i} (r_\phi x)^{-1} K_1(r_\phi x), \tag{10.15}$$

$$|i\mathcal{M}_{\phi \to 2N_i}|^2 = \sum_{\text{spin}} \left| \overline{u(p_1)} \frac{f_i}{\sqrt{2}} v(p_2) \right|^2 = f_i^2 (m_\phi^2 - 4m_{N_i}^2) \tag{10.16}$$

$$\Gamma_{\phi \to 2N_i} = \frac{1}{32\pi g_\phi m_\phi} \sqrt{1 - \frac{4m_{N_i}^2}{m_\phi^2}} \times f_i^2 (m_\phi^2 - 4m_{N_i}^2) \tag{10.17}$$

$$= \frac{f_i^2 m_\phi}{32\pi g_\phi} \left(1 - \frac{4m_{N_i}^2}{m_\phi^2}\right)^{\frac{3}{2}} \text{ (similar as } \phi \to 2\chi). \tag{10.18}$$

ϕ is produced from N_i via this process at $T \sim m_\phi$, and it decays as $\phi \to 2\chi$. In order to produce ϕ (i.e. χ) as much as the observed DM relic density, Y_{N_i} must be somewhat large at $T \sim m_\phi$. It is realized when m_ϕ is light ($\sim O(10^5)$ GeV) or N_i is non-thermally produced from inflaton.

Third, ${\gamma^\phi}_{2\chi}$ is given as follows:

$$\gamma^\phi{}_{2\chi} = \frac{g_\phi}{2\pi^2} m_\phi^3 \Gamma_{\phi \to 2\chi} (r_\phi x)^{-1} K_1(r_\phi x), \tag{10.19}$$

$$\Gamma_{\phi \to 2\chi} = \frac{1}{g_\phi} \frac{1}{2m_\phi} \frac{1}{2!} \int \frac{d^3 p_1}{2E_1 (2\pi)^3} \int \frac{d^3 p_2}{2E_2 (2\pi)^3} \tag{10.20}$$

$$\times (2\pi)^4 \delta(m_\phi - E_1 - E_2) \delta^3(\mathbf{p}_1 + \mathbf{p}_2) \times |m_\phi^2 / v_\phi|^2 \tag{10.21}$$

$$= \frac{m_\phi^3}{32\pi g_\phi v_\phi^2} \sqrt{1 - \frac{4m_\chi^2}{m_\phi^2}}. \tag{10.22}$$

χ is produced from ϕ via this process (or directly done from N_i via $2N_i \to 2\chi$).

Last, ${\gamma^{2N_i}}_{2\chi}$ can be evaluated by narrow width approximation (See §B.9):

$$ {\gamma^{2N_i}}_{2\chi} \simeq {\gamma^{2N_i}}_{\phi} {B^{\phi}}_{2\chi} = {\gamma^{\phi}}_{2N_i} {B^{\phi}}_{2\chi} \sim {\gamma^{\phi}}_{2N_i}. \tag{10.23} $$

Here, the branching ratio of $\phi \to 2\chi$ is

$$ {B^{\phi}}_{2\chi} = \frac{\Gamma_{\phi\to 2\chi}}{\Gamma_{\phi\to 2\chi} + \sum_i \Gamma_{\phi\to 2N_i}} = \frac{m_\phi^2}{m_\phi^2 + 2\sum_i m_{N_i}^2} \sim 1. \tag{10.24} $$

χ is directly produced from N_i via this process (or indirectly done from $2N_i \to \phi \to 2\chi$). This process occurs at $T \sim m_\phi$. Therefore, in order to produce χ as much as the observed DM relic density, Y_{N_i} must be somewhat large at $T \sim m_\phi$. It is realized when m_ϕ is light ($\sim O(10^5)$ GeV) or N_i is non-thermally produced from inflaton. It is same as indirectly production of χ.

10.2 The approximation formula

Next, we derive the approximation formulae of the present density of χ. We consider two scenarios: N_i is produced by inflaton (non-thermally produced/Scenario C-nt) or Standard Model particles (thermally produced/Scenario C-t).

First, we define $Y_D := Y_\chi + 2Y_\phi + \sum_i Y_{N_i}$. The Boltzmann equation of Y_D is given as follows:

$$ \frac{H(m_\chi)s(m_\chi)}{x^4}\frac{dY_D}{dx} = -\sum_i [N_i \leftrightarrow LH,\, \overline{LH}]. \tag{10.25} $$

Next, we integrate it with the boundary conditions $Y_\phi(\infty) = Y_{N_i}(\infty) = Y_\chi(x_R) = Y_\phi(x_R) = 0$ shown as follows:

$$ \begin{aligned} Y_\chi(\infty) =& Y_D(\infty) && (10.26)\\ =& \sum_i Y_{N_i}(x_R) - \sum_i \frac{1}{H(m_\chi)s(m_\chi)} \int_{x_R}^{\infty} x^4 [N_i \leftrightarrow L_a H,\, \overline{L}_a \overline{H}] && (10.27)\\ =& \sum_i \Big\{ Y_{N_i}(x_R) + \big[Y_{N_i}(\infty) - Y_{N_i}(x_R)\big] && (10.28)\\ & - 2\frac{1}{H(m_\chi)s(m_\chi)} \int_{x_R}^{\infty} x^4 \big([\phi \leftrightarrow 2N_i] - [2N_i \leftrightarrow 2\chi]\big) \Big\} && (10.29)\\ & (\text{Here, we use the Boltzmann equasion of } N_i,) && (10.30)\\ \simeq& -\frac{2}{H(m_\chi)s(m_\chi)} \sum_i \int_{x_R}^{\infty} x^4 \frac{{Y_{N_i}(x)}^2}{{Y_{N_i}^{\rm eq}(x)}^2} \big(-{\gamma^{\phi}}_{2N_i} - {\gamma^{\phi}}_{2N_i} {\rm Br}^{\phi}{}_{2\chi}\big) && (10.31)\\ =& \frac{4}{H(m_\chi)s(m_\chi)} \sum_i \frac{g_\phi m_\phi^3 \Gamma_{\phi\to 2N_i}}{2\pi^2} \int_{x_R}^{\infty} x^4 \frac{{Y_{N_i}(x)}^2}{{Y_{N_i}^{\rm eq}(x)}^2} (r_\phi x)^{-1} K_1(r_\phi x). && (10.32) \end{aligned} $$

In order to evaluate the present DM yield $Y_\chi(\infty)$, we must estimate $Y_{N_i}(x)$.

In Scenario C-nt, $Y_{N_i}(x)$ can be approximated as the initial condition $Y_{N_i}(x_R)$. By using (10.32), the approximation formula for the present yield of χ is given as follows:

$$Y_\chi^{\rm nontherm}(\infty) = \frac{4}{H(m_\chi)s(m_\chi)} \sum_i \frac{g_\phi m_\phi^3 \Gamma_{\phi\to 2N_i}}{2\pi^2} \int_0^\infty x^4 \frac{Y_{N_i}(x_R)^2}{\left(\pi^{-2} g_{N_i} m_\chi^3 s(m_\chi)^{-1}\right)^2} (r_\phi x)^{-1} K_1(r_\phi x) \tag{10.33}$$

$$= \sum_i \frac{3\pi^3 g_\phi s(m_\chi) \Gamma_{\phi\to 2N_i} Y_{N_i}(x_R)^2}{g_{N_i}^2 H(m_\chi) m_\phi^2 m_\chi} \tag{10.34}$$

$$= \frac{\pi^{5/2}}{32\sqrt{5}} \sum_i \frac{|f_i|^2 g_{*S} \left(1 - 4m_{N_i}^2/m_\phi^2\right)^2}{G^{1/2} g_*^{1/2} g_{N_i}^2 m_\phi} Y_{N_i}(x_R)^2. \tag{10.35}$$

Using this formula, we show the parametric region where the present χ density is equal to the DM relic density (Figure 23). For example, when $m_\chi = 6$TeV, $m_\phi = 10^8$GeV and $fY_N(x_R) = 10^{-12}$, the present density of χ is equal to the observed DM relic density. We show the numerical solution for the Boltzmann equations with these parameter, in next subsection.

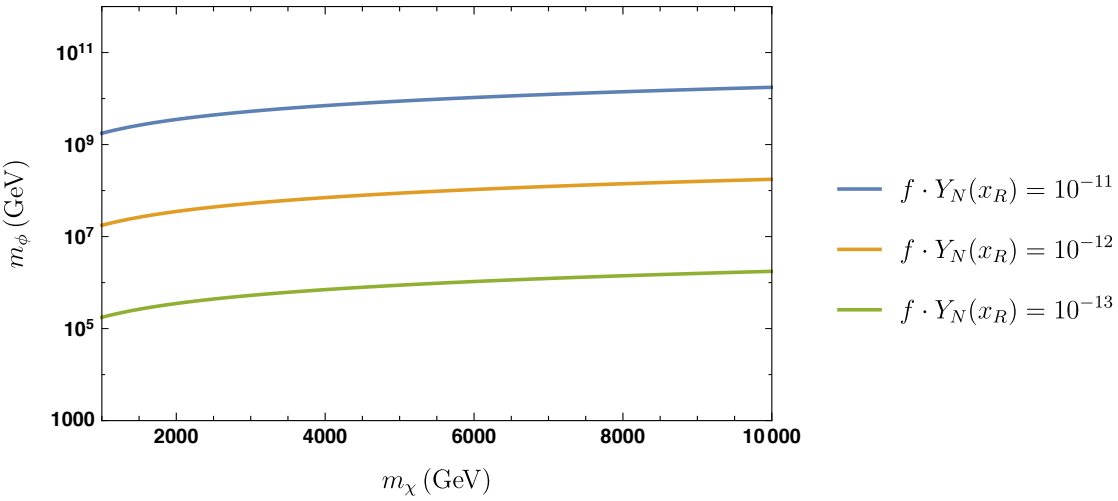

Figure 23: The parametric region where the density of χ is equal to DM relic density. Here, we vary $fY_N(x_R)$ from 10^{-11} to 10^{-13}.

Next we estimate the present yield of χ in Scenario C-t. We can estimate $Y_{N_i}(x)$ by

integrating the Boltzmann equation for N_i as follows:

$$Y_{N_i}^{\mathrm{b,\,therm}}(x) \simeq -\frac{1}{H(m_\chi)s(m_\chi)}\int_{x_R}^{x} x^4[N_i \leftrightarrow LH,\, \overline{LH}] \tag{10.36}$$

$$\simeq +\frac{1}{H(m_\chi)s(m_\chi)}\frac{g_{N_i}m_{N_i}^3\Gamma_{N_i\to LH,\overline{LH}}}{2\pi^2}\int_{x_R}^{x} x^4(r_{N_i}x)^{-1}K_1(r_{N_i}x) \tag{10.37}$$

$$\simeq +\frac{1}{H(m_\chi)s(m_\chi)}\frac{g_{N_i}m_{N_i}^3\Gamma_{N_i\to LH,\overline{LH}}}{2\pi^2} \tag{10.38}$$

$$\times (4r_{N_i}^{-5})\mathrm{Meijer}\big[\{\{1\},\,\{\}\},\,\{\{3/2,\,5/2\},\,\{0\}\},\,(r_{N_i}^2x_i^2)/4\big] \tag{10.39}$$

$$= +\frac{1}{H(m_\chi)s(m_\chi)}\frac{g_{N_i}m_{N_i}^3\Gamma_{N_i\to LH,\overline{LH}}}{2\pi^2}\frac{x^3}{3r_{N_i}^2}+O(x^5). \tag{10.40}$$

Using this formula and (10.32), we can get the approximation formula for $Y_\chi(\infty)$ in Scenario C-t:

$$Y_\chi^{\mathrm{therm}}(\infty) \simeq \frac{4}{H(m_\chi)s(m_\chi)}\sum_i \frac{g_\phi m_\phi^3\Gamma_{\phi\to 2N_i}}{2\pi^2}\int_0^\infty x^4\frac{Y_{N_i}^{\mathrm{b,\,therm}}(x)^2}{\left(\pi^{-2}g_{N_i}m_\chi^3 s_{m_\chi}^{-1}\right)^2}(r_\phi x)^{-1}K_1(r_\phi x) \tag{10.41}$$

$$= \frac{3^7\cdot 5^{9/2}\cdot 7^2}{2^{17}\pi^{21/2}}\sum_i \frac{|f_i|^2 m_{N_i}^4\left(1-\frac{4m_{N_i}^2}{m_\phi^2}\right)^{3/2}\left|\sum_a |y_{ai}^\nu|^2\right|^2}{G^{3/2}g_*^{3/2}g_{*S}m_\phi^7}. \tag{10.42}$$

Using this formula, we show the plot of m_ϕ vs $\Omega_\chi/\Omega_{\mathrm{CDM}}$ (Figure 24). Here, we set the parameters as follows:

$$\begin{aligned} f_1 =& 2\times 10^{-11},\ f_2 = 7\times 10^{-11},\ f_3 = 9\times 10^{-11},\ v_\phi = 10^{15}\mathrm{GeV},\ m_\chi = 6\mathrm{TeV},\\ O =& \begin{pmatrix} \cos(\pi/3) & \sin(\pi/3) & \\ -\sin(\pi/3) & \cos(\pi/3) & \\ & & 1 \end{pmatrix}\begin{pmatrix} 1 & & \\ & \cos(\pi/4) & \sin(\pi/4) \\ & -\sin(\pi/4) & \cos(\pi/4) \end{pmatrix}\\ &\times \begin{pmatrix} \cos(\pi/5) & & \sin(\pi/5) \\ & 1 & \\ -\sin(\pi/5) & & \cos(\pi/5) \end{pmatrix},\ (\mathrm{Casas}-\mathrm{Ibarra\,parametrization.}),\\ m_{\nu_1} =& 0,\ \mathrm{neutrino\,parameter\,is\,normal\,hierarchy.} \end{aligned} \tag{10.43}$$

These parameters are set so that the constraints from cosmic ray experiments can be avoided. In Figure 24, We can see that the present yield of χ is the same as the observed DM relic density when $m_\phi = 10^5$GeV. We show the numerical solution for the Boltzmann equations with these parameters, in next subsection.

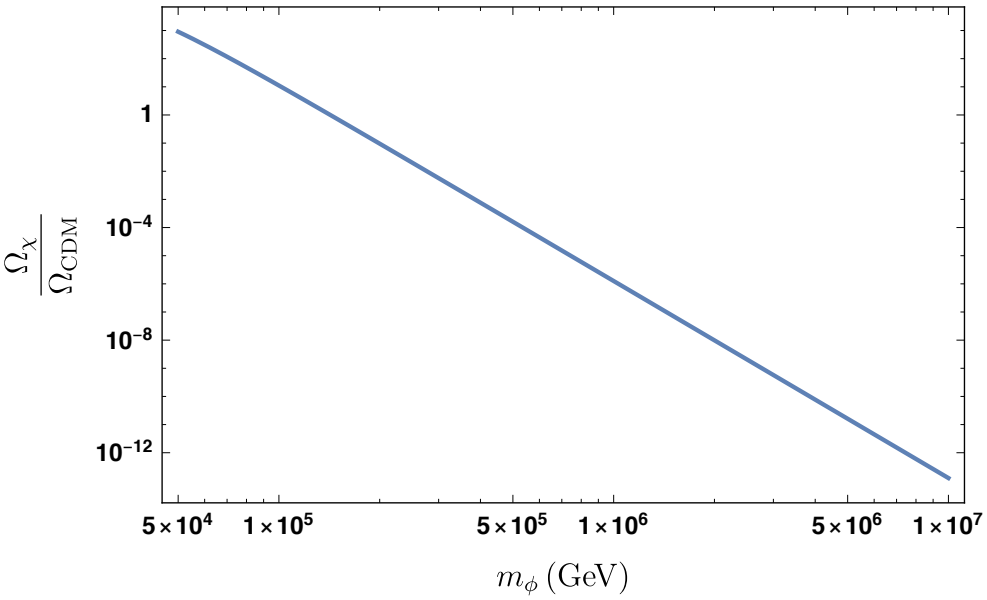

Figure 24: plot of m_ϕ vs $\Omega_\chi/\Omega_{\rm CDM}$. Here, we set the parameters as (10.43). For simplicity, we set i as $i = 1$.

10.3 The numerical solutions for the Boltzmann equations

Using the parameters in (10.43), $m_\phi = 10^8$GeV and the initial condition $Y_N(x_R) = 10^{-12}/f_1$, we estimate the numerical solutions for Boltzmann equation of Scenario C-nt in Figure 25. χ is produced at $T \sim m_\phi$ by the resonant $NN \to \chi\chi$ process. The decay of ϕ also occurs the production of χ.

Using the parameters in (10.43), $m_\phi = 10^5$GeV and the initial condition $Y_N(x_R) = 0$ (thermal N_R production), we estimate the numerical solutions for Boltzmann equation of Scenario C-t in Figure 26. χ is produced by $NN \to \chi\chi$ and $\phi \to \chi\chi$, the same as Figure 25. Both the production of ϕ by $NN \to \phi$ and the one χ by $NN \to \chi\chi$ occur at $T \sim m_\phi$. Therefore, Y_N must be large at $T \sim m_\phi$. This is the reason why ϕ must be light (10^5 GeV) [21].

Combining the above results, both Scenario C-nt and C-t are possible.

11 Summary of Part III

In the above sections, we show that TeV scale Majoron can be produced as much as the observed dark matter relic density. We consider three scenarios.

In Scenario A, we introduce the coupling $m_{ij}\overline{\nu^c_{Ri}}\nu_{Rj}$ which softly breaks the Lepton number symmetry. These couplings occur the $N_2 \to N_1\chi$ process, then, the Majoron

[21] When N is non-thermally produced, ϕ can have heavy mass, shown as Figure 23

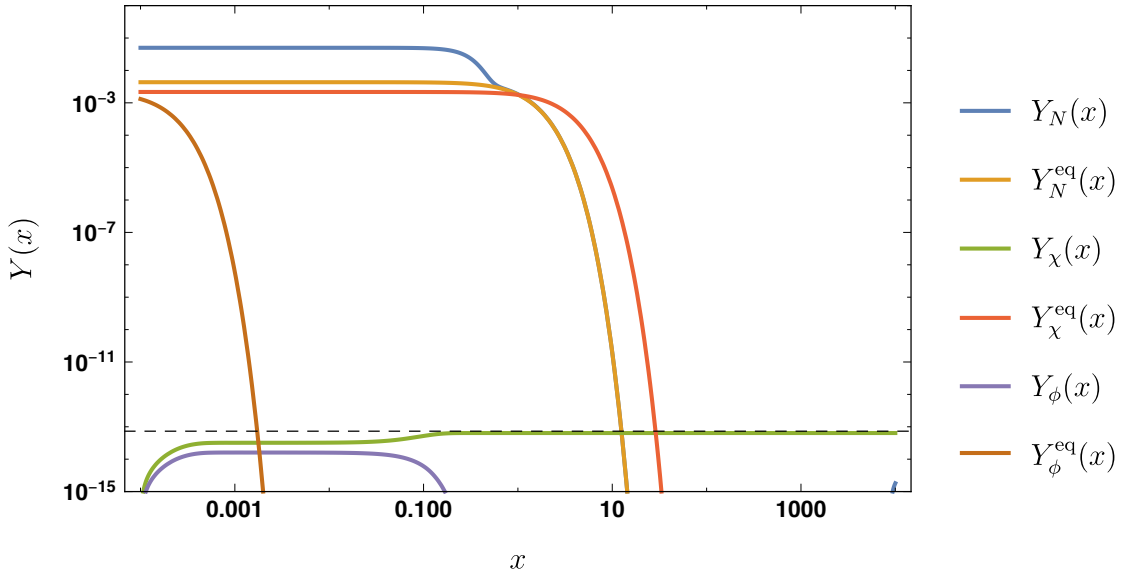

Figure 25: The solution for the Boltzmann equations in Scenario C-nt. Dashed line is the observed DM relic density.

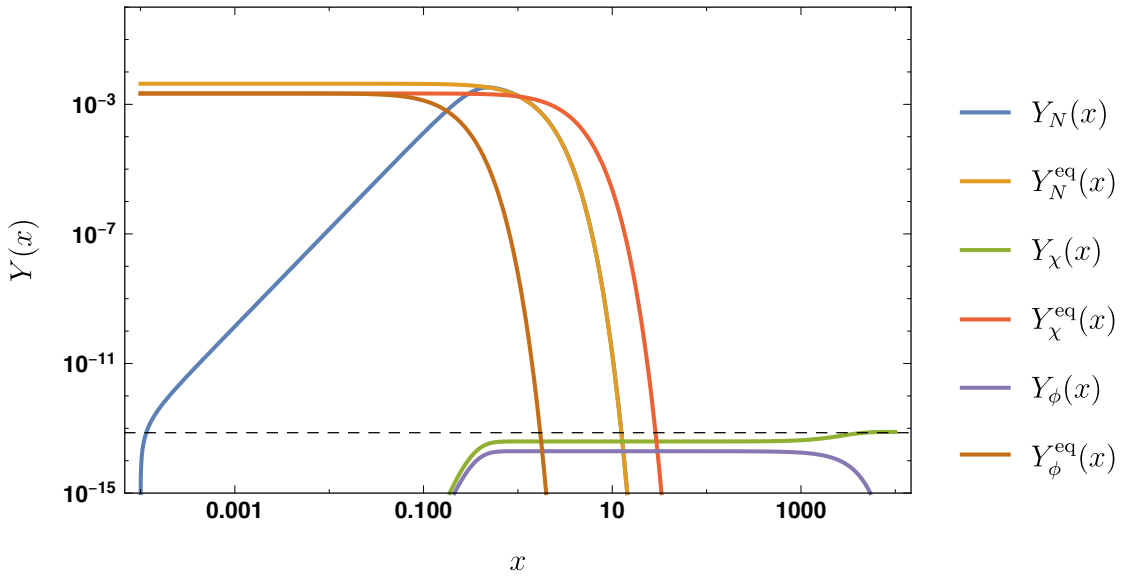

Figure 26: The solution for the Boltzmann equations of Scenario C-t. Dashed line is the observed DM relic density.

can be produced via this process.

In Scenario B, the Majoron can be produced via $HH^\dagger \to \chi\chi$. These couplings are weak because χ is pseudo Nambu Goldstone boson, therefore, we use the UV freeze-in mechanism.

In Scenario C, the Majoron can be produced via $NN \to \phi \to \chi\chi$ processes. In this scenario, χ and ϕ are produced at $T \sim m_\phi$. Y_N must be large at this temperature so that Majoron is produced as much as the observed DM relic density. When N is non-thermally produced (Scenario C-nt) or $m_\chi \sim O(10^5)$ GeV (Scenario C-t), Y_N can be large at $T \sim m_\chi$.

In all of these scenarios, we can see that Majoron is produced as much as the observed DM relic density.

Part IV
The QCD axion and the lepton number symmetry

12 The strong CP problem and the QCD axion models

In this section, we briefly explain the strong CP problem and the QCD axion models. See [157, 158] for a detailed review of these themes.

12.1 The strong CP problem

The standard model has the following theta terms: [22]

$$\mathcal{L}_{\rm SM} \supset \frac{\theta_2 g^2}{16\pi^2}{\rm Tr}W\tilde{W} + \frac{\theta_3 g_s^2}{16\pi^2}{\rm Tr}G\tilde{G}. \tag{12.1}$$

We can set $\theta_2 = 0$ by Baryon number transformation, however cannot set $\theta_3 = 0$. We would naively expect that θ_3 has $O(1)$ value.

On the other hand, the neutron electric dipole moment depends on θ_3:

$$d_n = 2.4(1.0) \times 10^{-16}\theta_3\, e\cdot{\rm cm}. \tag{12.2}$$

Here we use the results from QCD sum-rules [159]. There are different methods to estimate the neutron EDM: chiral perturbation theory: [160–162], holography [163] and lattice QCD [164, 165]. The latest constraint for d_n is given by [166]:

$$|d_n| < 1.8 \times 10^{-26} e\cdot{\rm cm}. \tag{12.3}$$

Therefore, θ_3 is unnaturally small: $|\theta_3| < 10^{-10}$. This smallness is called as "strong CP problem".

QCD axion model is the well-known solution for the strong CP model. We explain this model in next subsection.

12.2 The QCD axion models

12.2.1 Peccei-Quinn-Weinberg-Wilczek (PQWW) axion model

In this section, we explain the QCD axion models.

[22] $\tilde{X}_{\mu\nu} = \frac{1}{2}\epsilon_{\mu\nu\rho\sigma}X^{\rho\sigma}$

PQWW axion model [167–170] is the original model of axion. The Yukawa couplings of PQWW axion are given as follows:

$$\mathcal{L} \supset - y_u \overline{Q}_L u_R \tilde{H}_1 - y_d \overline{Q}_L d_R H_2 - y_e \overline{L} e_R H_2 + \text{H.c.} \tag{12.4}$$

Here, H_1 and H_2 are different Higgs particles. When these get nonzero electro-weak VEVs, $H_{1,2}$ are written as follows:

$$H_1 = \begin{pmatrix} \frac{v_1 G^+ - v_2 A^+}{v} \\ \frac{v_1+h_1}{\sqrt{2}} \exp \frac{i(v_1 g^0 - v_2 a)}{v_1 v} \end{pmatrix}, \; H_2 = \begin{pmatrix} \frac{v_2 G^+ + v_1 A^+}{v} \\ \frac{v_2+h_2}{\sqrt{2}} \exp \frac{i(v_2 g^0 + v_1 a)}{v_2 v} \end{pmatrix}, \; v = \sqrt{v_1^2 + v_2^2}. \tag{12.5}$$

This Model has the following symmetry:

$$Q_L \to e^{i\alpha_{QL}} Q_L, \; u_R \to e^{i\alpha_{uR}} u_R, \; d_R \to e^{i\alpha_{dR}} d_R, \; L \to e^{i\alpha_L} L, \tag{12.6}$$

$$e_R \to e^{i\alpha_{eR}} e_R, \; H_1 \to e^{i\alpha_1} H_1, \; H_2 \to e^{i\alpha_2} H_2, \tag{12.7}$$

$$0 = -\alpha_{QL} + \alpha_{uR} - \alpha_1, \; 0 = -\alpha_{QL} + \alpha_{dR} + \alpha_2, \tag{12.8}$$

$$0 = -\alpha_L + \alpha_{eR} + \alpha_2, \; \alpha_1 = -\alpha v_2/v_1, \; \alpha_2 = +\alpha v_1/v_2. \tag{12.9}$$

This symmetry is called as "Peccei-Quinn (PQ) symmetry". This is broken by electro-weak VEVs, and its (pseudo) NG boson is called as "axion".

By the redefinition: $u \to e^{-iv_2 a\gamma^5/(2v_1 v)} u$, $d \to e^{-iv_1 a\gamma^5/(2v_2 v)} d$, $e \to e^{-iv_1 a\gamma^5/(2v_2 v)} e$, we can derive the effective couplings of $a\mathrm{Tr}G\tilde{G}$ ($N_g(=3)$: the number of generation):

$$\mathcal{L} \supset \frac{g_s^2}{16\pi^2} \left[\theta - (v_1/v_2 + v_2/v_1) N_g \frac{a}{v} \right] \mathrm{Tr} G\tilde{G}. \tag{12.10}$$

Then, the energy density of axion potential is written as follows:

$$V(a) = \Lambda^4 \Big\{ 1 - \cos \left[\theta - (v_1/v_2 + v_2/v_1) N_g \frac{a}{v} \right] \Big\}. \tag{12.11}$$

Therefore, the VEV of axion is $\langle a \rangle = \theta(v_1/v_2 + v_2/v_1)/v$. Then, QCD theta term becomes zero:

$$\mathcal{L} \supset \frac{g_s^2}{16\pi^2} \left[\theta - N_g (v_1/v_2 + v_2/v_1) \frac{a}{v} \right] \mathrm{Tr} G\tilde{G} \to 0. \tag{12.12}$$

Therefore, the strong CP problem can be solved.

Next, we consider the coupling between axion and SM particles. By redefinition: $u \to e^{-iv_2 a\gamma^5/(2v_1 v)} u$, $d \to e^{-iv_1 a\gamma^5/(2v_2 v)} d$, $e \to e^{-iv_1 a\gamma^5/(2v_2 v)} e$, we can derive the couplings

between axion and SM particles: [23]

$$\mathcal{L} \supset \mathcal{L}_{au} + \mathcal{L}_{ad} + \mathcal{L}_{ae}, \tag{12.13}$$

$$\mathcal{L}_{au} = \frac{v_2}{2v_1 v}\partial_\mu a \bar{u}\gamma^\mu\gamma^5 u - \frac{e^2}{8\pi^2}\Big(+\frac{2}{3}\Big)^2 \cdot 3 \cdot N_g \frac{v_2}{2v_1 v} a F\tilde{F}, \tag{12.14}$$

$$\mathcal{L}_{ad} = \frac{v_1}{2v_2 v}\partial_\mu a \bar{d}\gamma^\mu\gamma^5 d - \frac{e^2}{8\pi^2}\Big(-\frac{1}{3}\Big)^2 \cdot 3 \cdot N_g \frac{v_1}{2v_2 v} a F\tilde{F}, \tag{12.15}$$

$$\mathcal{L}_{ae} = \frac{v_1}{2v_2 v}\partial_\mu a \bar{e}\gamma^\mu\gamma^5 e - \frac{e^2}{8\pi^2}(-1)^2 \cdot N_g \frac{v_1}{2v_2 v} a F\tilde{F}. \tag{12.16}$$

These couplings correspond to c_q^0 and $g_{a\gamma}^0$ in §C.2. f_a in §C.2 is given as $f_a^{-1} = (v_1/v_2 + v_2/v_1)N_g/v$ in this model.

The couplings c_q and $g_{a\gamma}$ [24] in PQWW model are given as $c_q = c_q^0 - Q_a$, $g_{a\gamma} = g_{a\gamma}^0 + \frac{e^2}{4\pi^2 f_a} N_c \mathrm{Tr} Q^2 Q_a$. These couplings are $O(v^{-1})$, because PQ symmetry is broken by electro-weak VEV. Therefore, PQWW axion model is ruled out by the axion experiments (please see §12.3 for a detail).

12.2.2 Kim-Shifman-Vainshtein-Zakharov (KSVZ) model

Next, we explain the invisible axion models. In these models, PQ symmetry is broken by the large VEV, and the axion-SM-SM couplings are suppressed by it. We can avoid the constraint by the axion experiments.

Kim-Shifman-Vainshtein-Zakharov (KSVZ) model [171,172] and Dine-Fischler-Srednicki-Zhitnitsky (DFSZ) models [173, 174] are well-known invisible axion models.

First, we explain KSVZ model. KSVZ model contains colored Fermions: Ψ_L, $\Psi_R \in (\mathbf{3}, \mathbf{1}, +y)$, and complex scalar S. These particles have PQ charges: $\mathrm{PQ}\Psi_L = -x\Psi_L$, $\mathrm{PQ}\Psi_R = -(x+1)\Psi_R$, $\mathrm{PQ}S = +S$. PQ symmetry is broken by the VEV of $S\big(= \frac{1}{\sqrt{2}}(f_a + \rho)e^{ia/f_a}\big)$. The Yukawa coupling of KSVZ axion models is given as follows:

$$\mathcal{L} \supset -yS\overline{\Psi_L}\Psi_R + \mathrm{H.c.} \tag{12.17}$$

By the redefinition $\Psi_R \to e^{-ia/f_a}\Psi_R = e^{-ia\gamma^5/f_a}\Psi_R$, the effective coupling of $a\mathrm{Tr}G\tilde{G}$ is given as follows:

$$\mathcal{L} \supset \frac{g_s^2}{16\pi^2}\Big[\theta - \frac{a}{f_a}\Big]\mathrm{Tr}G\tilde{G}. \tag{12.18}$$

Then, the strong CP problem is solved as PQWW axion model.

The axion-gluon-gluon coupling is suppressed by $f_a (\sim O(10^{8-12})\mathrm{GeV})$. It occurs axion-nucleon-nucleon coupling g_{aNN} as §C.2, and it is also suppressed by f_a.

In §12.3, we explain the experimental constraint on them.

[23] Here, we omit $a\mathrm{Tr}G\tilde{G}$ term.

[24] They are defined in §C.2.

12.2.3 Dine-Fischler-Srednicki-Zhitnitsky (DFSZ) model

Next, we explain DFSZ model [173,174]. DFSZ model is similar as PQWW axion model. The Yukawa couplings of DFSZ axion are given as follows:

$$\mathcal{L} \supset - y_u \overline{Q}_L u_R \tilde{H}_1 - y_d \overline{Q}_L d_R H_2 - y_e \overline{L} e_R H_2 - \kappa (S^\dagger)^2 H_1^\dagger H_2 + \text{H.c.} \tag{12.19}$$

H_1, H_2, S are written as follows:

$$H_1 = \begin{pmatrix} \frac{v_1 G^+ - v_2 A^+}{v} \\ \frac{v_1+\rho_1}{\sqrt{2}} e^{\frac{i}{v_1}(v_1 G_0 - v_2 A_0)/v} \end{pmatrix}, \; H_2 = \begin{pmatrix} \frac{v_2 G^+ + v_1 A^+}{v} \\ \frac{v_2+\rho_2}{\sqrt{2}} e^{\frac{i}{v_2}(v_2 G_0 + v_1 A_0)/v} \end{pmatrix}, \tag{12.20}$$

$$S = \frac{f_a + s}{\sqrt{2}} e^{i\chi_0/f_a}, \; v = \sqrt{v_1^2 + v_2^2}. \tag{12.21}$$

This Model has the following symmetry:

$$Q_L \to e^{i\alpha_{QL}} Q_L, \; u_R \to e^{i\alpha_{uR}} u_R, \; d_R \to e^{i\alpha_{dR}} d_R, \; L \to e^{i\alpha_L} L, \tag{12.22}$$

$$e_R \to e^{i\alpha_{eR}} e_R, \; H_1 \to e^{i\alpha_1} H_1, \; H_2 \to e^{i\alpha_2} H_2, \; S \to e^{i\alpha} S \tag{12.23}$$

$$0 = -\alpha_{QL} + \alpha_{uR} - \alpha_1, \; 0 = -\alpha_{QL} + \alpha_{dR} + \alpha_2, \tag{12.24}$$

$$0 = -\alpha_L + \alpha_{eR} + \alpha_2, \; \alpha_1/\alpha_2 = -v_2^2/v_1^2, \; 0 = -2\alpha - \alpha_1 + \alpha_2. \tag{12.25}$$

Therefore, $\alpha_1 = -\frac{2v_2^2}{v_1^2+v_2^2}\alpha$, $\alpha_2 = \frac{2v_1^2}{v_1^2+v_2^2}\alpha$. PQ transformation shift χ_0 and A_0 as follows:

$$\chi_0 \to \chi_0 + \alpha f_a, \tag{12.26}$$

$$A_0 \to A_0 - \frac{v_1 v}{v_2}\alpha_1 = A_0 + \frac{2v_1 v_2}{v}\alpha, \tag{12.27}$$

$$\left(A_0 \to A_0 + \frac{v_2 v}{v_1}\alpha_2 = A_0 + \frac{2v_1 v_2}{v}\alpha. \right) \tag{12.28}$$

Therefore, axion a and other CP odd scalar A' are defined as follows:

$$\chi_0 = \frac{f_a v}{\sqrt{(f_a v)^2 + (2v_1 v_2)^2}} a + \frac{2v_1 v_2}{\sqrt{(f_a v)^2 + (2v_1 v_2)^2}} A_0' \tag{12.29}$$

$$A_0 = \frac{2v_1 v_2}{\sqrt{(f_a v)^2 + (2v_1 v_2)^2}} a - \frac{f_a v}{\sqrt{(f_a v)^2 + (2v_1 v_2)^2}} A_0'. \tag{12.30}$$

By the redefinition (after the electro-weak symmetry breaking):

$$u \to e^{-i\alpha_u \gamma^5} u, \; d \to e^{-i\alpha_d \gamma^5} d, \; e \to e^{-i\alpha_\ell \gamma^5} e, \; \nu_L \to e^{-i\alpha_\ell \gamma^5} \nu_L \tag{12.31}$$

$$\alpha_u = + \frac{v_2^2}{v^2}\frac{a}{f_a}, \; \alpha_d = \alpha_\ell = + \frac{v_1^2}{v^2}\frac{a}{f_a}, \tag{12.32}$$

we can derive axion-SM-SM coupling: [25]

$$\mathcal{L} \supset \mathcal{L}_{au} + \mathcal{L}_{ad} + \mathcal{L}_{ae}, \tag{12.33}$$

$$\mathcal{L}_{au} = \frac{v_2^2}{v^2}\frac{\partial_\mu a}{f_a}\overline{u}\gamma^\mu\gamma^5 u - \frac{e^2}{8\pi^2}\Big(+\frac{2}{3}\Big)^2 \cdot 3 \cdot N_g \frac{v_2^2}{v^2}\frac{a}{f_a}F\tilde{F}, \tag{12.34}$$

$$\mathcal{L}_{ad} = \frac{v_1^2}{v^2}\frac{\partial_\mu a}{f_a}\overline{d}\gamma^\mu\gamma^5 d - \frac{e^2}{8\pi^2}\Big(-\frac{1}{3}\Big)^2 \cdot 3 \cdot N_g \frac{v_1^2}{v^2}\frac{a}{f_a}F\tilde{F}, \tag{12.35}$$

$$\mathcal{L}_{ae} = \frac{v_1^2}{v^2}\frac{\partial_\mu a}{f_a}\overline{e}\gamma^\mu\gamma^5 e - \frac{e^2}{8\pi^2}(-1)^2 \cdot N_g \frac{v_1^2}{v^2}\frac{a}{f_a}F\tilde{F}. \tag{12.36}$$

These couplings correspond to c_q^0 and $g_{a\gamma}^0$ in §C.2. f_a in §C.2 is given as $f_a^{-1} \to N_g f_a^{-1}$ in this model. The couplings c_q and $g_{a\gamma}$ [26] in PQWW model are given as $c_q = c_q^0 - Q_a$, $g_{a\gamma} = g_{a\gamma}^0 + \frac{e^2}{4\pi^2(f_a/N_g)} N_c \mathrm{Tr} Q^2 Q_a$. Furthermore, there are axion-nucleon-nucleon couplings g_{aNN} as §C.2, and they are suppressed by f_a. In §12.3, we explain the experimental constraint on them.

12.3 The experimental constraints on the couplings between the QCD axion and the SM particles

In this section, we explain the experimental constraints on the couplings between axion and standard model particles.

We define these couplings as follows:

$$\mathcal{L}_{aff} = \frac{g_{aff}}{2m_f}(\partial_\mu a)\overline{f}\gamma^\mu\gamma^5 f,\ \mathcal{L}_{a\gamma\gamma} = -\frac{g_{a\gamma\gamma}}{4}aF\tilde{F}. \tag{12.37}$$

$g_{a\gamma\gamma}$ is constrained by the axion helioscope (CAST [175]): $g_{a\gamma\gamma} < 6.6 \times 10^{-11}\mathrm{GeV}^{-1}$ for $m_a < 0.02$ eV, the haloscopes (ADMX [176–178]): $m_a < 1.9\mu$eV or $3.53\mu\mathrm{eV} < m_a$, and the horizontal branch (HB) [179, 180]: $g_{a\gamma\gamma} < 6.6 \times 10^{-11}$. We show the constraints on $g_{a\gamma\gamma}$ in Figure 27 and 28. g_{ann} is constrained by neutron star [182]: $g_{ann}^2 < 7.7 \times 10^{-20}$. We show the constraints on g_{ann} in Figure 29. g_{app} is constrained by neutron star [183]: $g_{app}^2 + 1.6 g_{ann}^2 < 1 \times 10^{-18}$. We show the constraints on g_{app} in Figure 30. g_{aee} is constrained by the red giants [184]: $|g_{aee}| < 4.3 \times 10^{-13}$, the white dwarf [185]: $|g_{aee}| < 2.8 \times 10^{-13}$. We show the constraints on g_{aee} in Figure 31. PQ scale f_a is restricted by these constraints: $f_a > O(10^9)$ GeV.

Axion behaves as dark matter. The relic density is given as follows [181, 186]:

$$\Omega h^2 \simeq \begin{cases} 0.12\Big(\frac{f_a}{1.92\times 10^{11}\mathrm{GeV}}\Big)^{1.165}, \text{(PQ is broken after reheating)} \\ 0.12 \cdot \theta^2\Big(\frac{f_a}{9\times 10^{11}\mathrm{GeV}}\Big)^{1.165}, \text{(PQ is broken before reheating)} \end{cases}. \tag{12.38}$$

[25] Here, we omit $a\mathrm{Tr}G\tilde{G}$ term.

[26] They are defined in §C.2.

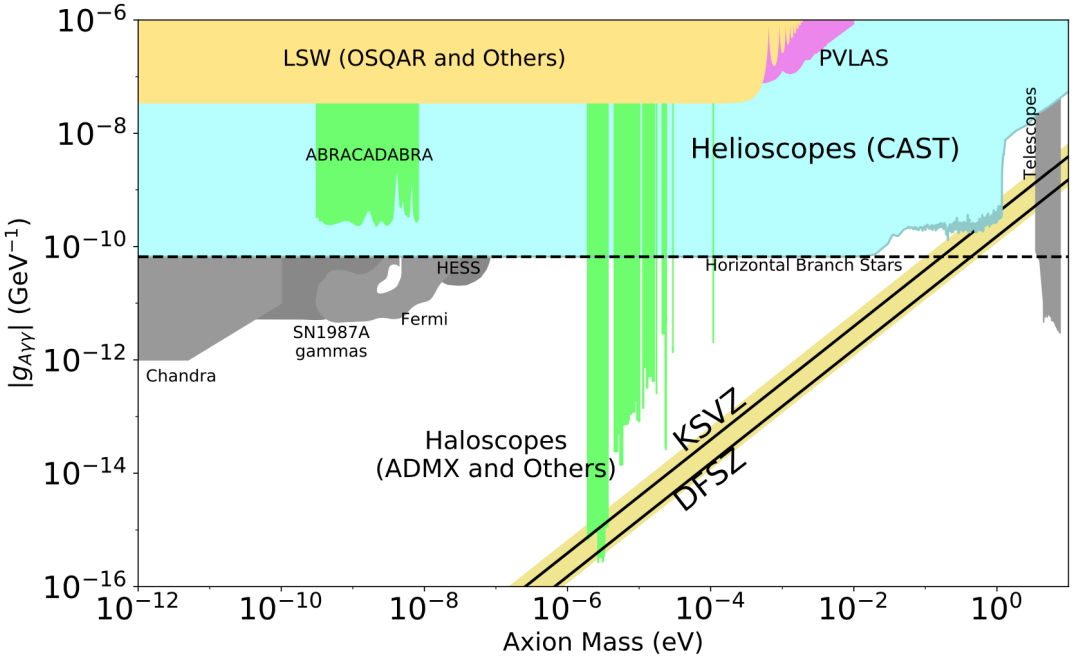

Figure 27: The experimental constraints on $g_{a\gamma\gamma}$ [181].

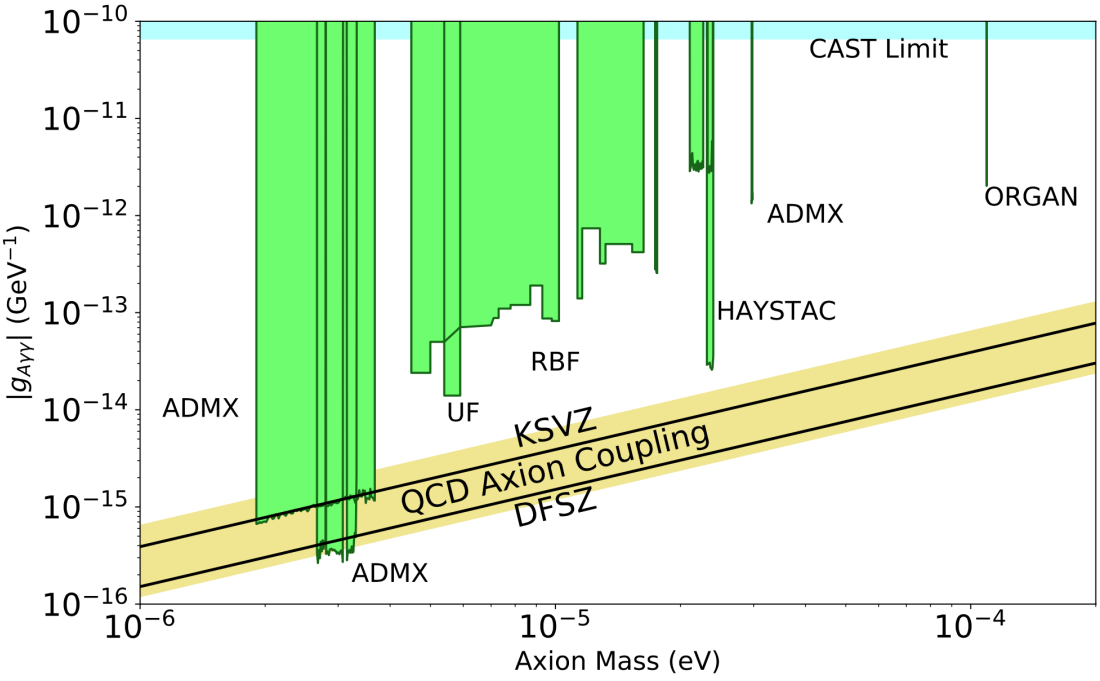

Figure 28: The experimental constraints on $g_{a\gamma\gamma}$ by the haloscopes [181].

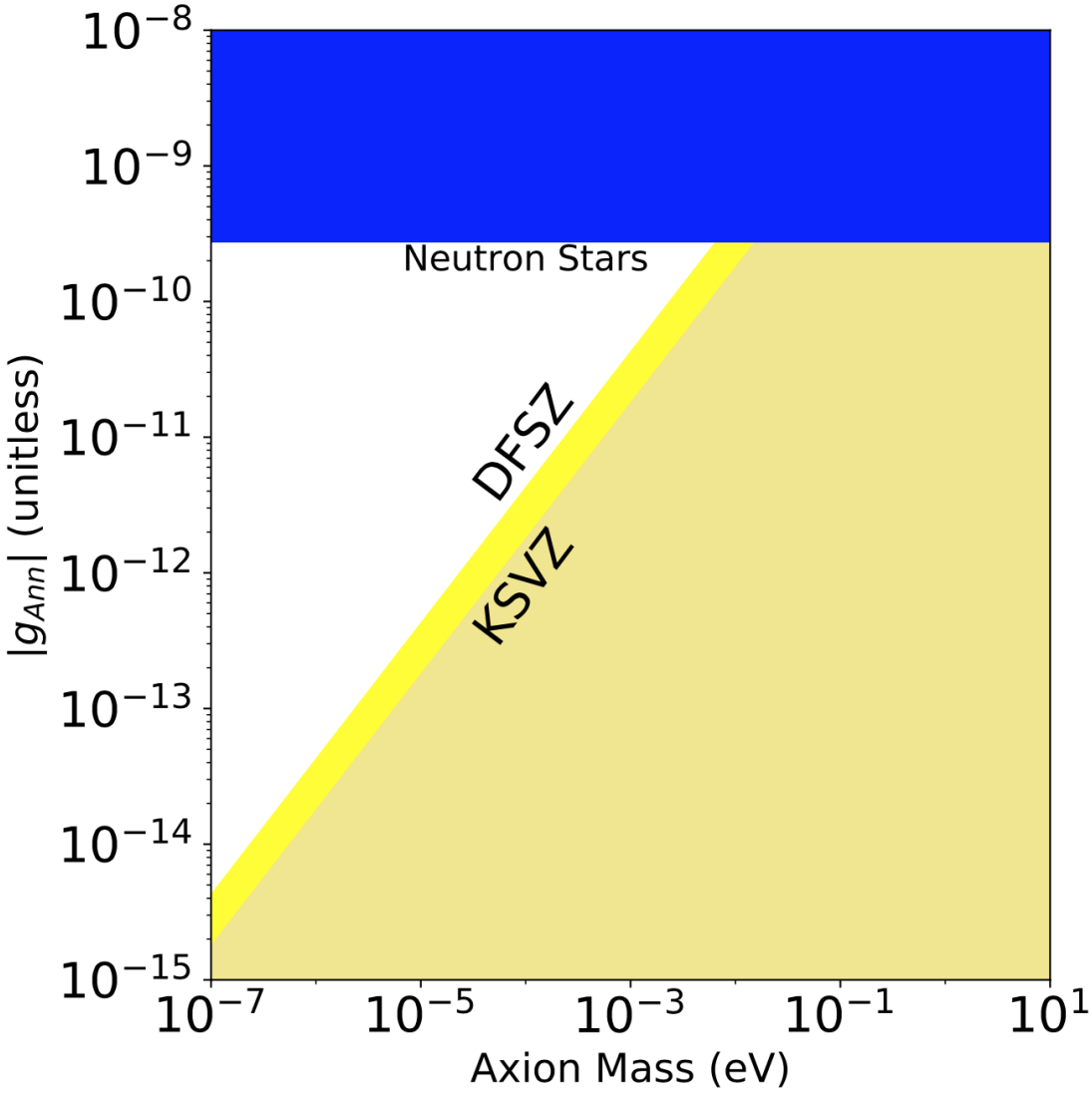

Figure 29: The experimental constraints on g_{ann} [181].

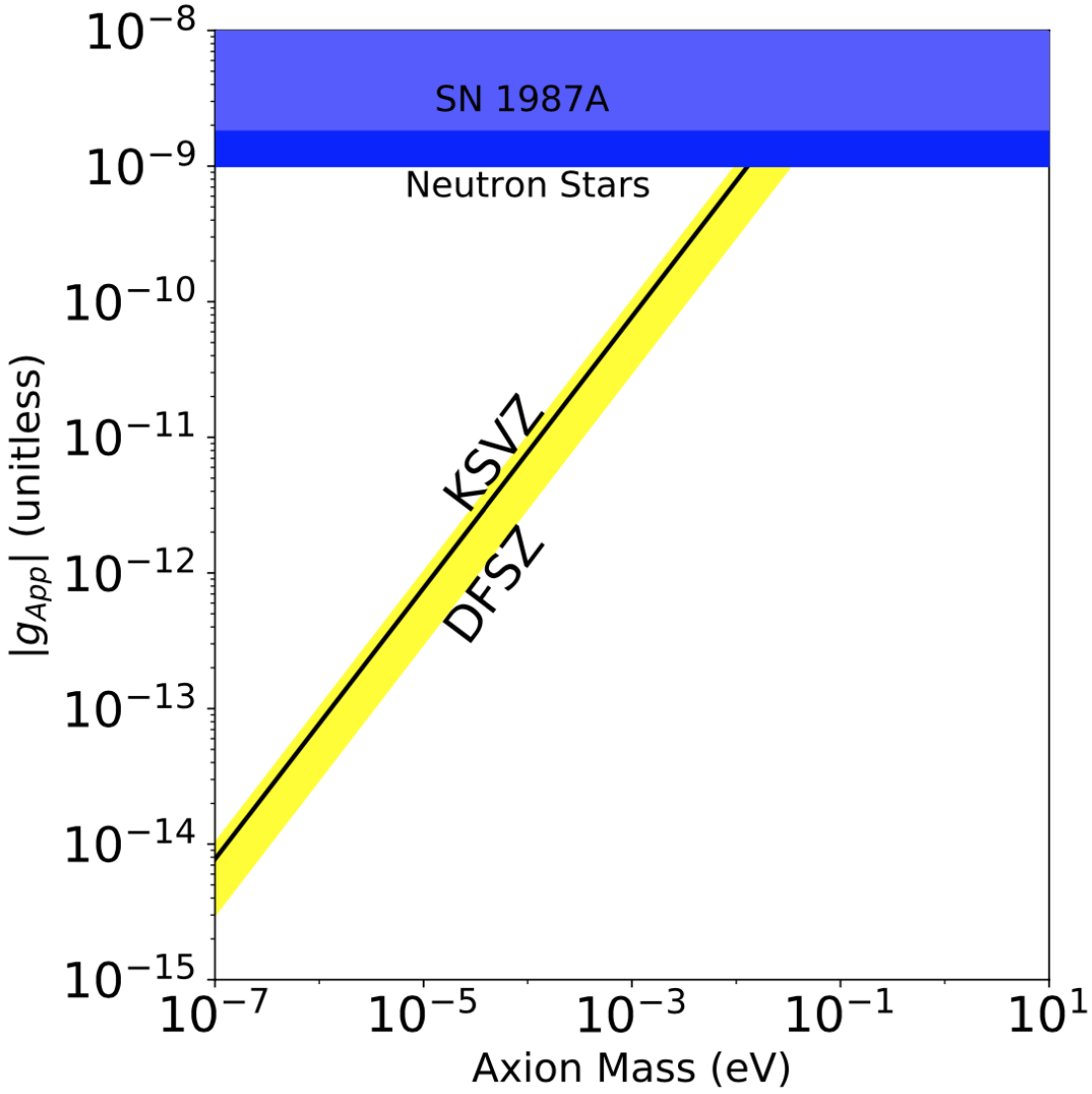

Figure 30: The experimental constraints on g_{app} [181].

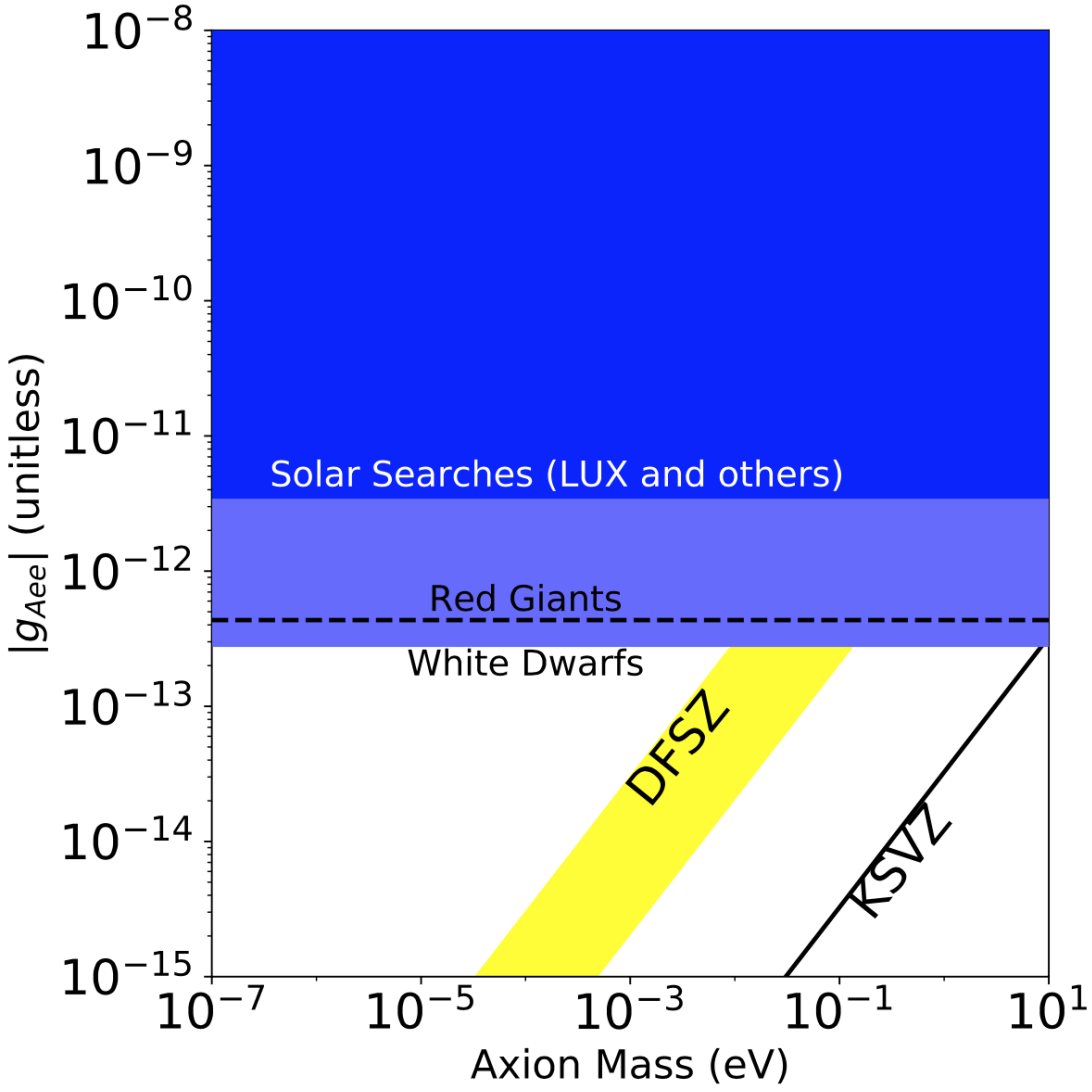

Figure 31: The experimental constraints on g_{aee} [181].

Therefore, f_a must be $f_a < O(10^{12})$GeV when $\theta \sim O(1)$.

Please see [157, 181] for a detailed review of axion experiments.

field	$SU(3)_C$	$SU(2)_L$	$U(1)_Y$	$U(1)_L$	spin
L	**1**	**2**	$-1/2$	$+1$	$1/2$
e_R	**1**	**1**	-1	$+1$	$1/2$
H	**1**	**2**	$+1/2$	$+0$	0
N_R	**1**	**1**	$+0$	$+1$	$1/2$
Ψ_L	**3**	**1**	$+x$	$+x$	$1/2$
Ψ_R	**3**	**1**	$+x$	$+(x-2)$	$1/2$
σ	**1**	**1**	$+0$	$+2$	0

Table 4: The particle contents in [187]

13 The relationship between the neutrino oscillation and the strong CP problem

Axion is NG boson of PQ symmetry. In this section, we show the relationship between neutrino oscillation and the strong CP problem.

Neutrino oscillations are detected by experiments using solar [7–17], atmospheric [19–21], reactor [23–29] and accelerator [30–35] neutrinos. There are two well-known methods which explain neutrino oscillation: "Dirac mass method" and "Majorana mass method". In Majorana mass method, neutrino masses are explained by the following dimension-5 effective operator:

$$\mathcal{L} \subset -\frac{1}{\Lambda}\overline{L^c}H\tilde{H}^\dagger L + \text{H.c.} \tag{13.1}$$

This operator breaks lepton number symmetry. In Majoron model [51,52], this symmetry breaking is explained by VEV of a complex scalar field. This model contains the NG boson of the lepton number symmetry breaking, called as "Majoron".

We can identify the lepton number symmetry and Majoron with the PQ symmetry and axion.

In [187], the axion in KSVZ model is identified as Majoron. The particle contents in [187] are shown in Table 4. In this model, both the masses of right-handed neutrino N_R and vector-like heavy quark Ψ are generated by the VEV of $\sigma(=(v_\sigma+\rho_\sigma)e^{ia/v_\sigma}/\sqrt{2})$. The field a works as axion, as KSVZ axion model. Furthermore, left-handed neutrino gains Majorana mass, as Type I seesaw model.

There are other models in which lepton number symmetry is identified as PQ symmetry (early researches [188–191] motivated by GUT, ones [186,187,191–200] by Type I seesaw, ones [201,202] by Zee Model, ones [203–207] by Type II (III) and other radiative seesaw models and ones by Dirac masses [208–211]). They are summarized in [157].

Next section, we construct the minimal model with $L = PQ$.

14 The minimal $L = PQ$ model

14.1 The identification of the colored fermion in the radiative seesaw model with the heavy quark in KSVZ axion model

KSVZ axion model contains heavy quark. Seesaw model also contains BSM heavy fermion (for example, N_R in type I seesaw). In order to construct minimal model with $L = PQ$, we identify heavy quark in KSVZ axion model with heavy fermion in seesaw model.

There are some radiative seesaw model with colored fermion [212–217]. [27] In this section, we identify the octet colored fermion in [212] as the colored heavy fermion in axion model. The particle contents of [212] are color-octet fermion $\Psi_R \in (\mathbf{8}, \mathbf{1}, +0)$ and complex doublet scalar $\eta \in (\mathbf{8}, \mathbf{2}, +1/2)$. In this model, neutrinos gain one-loop Majorana mass, as the scotogenic model [50]. In order to reconstruct this model as axion model, we introduce new complex scalar S, and give the Majorana mass of Ψ_R by the VEV of S. The axion model with color-octet Majorana Fermion is considered in [219]. We call the model constructed here as "Ma-xion model".

14.2 The field contents and the interactions in Ma-xion model

The field contents of Ma-xion model is shown in Table 5. The Yukawa couplings in

field	$SU(3)_C$	$SU(2)_L$	$U(1)_Y$	$U(1)_{\rm L} = U(1)_{\rm PQ}$	spin
Ψ_R	$\mathbf{8}$	$\mathbf{1}$	$+0$	$+1$	$1/2$
Φ	$\mathbf{8}$	$\mathbf{2}$	$+1/2$	$+0$	0
S	$\mathbf{1}$	$\mathbf{1}$	$+0$	-2	0

Table 5: The particle contents in Ma-xion model.

Ma-xion model are shown as follows:

$$\mathcal{L}_{Q\Phi q_R} = g_u^{ij}\,\overline{Q_i}\,\widetilde{\Phi^A}\,T^A\,u_{jR} + g_d^{ij}\,\overline{Q_i}\,\Phi^A\,T^A\,d_{jR} + \text{H.c.} \tag{14.1}$$

$$\mathcal{L}_{L\Phi\Psi_R} = h_\Psi^{ij}\widetilde{\Phi}^{A\dagger}\overline{\Psi_{jR}^A}L_i + \text{H.c.} \tag{14.2}$$

$$\mathcal{L}_{S\Psi_R\Psi_R} = -\frac{1}{2}\,y_\Psi^i\,S\,\overline{(\Psi_{iR}^A)^c}\Psi_{iR}^A + \text{H.c.} \tag{14.3}$$

The coupling g_u^{ij} and g_d^{ij} may occur FCNC processes. Here, we set these couplings as zero, for simplicity.

[27] For detail of them, please see §5.4 in [218].

Scalar potential in Ma-xion model is given as follows:

$$\begin{aligned} V =& -\mu^2 H^\dagger H - \mu_S^2 S^\star S + M_\Phi^2 \Phi^{A\dagger}\Phi^A + \lambda (H^\dagger H)^2 \\ &+ \lambda_S (S^\star S)^2 + \lambda_{SH}(S^\star S)(H^\dagger H) + \lambda_{S\Phi}(S^\star S)\Phi^{A\dagger}\Phi^A \\ &+ \lambda_3 (H^\dagger H)\Phi^{A\dagger}\Phi^A + \lambda_4 |H^\dagger \Phi|^2 + \frac{1}{2}\Big\{\lambda_5 (H^\dagger \Phi^A)^2 + \text{H.c.}\Big\} + \cdots \end{aligned} \tag{14.4}$$

We set the parameters of scalar potential so that S gains nonzero VEV: $S = \frac{1}{\sqrt{2}}(f_a + \rho)e^{ia/f_a}$. It breaks lepton number symmetry (=PQ symmetry). After that, Ψ_R gains Majorana mass: $M_{\Psi_i} = y_\Psi^i \langle S\rangle = y_\Psi^i f_a/\sqrt{2}$ and the angular part of S works as axion. $\Phi^A = \begin{pmatrix} H^{+A} \\ (H^A + i\, A^A)/\sqrt{2} \end{pmatrix}$ gains the following masses after electro-weak symmetry breaking:

$$M_{H,A}^2 = M_\Phi^2 + \frac{1}{2}\lambda_{S\Phi} f_a^2 + \frac{1}{2}(\lambda_3 + \lambda_4 \pm \lambda_5) v^2 \tag{14.5}$$

$$M_{H^\pm}^2 = M_\Phi^2 + \frac{1}{2}\lambda_{S\Phi} f_a^2 + \frac{1}{2}\lambda_3 v^2 \tag{14.6}$$

14.3 The interactions between the QCD axion and the SM particles, and the constraints on them

By the redefinition $\Psi_R^A \to e^{-i\frac{a(x)}{2f_a}\gamma^5}\Psi_R^A$, $L \to e^{+i\frac{a(x)}{2f_a}\gamma^5} L$, $e_R \to e^{-i\frac{a(x)}{2f_a}\gamma^5} e_R$, we can derive the axion-gluon-gluon coupling: [28]

$$\mathcal{L} \supset \frac{g_s^2}{16\pi^2}\Big(\theta \text{Tr} T_{\mathbf{3}}^a T_{\mathbf{3}}^b - \frac{n_\Psi a(x)}{2f_a}\text{Tr} T_{\mathbf{8}}^a T_{\mathbf{8}}^b\Big)\tilde{G}^a G^b \tag{14.7}$$

$$= \frac{g_s^2}{16\pi^2}\Big(\theta - \frac{3n_\Psi a(x)}{f_a}\Big)\text{Tr}\tilde{G}G, \tag{14.8}$$

and the axion-lepton coupling:

$$\mathcal{L} \supset -\frac{\partial_\mu a}{2f_a}\Big(\overline{L}\gamma^\mu\gamma^5 L - \overline{e}_R\gamma^\mu\gamma^5 e_R\Big) \tag{14.9}$$

$$= \frac{\partial_\mu a}{2f_a}\Big(\overline{e}\gamma^\mu e + \overline{\nu}_L\gamma^\mu\nu_L\Big). \tag{14.10}$$

Then axion potential is written as follows:

$$V_a = \Lambda^4\Big\{1 - \cos\Big(\theta - \frac{3\, n_\Psi\, a(x)}{f_a}\Big)\Big\}. \tag{14.11}$$

[28] n_Ψ is defined as the number of Ψ_{jR} $(j = 1, \cdots, n_\Psi)$.

Then, QCD θ term becomes zero, therefore, the strong CP problem is solved:

$$\mathcal{L} = \frac{g^2}{16\pi^2}\left(\theta - \frac{3n_\Psi a(x)}{v_a}\right)\mathrm{Tr}\tilde{G}G \to 0. \tag{14.12}$$

Next, we consider the experimental constraint from the axion-electron coupling. First, we define the axion emission diagram from electron line as $ik_\mu\mathcal{M}^\mu$. When replacing the axion emission with the photon one, the replaced amplitude is given as $i\epsilon_\mu^{(*)}\mathcal{M}$. Therefore, the axion emission amplitude becomes zero: $ik_\mu\mathcal{M}^\mu \to 0$, by using Ward-Takahashi identity. Therefore, there are no experimental constraints from the axion-electron coupling.

Therefore, f_a is constrained by only the axion-nucleon-nucleon coupling. The constraint on this coupling from supernova is given as follows [183]:

$$\frac{f_a}{3n_\Psi} \gtrsim 4.4 \times 10^8 \mathrm{GeV}. \tag{14.13}$$

14.4 The explanation of the neutrino oscillation and the dark matter relic density

The invisible axion can explain the dark matter relic density. It is given as follows (θ_i is the misalignment angle of the axion): [181]

$$\Omega_a h^2 \approx 0.12 \cdot \theta^2 \left(\frac{f_a/(3n_\Psi)}{9\times 10^{11}\mathrm{GeV}}\right)^{1.165}. \tag{14.14}$$

Here, we assume that the PQ symmetry is broken during inflation, so that the axion domain wall problem does not happen. [29]

Furthermore, the Ma-xion model can explain the neutrino oscillation. The neutrino mass matrix is generated by the 1-loop diagram in Figure 32. It is evaluated as follows: [30]

$$(\mathcal{M}_\nu)_{ij} = -\frac{1}{4\pi^2}\sum_k h_\Psi^{ik}h_\Psi^{jk}M_{\Psi k}\left(\frac{M_H^2}{M_{\Psi k}^2 - M_H^2}\ln\frac{M_H^2}{M_{\Psi k}^2} - \frac{M_A^2}{M_{\Psi k}^2 - M_A^2}\ln\frac{M_A^2}{M_{\Psi k}^2}\right). \tag{14.15}$$

In the limit of $2\lambda_5 v^2 \ll m_0^2 = (M_H^2 + M_A^2)/2$, this becomes as follows:

$$(\mathcal{M}_\nu)_{ij} \simeq \frac{1}{4\pi^2}\lambda_5 v^2 \sum_k h_\Psi^{ik}h_\Psi^{jk}M_{\Psi k}\frac{M_{\Psi k}^2\ln\frac{M_{\Psi k}^2}{m_0^2} - M_{\Psi k}^2 + m_0^2}{(M_{\Psi k}^2 - m_0^2)^2}. \tag{14.16}$$

[29] If the PQ symmetry is broken after inflation, the axion domain wall problem happens. It is because the domain wall number $3n_\Psi$ is larger than 1.

[30] Here, we define m_0 as $M_H^2 + M_A^2 = 2m_0^2$, and use $M_H^2 - M_A^2 = \lambda_5 v^2$.

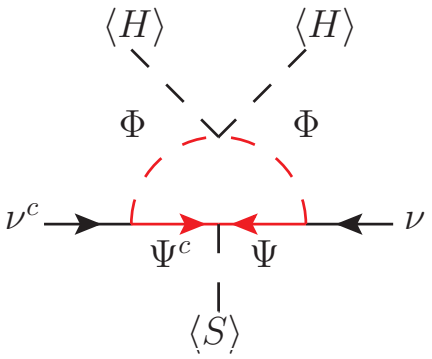

Figure 32: Neutrino mass

Furthermore, using the another limit: $M_{H,A} \ll M_{\Psi_k}$, this becomes similar to the neutrino mass in Type I seesaw:

$$(\mathcal{M}_\nu)_{ij} \simeq \frac{\lambda_5 v^2}{4\pi^2} \sum_k \frac{h_\Psi^{ik} h_\Psi^{jk}}{M_{\Psi k}}. \tag{14.17}$$

15 Summary of Part IV

We can construct the minimal model, in which we identify the Peccei Quinn symmetry in the KSVZ axion model with the lepton number symmetry in Majoron model. We use the radiative seesaw model with the color octet fermion, and we identify this as the heavy quark in the KSVZ axion model. Then, the neutrino oscillation can be explained by the 1-loop diagram of neutrino mass. Both the strong CP problem and the existence of dark matter are explained by the QCD axion. In order to avoid the domain wall problem, the PQ symmetry must be broken before reheating temperature. The scale of PQ scale is mainly constrained by the supernova.

Part V
Conclusion

Neutrino oscillation is the strong hint which indicates the BSM physics coupling to SM lepton sector. Furthermore, the other problems of SM are also serious (for example, muon g-2 anomaly, dark matter, strong CP problem, and etc). Therefore, we focus on the relationships between neutrino Majorana mass and other physics.

In Part II, we focus on the muon g-2 anomaly. It indicates the BSM physics which couple to SM lepton sector. Therefore, they may be identified as the BSM in seesaw models. We use the type II seesaw model to explain the muon g-2 anomaly. It is because it can explain neutrino mass with $O(1)$ Yukawa couplings and TeV scale BSM particles. In order to make the Δa positive definite, a double charged scalar k^{++} is introduced. Then, LFV constraints indicates the existence of the discrete lepton flavor symmetry $\mathbb{Z}_3$. Furthermore, double charged scalars mainly decay to $\mu^- + \tau^-$ in our model. Therefore, the muon g-2 anomaly and the neutrino oscillation indicate the importance of the $\mathbb{Z}_3$ conserving LFV processes and the decay processes from double charged scalar to $\mu^- + \tau^-$ final states.

In Part III, we focus on the dark matter. Among the models explaining neutrino oscillation and dark matter, we consider the TeV scale Majoron dark matter. TeV scale Majoron dark matter can solve the anomalous results in positron fraction detected by the cosmic ray experiments. Furthermore, the Majoron dark matter can be tested by the neutrino telescopes ($\chi \to \nu\nu$). However, it is not obvious that the TeV scale Majoron can be produced as much as the observed dark matter relic density. We can see that three production mechanisms for the TeV scale Majoron dark matter are possible. Therefore, the observed dark matter may be TeV scale Majoron. The neutrino oscillation and the dark matter relic density indicate the importance for the indirect detections of dark matter by the cosmic ray experiments.

In Part IV, we focus on the strong CP problem. Lepton number symmetry is broken in seesaw models, and PQ symmetry is done in axion models. Therefore, it is important to identify them. Some seesaw models contain heavy fermions, therefore, we identify them as the heavy "colored" fermion in KSVZ axion models. In this model, axion can explain the observed dark matter relic density. In order to avoid the domain wall problem in this model, the PQ symmetry breaking must occur before reheating temperature. Combining the above results, the neutrino oscillation and the strong CP problem indicate that the observed dark matter is axion (= Majoron) coupling to SM lepton and nucleons, SM lepton couples to heavy colored particles, and the PQ (=L) scale of this model constrains the reheating temperature.

Throughout this thesis, we consider what is indicated by neutrino oscillation and

other BSM physics. They can be tested by future experiments; colliders, cosmic ray experiments, axion detectors, neutrino telescopes, and so on. We want to discover these new physics in future.

Acknowledgment

I am very very grateful to my supervisors: Koji Tsumura and Koichi Yoshioka; my collaborators: Yoshihiko Abe, Nabarun Chakrabarty, Cheng-Wei Chiang, Yu Hamada, Ernest Ma and Kenta Suzuki; faculty staffs in Kyoto University: Masafumi Fukuma, Hiroyuki Hata, Hikaru Kawai, Katsuyuki Sugiyama, and Kentaroh Yoshida.

A Appendix for Part II

A.1 The calculation of the lepton g-2 and the LFV processes

We want to lepton g-2 and LFV process in this part.

In §A.1.1, we derive the contribution to lepton g-2 and $\ell_a \to \ell_b\gamma$ from the effective dipole operator

$$\mathcal{L} = \overline{\ell_b}\sigma^{\mu\nu}(A_L^{ba}P_L + A_R^{ba}P_R)\ell_a F_{\mu\nu},\ \left(\sigma^{\mu\nu} = \frac{i}{2}[\gamma^\mu,\gamma^\nu],\ A_L^{ba} = A_R^{\dagger ba}\right). \tag{A.1}$$

In §A.1.2, we calculate the coefficient of effective dipole operator $A_{L,R}^{ba}$, from somewhat general Yukawa couplings:

$$\mathcal{L} = H_i^{++}\overline{\ell_a^C}(f_{iL}^{ab}P_L + f_{iR}^{ab}P_R)\ell_b + h_i^{aj}H_i^+\overline{\ell_a^C}\nu_{Lj} + \text{H.c.} \tag{A.2}$$

In §A.1.3, we calculate $\mathrm{Br}(\ell_a \to \ell_b\gamma)/\mathrm{Br}(\ell_a \to \nu_a\ell_e\overline{\nu_e})$ and $\mathrm{Br}(\ell_a \to \ell_b\ell_c\overline{\ell_d})/\mathrm{Br}(\ell_a \to \nu_a\ell_e\overline{\nu_e})$ $(b \neq c,\ a \neq e)$, under the above general Yukawa couplings. In §A.1.4, we evaluate the loop integral used in §A.1.2. In §A.1.5, we evaluate the integral over n-body phase space used in §A.1.3.

A.1.1 The calculation from the effective dipole operator

In this section, we consider the dipole effective action

$$\mathcal{L} = \overline{\ell_b}\sigma^{\mu\nu}(A_L^{ba}P_L + A_R^{ba}P_R)\ell_a F_{\mu\nu},\ \left(\sigma^{\mu\nu} = \frac{i}{2}[\gamma^\mu,\gamma^\nu],\ A_L^{ba} = A_R^{\dagger ba}\right). \tag{A.3}$$

It is useful to rewrite this Lagrangian in momentum space [31]

$$\begin{aligned} i\int d^Dx\mathcal{L} =& i\int d^Dx\int\frac{d^Dk_1}{(2\pi)^D}\int\frac{d^Dk_2}{(2\pi)^D}\int\frac{d^Dk_3}{(2\pi)^D}\overline{\ell_b}(k_2)\sigma^{\mu\nu}(A_L^{ba}P_L+A_R^{ba}P_R)\ell_a(k_1)\\ &\times\{-ik_{3\mu}A_\nu(k_3)+ik_{3\nu}A_\mu(k_3)\}e^{-i(k_1+k_2+k_3)x}\\ =&2\int\frac{d^Dk_1}{(2\pi)^D}\int\frac{d^Dk_2}{(2\pi)^D}\overline{\ell_b}(-k_2)\sigma^{\mu\nu}(A_L^{ba}P_L+A_R^{ba}P_R)\ell_a(k_1)\\ &\times(-k_1+k_2)_\mu A_\nu(-k_1+k_2). \end{aligned} \tag{A.4}$$

Then, we can calculate the amplitude of $\ell_a(k_a)\to\ell_b(k_b)\gamma(k_a-k_b)$ from the dipole Lagrangian

$$i\mathcal{M} =2\epsilon_\mu^*(k_a-k_b)\overline{u}(k_b)\sigma^{\nu\mu}(A_L^{ba}P_L+A_R^{ba}P_R)u(k_a)(k_b-k_a)_\nu \tag{A.5}$$

$$=2i\epsilon_\mu^*(k_a-k_b)\overline{u}(k_b)(m_{\ell_b}-\not{k_a})\gamma^\mu(A_L^{ba}P_L+A_R^{ba}P_R)u(k_a). \tag{A.6}$$

Then, squared amplitude are

$$\begin{aligned} \sum_{d.o.f}|\mathcal{M}|^2 =& -4\mathrm{Tr}(\not{k_b}+m_{\ell_b})(\not{k_a}-m_{\ell_b})\gamma^\mu(A_L^{ba}P_L+A_R^{ba}P_R)\\ &\times(\not{k_a}+m_{\ell_a})(A_L^{ba*}P_R+A_R^{ba*}P_L)\gamma_\mu(\not{k_a}-m_{\ell_b}) \end{aligned} \tag{A.7}$$

$$=8(m_{\ell_a}^2-m_{\ell_b}^2)^2(|A_L^{ab}|^2+|A_R^{ab}|^2). \tag{A.8}$$

Therefore, Decay width of $\ell_a\to\ell_b\gamma$ is

$$\begin{aligned} \Gamma(\ell_a\to\ell_b\gamma) =&\frac{1}{2m_{\ell_a}}\frac{1}{2!}\int\frac{d^3k_b}{(2\pi)^32E_{k_b}}\int\frac{d^3k_\gamma}{(2\pi)^32E_{k_\gamma}}(2\pi)^4\delta^4(k_a-k_b-k_\gamma)\\ &\times 8(m_{\ell_a}^2-m_{\ell_b}^2)^2\big(|A_L^{ab}|^2+|A_R^{ab}|^2\big) \end{aligned} \tag{A.9}$$

$$=\frac{1}{2m_{\ell_a}}\frac{1}{2!}8(m_{\ell_a}^2-m_{\ell_b}^2)^2\big(|A_L^{ab}|^2+|A_R^{ab}|^2\big)\frac{2}{2\pi}\frac{(m_{\ell_a}^2-m_{\ell_b}^2)}{8m_{\ell_a}^2} \tag{A.10}$$

$$=\frac{(m_{\ell_a}^2-m_{\ell_b}^2)^3}{4\pi m_a^3}\big(|A_L^{ba}|^2+|A_R^{ba}|^2\big). \tag{A.11}$$

The contribution to lepton anomalous dipole moment from effective action is written as follows (see §1.2)

$$\Delta a_{\ell_a} =-\frac{2m_{\ell_a}}{e}(A_L+A_R)^{aa}. \tag{A.12}$$

[31] $A(x)=\int\frac{d^Dp}{(2\pi)^D}A(p)e^{-ipx}$, $F_{\mu\nu}(x)=\partial_\mu A_\nu-\partial_\nu A_\mu=\int\frac{d^Dp}{(2\pi)^D}(-ip_\mu A_\nu+ip_\nu A_\mu)e^{-ipx}=\int\frac{d^Dp}{(2\pi)^D}F_{\mu\nu}(p)e^{-ipx}$

A.1.2 The calculation of the lepton g-2 and the LFV processes from Yukawa coupling

In this section, we calculate the coefficient of the effective action in §A.1.1 ($A^{ba}_{L,\,R}$), from the following general Yukawa coupling [32]

$$\mathcal{L} = H_i^{++}\overline{\ell_a^C}(f^{ab}_{iL}P_L + f^{ab}_{iR}P_R)\ell_b + h_i^{aj}H_i^{+}\overline{\ell_a^C}\nu_{Lj} + \text{H.c.} \tag{A.13}$$

First, we rewrite the amplitude of $\ell_a(p_3) \to \ell_b(-p_2)\gamma(-p_1)$ written by the effective action

$$\begin{aligned} i\mathcal{M} =& 2\epsilon^*_\mu(-p_1)\overline{u}(-p_2)\sigma^{\nu\mu}(A^{ba}_L P_L + A^{ba}_R P_R)u(p_3)(-p_2-p_3)_\nu \qquad (A.14)\\ =& 2i\overline{u}(-p_2)\not{\epsilon}^*(-p_1)\\ & \times\Big\{(m_{\ell_b}A^{ba}_L + m_{\ell_a}A^{ba}_R)P_L + (m_{\ell_b}A^{ba}_R + m_{\ell_a}A^{ba}_L)P_R\Big\}u(p_3)\\ & + 4i\Big\{p_2\epsilon^*(-p_1)\Big\}\overline{u}(-p_2)(A^{ba}_L P_L + A^{ba}_R P_R)u(p_3). \qquad (A.15)\end{aligned}$$

Please pay attention that this amplitude contain the term with $\not{\epsilon}^*(-p_1)$ and the one with $p_2\epsilon^*(-p_1)$.

We will calculate the amplitude from the general Yukawa interaction. Then, we can write $A^{ab}_{L,\,R}$ as a function of Yukawa coupling, even if we keep only $p_2\epsilon^*(-p_1)$ terms. Therefore, we will ignore $\not{\epsilon}^*(-p_1)$ terms in this subsubsection.

First we calculate the H^+'s contribution to the LFV amplitude

$$\begin{aligned} i\mathcal{M}_{H_i^+} =& (ih_i^{*bj})(ih_i^{\mathrm{T}ja})\int\frac{d^D\ell}{(2\pi)^D}\overline{u}(-p_2)P_R\frac{i\not{\ell}}{\ell^2}P_L u(p_3)\epsilon^{*\mu}(-p_1)\\ & \times\frac{i}{(\ell+p_2)^2 - M^2_{H_i^+}}\Big\{-ie(-2\ell-p_2+p_3)_\mu\Big\}\frac{i}{(\ell-p_3)^2-M^2_{H_i^+}} \qquad (A.16)\\ \to& 2e[h_ih_i^\dagger]^{ab}(C_{22}-C_{23}+C_2)(0,M_{H_i^+})\Big\{p_2\epsilon^*(-p_1)\Big\}\overline{u}(-p_2)(m_{\ell_b}P_L + m_{\ell_a}P_R)u(p_3) \qquad (A.17)\end{aligned}$$

Here, $\to$ means that we ignore the $\not{\epsilon}^*(-p_1)$ terms. C_{00}, C_{22} and etc. are defined in §A.1.4. When we compare $i\mathcal{M}_{H_i^+}$ with the amplitude written by the effective action (A.15), we

[32] H_i^{++} and H_i^+ are written in mass basis.

can write the contribution from H_i^+ to $A_{L,\,R}$ as

$$A_L^{H^+ba} = \frac{1}{4i} \times 2e \sum_i [h_i h_i^\dagger]^{ab} (C_{22} - C_{23} + C_2)(0, M_{H_i^+}) m_{\ell_b} \tag{A.18}$$

$$\simeq \frac{e}{24(4\pi)^2} \sum_i \frac{[h_i h_i^\dagger]^{ab} m_{\ell_b}}{M_{H_i^+}^2}, \tag{A.19}$$

$$A_R^{H^+ba} = \frac{1}{4i} \times 2e \sum_i [h_i h_i^\dagger]^{ab} (C_{22} - C_{23} + C_2)(0, M_{H_i^+}) m_{\ell_a} \tag{A.20}$$

$$\simeq \frac{e}{24(4\pi)^2} \sum_i \frac{[h_i h_i^\dagger]^{ab} m_{\ell_a}}{M_{H_i^+}^2}. \tag{A.21}$$

Next, we calculate the contributions to dipole effective coupling from H_i^{++} Yukawa coupling. Two contributions from H_i^{++} exist. We define $i\mathcal{M}_{H_i^{++}1}$ in which a photon emits from the internal scalar line, $i\mathcal{M}_{H_i^{++}2}$ in which a photon emits from the internal Fermion line. First, we calculate $i\mathcal{M}_{H_i^{++}1}$ shown as follows

$$\begin{aligned} i\mathcal{M}_{H_i^{++}1} = \int \frac{d^D\ell}{(2\pi)^D} \overline{u}(-p_2)\big\{i(2f_{iL}^{\dagger bc} P_R + 2f_{iR}^{\dagger bc} P_L)\big\} \frac{i(\not{\ell} + m_{\ell_c})}{\ell^2 - m_{\ell_c}^2} \big\{i(2f_{iL}^{ca} P_L + 2f_{iR}^{ca} P_R)\big\} u(p_3) \\ \times \epsilon^{*\mu}(-p_1) \frac{i}{(\ell + p_2)^2 - M_{H_i^{++}}^2} \big\{ -2ie(-2\ell - p_2 + p_3)_\mu \big\} \frac{i}{(\ell - p_3)^2 - M_{H_i^{++}}^2} \end{aligned} \tag{A.22}$$

$$\begin{aligned} \to & 16e\big\{p_2 \epsilon^*(-p_1)\big\}(C_{22} - C_{23} + C_2)(\ell_c, M_{H_i^{++}}) \\ & \times \overline{u}(-p_2)\big\{(m_{\ell_b} f_{iL}^{\dagger bc} f_{iL}^{ca} + m_{\ell_a} f_{iR}^{\dagger bc} f_{iR}^{ca}) P_L + (m_{\ell_b} f_{iR}^{\dagger bc} f_{iR}^{ca} + m_{\ell_a} f_{iL}^{\dagger bc} f_{iL}^{ca}) P_R\big\} u(p_3) \\ & - 16e\big\{p_2 \epsilon^*(-p_1)\big\}(2C_2 + C_0)(\ell_c, M_{H_i^{++}}) m_{\ell_c} \overline{u}(-p_2)(f_{iR}^{\dagger bc} f_{iL}^{ca} P_L + f_{iL}^{\dagger bc} f_{iR}^{ca} P_R) u(p_3). \end{aligned} \tag{A.23}$$

We compare this with (A.15), then, we can know the effective coupling which correspond

to $\mathcal{M}_{H_i^{++}1}$:

$$A_L^{H^{++}1ba} = \frac{1}{4i} \times 16e \sum_i (C_{22} - C_{23} + C_2)(\ell_c, M_{H_i^{++}})(m_{\ell_b} f_{iL}^{\dagger bc} f_{iL}^{ca} + m_{\ell_a} f_{iR}^{\dagger bc} f_{iR}^{ca})$$
$$- \frac{1}{4i} \times 16e \sum_i (2C_2 + C_0)(\ell_c, M_{H_i^{++}}) m_{\ell_c} f_{iR}^{\dagger bc} f_{iL}^{ca} \tag{A.24}$$
$$\simeq \frac{e}{3(4\pi)^2} \sum_i \frac{m_{\ell_b} f_{iL}^{\dagger bc} f_{iL}^{ca} + m_{\ell_a} f_{iR}^{\dagger bc} f_{iR}^{ca} + 6 m_{\ell_c} f_{iR}^{\dagger bc} f_{iL}^{ca}}{M_{H_i^{++}}^2}, \tag{A.25}$$
$$A_R^{H^{++}1ba} = \frac{1}{4i} \times 16e \sum_i (C_{22} - C_{23} + C_2)(\ell_c, M_{H_i^{++}})(m_{\ell_b} f_{iR}^{\dagger bc} f_{iR}^{ca} + m_{\ell_a} f_{iL}^{\dagger bc} f_{iL}^{ca})$$
$$- \frac{1}{4i} \times 16e \sum_i (2C_2 + C_0)(\ell_c, M_{H_i^{++}}) m_{\ell_c} f_{iL}^{\dagger bc} f_{iR}^{ca} \tag{A.26}$$
$$\simeq \frac{e}{3(4\pi)^2} \sum_i \frac{m_{\ell_b} f_{iR}^{\dagger bc} f_{iR}^{ca} + m_{\ell_a} f_{iL}^{\dagger bc} f_{iL}^{ca} + 6 m_{\ell_c} f_{iL}^{\dagger bc} f_{iR}^{ca}}{M_{H_i^{++}}^2}. \tag{A.27}$$

Next, we calculate $i\mathcal{M}_{H_i^{++}2}$ shown as follows:

$$i\mathcal{M}_{H_i^{++}2} = \epsilon^{*\mu}(-p_1) \int \frac{d^D \ell}{(2\pi)^D} \overline{u}(-p_2)$$
$$\times \big\{ 2i(f_{iL}^{\dagger bc} P_R + f_{iR}^{\dagger bc} P_L) \big\} \frac{i(\cancel{-\ell - p_2} + m_{\ell_c})}{(\ell + p_2)^2 - m_{\ell_c}^2} ie\gamma^\mu \frac{i(\cancel{-\ell + p_3} + m_{\ell_c})}{(\ell - p_3)^2 - m_{\ell_c}^2}$$
$$\times \big\{ 2i(f_{iL}^{ca} P_L + f_{iR}^{ca} P_R) \big\} u(p_3) \frac{i}{\ell^2 - M_{H_i^{++}}^2} \tag{A.28}$$
$$\to 8e \big\{ p_2 \epsilon^*(-p_1) \big\} (C_{22} - C_{23} + C_2)(M_{H_i^{++}}, m_{\ell_c})$$
$$\times \overline{u}(-p_2) \big\{ (m_{\ell_b} f_{iL}^{\dagger bc} f_{iL}^{ca} + m_{\ell_a} f_{iR}^{\dagger bc} f_{iR}^{ca}) P_L + (m_{\ell_b} f_{iR}^{\dagger bc} f_{iR}^{ca} + m_{\ell_a} f_{iL}^{\dagger bc} f_{iL}^{ca}) P_R \big\} u(p_3)$$
$$+ 16e m_{\ell_c} \big\{ p_2 \epsilon^*(-p_1) \big\} C_2(M_{H_i^{++}}, m_{\ell_c}) \overline{u}(-p_2)(f_{iR}^{\dagger bc} f_{iL}^{ca} P_L + f_{iL}^{\dagger bc} f_{iR}^{ca} P_R) u(p_3) \tag{A.29}$$

After comparing this with (A.15), we can get the effective couplings as follows:

$$A_L^{H^{++}2ba} = \frac{1}{4i} \times 8e \sum_i (C_{22} - C_{23} + C_2)(M_{H_i^{++}}, m_{\ell_c})(m_{\ell_b} f_{iL}^{\dagger bc} f_{iL}^{ca} + m_{\ell_a} f_{iR}^{\dagger bc} f_{iR}^{ca}) + \frac{1}{4i} \times 16e \sum_i m_{\ell_c} C_2(M_{H_i^{++}}, m_{\ell_c}) f_{iR}^{\dagger bc} f_{iL}^{ca} \tag{A.30}$$

$$\simeq \frac{e}{3(4\pi)^2} \sum_i \frac{m_{\ell_b} f_{iL}^{\dagger bc} f_{iL}^{ca} + m_{\ell_a} f_{iR}^{\dagger bc} f_{iR}^{ca}}{M_i^{++2}} - \frac{e}{(4\pi)^2} \sum_i \frac{\{3 - 2\ln(M_i^{++2}/m_{\ell_c}^2)\} m_{\ell_c} f_{iR}^{\dagger bc} f_{iL}^{ca}}{M_i^{++2}}, \tag{A.31}$$

$$A_R^{H^{++}2ba} = \frac{1}{4i} \times 8e \sum_i (C_{22} - C_{23} + C_2)(M_{H_i^{++}}, m_{\ell_c})(m_{\ell_b} f_{iR}^{\dagger bc} f_{iR}^{ca} + m_{\ell_a} f_{iL}^{\dagger bc} f_{iL}^{ca}) + \frac{1}{4i} \times 16e \sum_i m_{\ell_c} C_2(M_{H_i^{++}}, m_{\ell_c}) f_{iL}^{\dagger bc} f_{iR}^{ca} \tag{A.32}$$

$$\simeq \frac{e}{3(4\pi)^2} \sum_i \frac{m_{\ell_b} f_{iR}^{\dagger bc} f_{iR}^{ca} + m_{\ell_a} f_{iL}^{\dagger bc} f_{iL}^{ca}}{M_i^{++2}} - \frac{e}{(4\pi)^2} \sum_i \frac{\{3 - 2\ln(M_i^{++2}/m_{\ell_c}^2)\} m_{\ell_c} f_{iL}^{\dagger bc} f_{iR}^{ca}}{M_i^{++2}}. \tag{A.33}$$

Using the above results, total contribution from H^{++} ($A_{L,R}^{H^{++}ba} := A_{L,R}^{H^{++}1ba} + A_{L,R}^{H^{++}2ba}$) can be written as follows:

$$A_L^{H^{++}ba} = A_L^{H^{++}1ba} + A_L^{H^{++}2ba} \tag{A.34}$$

$$= \frac{e}{3(4\pi)^2} \sum_i \frac{1}{M_{H_i^{++}}^2} \Big[2m_{\ell_b} f_{iL}^{\dagger bc} f_{iL}^{ca} + 2m_{\ell_a} f_{iR}^{\dagger bc} f_{iR}^{ca} + \{ -3 + 6\ln(M_i^{++2}/m_{\ell_c}^2) \} m_{\ell_c} f_{iR}^{\dagger bc} f_{iL}^{ca} \Big], \tag{A.35}$$

$$A_R^{H^{++}ba} = \frac{e}{3(4\pi)^2} \sum_i \frac{1}{M_{H_i^{++}}^2} \Big[2m_{\ell_b} f_{iR}^{\dagger bc} f_{iR}^{ca} + 2m_{\ell_a} f_{iL}^{\dagger bc} f_{iL}^{ca} + \{ -3 + 6\ln(M_i^{++2}/m_{\ell_c}^2) \} m_{\ell_c} f_{iL}^{\dagger bc} f_{iR}^{ca} \Big]. \tag{A.36}$$

A.1.3 The branching ratio of the LFV processes

In this subsubsection, we calculate $\mathrm{Br}(\ell_a \to \ell_b \gamma)/\mathrm{Br}(\ell_a \to \nu_a \ell_e \overline{\nu_e})$ and $\mathrm{Br}(\ell_a \to \ell_b \ell_c \overline{\ell_d})/\mathrm{Br}(\ell_a \to \nu_a \ell_e \overline{\nu_e})$ ($b \neq c$, $a \neq e$).

First, we calculate the amplitude of $\ell_a(p_a) \to \ell_b(p_b)\ell_c(p_c)\overline{\ell_d}(p_d)$:

$$i\mathcal{M}(\ell_a \to \ell_b\ell_c\overline{\ell_d}) \tag{A.37}$$

$$= \sum_i \overline{u}(p_d)(2f_{iL}^{da}P_L + 2f_{iR}^{da}P_R)u(p_a)\frac{i}{(p_b+p_c)^2 - M_{H_i^{++}}^2}\overline{u}(p_b)(2f_{iL}^{\dagger bc}P_R + 2f_{iR}^{\dagger bc}P_L)v(p_c) \tag{A.38}$$

Then, the decay width of $\ell_a(p_a) \to \ell_b(p_b)\ell_c(p_c)\overline{\ell_d}(p_d)$ is given as follows [33]:

$$\Gamma(\ell_a \to \ell_b\ell_c\overline{\ell_d}) \tag{A.39}$$

$$\begin{aligned}
=&\frac{1}{2}\frac{1}{2m_{\ell_a}}\int \frac{d^3p_b}{(2\pi)^3 2E_b}\frac{d^3p_c}{(2\pi)^3 2E_c}\frac{d^3p_d}{(2\pi)^3 2E_d}(2\pi)^4\delta^4(p_a - p_b - p_c - p_d) \\
&\times \frac{1}{\{(p_b+p_c)^2 - M_{H_i^{++}}^2\}}\frac{1}{\{(p_b+p_c)^2 - M_{H_j^{++}}^2\}} \\
&\times 16\mathrm{Tr}(f_{iL}^{da}P_L + f_{iR}^{da}P_R)(\not{p_a} + m_{\ell_a})(f_{jL}^{\dagger ad}P_R + f_{jR}^{\dagger ad}P_L)(\not{p_d} + m_{\ell_d}) \\
&\times \mathrm{Tr}(f_{iL}^{\dagger bc}P_R + f_{iR}^{\dagger bc}P_L)(\not{p_c} - m_{\ell_c})(f_{jL}^{cb}P_L + f_{jR}^{cb}P_R)(\not{p_b} + m_{\ell_b})
\end{aligned} \tag{A.40}$$

$$\simeq \frac{1}{6(4\pi)^3}m_{\ell_a}^5\sum_{ij}\frac{1}{M_{H_i^{++}}^2 M_{H_j^{++}}^2}(f_{iL}^{da}f_{jL}^{\dagger ad} + f_{iR}^{da}f_{jR}^{\dagger ad})(f_{iL}^{\dagger bc}f_{jL}^{cb} + f_{iR}^{\dagger bc}f_{jR}^{cb}) \tag{A.41}$$

Next, we calculate the decay width of $\ell_a(p_1) \to \nu_a(p_2)\ell_b(p_3)\overline{\nu_b}(p_4)$, $(a \neq b)$. The amplitude is given as follows:

$$\begin{aligned}
i\mathcal{M} =& \frac{ig}{\sqrt{2}}\overline{u}(p_2)\gamma^\mu P_L u(p_1) \times \frac{ig}{\sqrt{2}}\overline{u}(p_3)\gamma^\nu P_L v(p_4) \\
&\times \frac{-i}{(p_3+p_4)^2 - m_W^2} \times \left\{\eta_{\mu\nu} - (p_3+p_4)_\mu(p_3+p_4)_\nu/m_W^2\right\}.
\end{aligned} \tag{A.42}$$

Then, we can calculate the decay width:

$$\begin{aligned}
&\Gamma(\ell_a \to \nu_a\ell_b\overline{\nu_b}) \\
=&\frac{1}{2}\frac{1}{2m_{\ell_a}}\frac{1}{2\pi}\int_{m_{\ell_b}^2}^{m_{\ell_a}^2} dm_{34}^2 d\Phi_2(p_1, p_{34}, p_2)d\Phi_2(p_{34}, p_3, p_4) \\
&\times \frac{g^4}{4}\mathrm{Tr}\not{p_2}\gamma^\mu P_L(\not{p_1} - m_{\ell_a})P_R\gamma^\rho\mathrm{Tr}(\not{p_3} - m_{\ell_b})\gamma^\nu P_L\not{p_4}P_R\gamma^\sigma \\
&\times \frac{1}{(m_{34}^2 - m_W^2)^2}\left\{\eta_{\mu\nu} - (p_3+p_4)_\mu(p_3+p_4)_\nu/m_W^2\right\}\left\{\eta_{\rho\sigma} - (p_3+p_4)_\rho(p_3+p_4)_\sigma/m_W^2\right\} \\
\simeq&\frac{G_F^2 m_{\ell_a}^5}{3(4\pi)^3}
\end{aligned} \tag{A.43}$$

[33] Here, we used the formulae for the integral over n-body phase space in §A.1.5.

Using the above results, $\mathrm{Br}(\ell_a \to \ell_b\gamma)/\mathrm{Br}(\ell_a \to \nu_a\ell_e\overline{\nu_e})$ is given as follows:

$$\mathrm{Br}(\ell_a \to \ell_b\gamma)/\mathrm{Br}(\ell_a \to \nu_a\ell_e\overline{\nu_e}) \tag{A.44}$$

$$=\frac{(m_{\ell_a}^2 - m_{\ell_b}^2)^3}{4\pi m_{\ell_a}^3 \Lambda^2}\left(|A_L^{ba}|^2 + |A_R^{ba}|^2\right) \times \frac{3(4\pi)^3}{G_F^2 m_{\ell_a}^5}, \tag{A.45}$$

and $\mathrm{Br}(\ell_a \to \ell_b\ell_c\overline{\ell_d})/\mathrm{Br}(\ell_a \to \nu_a\ell_e\overline{\nu_e})$ $(b \neq c,\ a \neq e)$ is given as follows:

$$\mathrm{Br}(\ell_a \to \ell_b\ell_c\overline{\ell_d})/\mathrm{Br}(\ell_a \to \nu_a\ell_e\overline{\nu_e}) \tag{A.46}$$

$$=\frac{1}{6(4\pi)^3} m_{\ell_a}^5 \sum_{ij} \frac{1}{M_{H_i^{++}}^2 M_{H_j^{++}}^2}(f_{iL}^{da} f_{jL}^{\dagger ad} + f_{iR}^{da} f_{jR}^{\dagger ad})(f_{iL}^{\dagger bc} f_{jL}^{cb} + f_{iR}^{\dagger bc} f_{jR}^{cb}) \times \frac{3(4\pi)^3}{G_F^2 m_{\ell_a}^5} \tag{A.47}$$

$$=\frac{1}{2G_F^2} \sum_{ij} \frac{1}{M_{H_i^{++}}^2 M_{H_j^{++}}^2}(f_{iL}^{da} f_{jL}^{\dagger ad} + f_{iR}^{da} f_{jR}^{\dagger ad})(f_{iL}^{\dagger bc} f_{jL}^{cb} + f_{iR}^{\dagger bc} f_{jR}^{cb}). \tag{A.48}$$

A.1.4 The calculation of the loop integral

In this section, we evaluate the loop integral in the LFV process $\ell_a(p_3) \to \ell_b(-p_2)\gamma(-p_1)$. First, we define loop integral $C_2(M_1,\, M_2)$ and $C_3(M_1,\, M_2)$ as folows:

$$C_2(M_1, M_2)p_{2\mu} + C_3(M_1, M_2)p_{3\mu} \tag{A.49}$$

$$=: \int \frac{d^D\ell}{(2\pi)^D} \frac{\ell_\mu}{(\ell^2 - M_1^2)\{(\ell + p_2)^2 - M_2^2\}\{(p_3 - \ell)^2 - M_2^2\}} \tag{A.50}$$

$$\simeq 2\int_0^1 dx \int_0^{1-x} dy \int \frac{d^Dq}{(2\pi)^D} \frac{-(xp_2 - yp_3)_\mu}{\left\{q^2 - M_1^2(1-x-y) - (x+y)M_2^2\right\}^3} \quad (m_\ell \ll M_1 \text{ or } m_\ell \ll M_2) \tag{A.51}$$

Therefore, C_2 and C_3 are written as follows:

$$\begin{aligned}
&C_2(M_1, M_2) \\
&\simeq -C_3(M_1, M_2) \\
&= -2\int_0^1 dx \int_0^{1-x} dy \int \frac{d^Dq}{(2\pi)^D} \frac{x}{\left\{q^2 - M_1^2(1-x-y) - (x+y)M_2^2\right\}^3} \\
&= \frac{i}{(4\pi)^2}\int_0^1 dx \int_0^{1-x} dy \frac{x}{M_1^2(1-x-y) + (x+y)M_2^2} \\
&= \frac{i}{(4\pi)^2}\frac{-3M_1^4 + 4M_1^2M_2^2 - M_2^4 - 2M_1^4\ln(M_2^2/M_1^2)}{4(M_1^2 - M_2^2)^3}.
\end{aligned} \tag{A.52}$$

Next, we define C_{00}, C_{22}, C_{23}, C_{33} as follows:

$$
\begin{aligned}
&C_{00}(M_1,M_2)\eta_{\mu\nu}+C_{22}(M_1,M_2)p_{2\mu}p_{2\nu}\\
&+C_{23}(M_1,M_2)(p_{2\mu}p_{3\nu}+p_{3\mu}p_{2\nu})+C_{33}(M_1,M_2)p_{3\mu}p_{3\nu} &\text{(A.53)}\\
=&\int\frac{d^D\ell}{(2\pi)^D}\frac{\ell_\mu\ell_\nu}{(\ell^2-M_1^2)\{(\ell+p_2)^2-M_2^2\}\{(p_3-\ell)^2-M_2^2\}} &\text{(A.54)}\\
=&2\int_0^1dx\int_0^{1-x}dy\int\frac{d^Dq}{(2\pi)^D}\\
&\times\frac{\{q-(xp_2-yp_3)\}_\mu\{q-(xp_2-yp_3)\}_\nu}{\left\{q^2-x^2m_{\ell_b}^2-xy(m_{\ell_a}^2+m_{\ell_b}^2)-y^2m_{\ell_a}^2-M_1^2(1-x-y)+x(m_{\ell_b}^2-M_2^2)+y(m_{\ell_a}^2-M_2^2)\right\}^3} &\text{(A.55)}\\
=&2\int_0^1dx\int_0^{1-x}dy\int\frac{d^Dq}{(2\pi)^D}\\
&\times\frac{q^2g_{\mu\nu}/D+(xp_2-yp_3)_\mu(xp_2-yp_3)_\nu}{\left\{q^2-x^2m_{\ell_b}^2-xy(m_{\ell_a}^2+m_{\ell_b}^2)-y^2m_{\ell_a}^2-M_1^2(1-x-y)+x(m_{\ell_b}^2-M_2^2)+y(m_{\ell_a}^2-M_2^2)\right\}^3} &\text{(A.56)}\\
\simeq&2\int_0^1dx\int_0^{1-x}dy\int\frac{d^Dq}{(2\pi)^D}\frac{q^2g_{\mu\nu}/D+x^2p_{2\mu}p_{2\nu}-xy(p_{2\mu}p_{3\nu}+p_{3\mu}p_{2\nu})+y^2p_{3\mu}p_{3\nu}}{\left\{q^2-M_1^2(1-x-y)-(x+y)M_2^2\right\}^3} &\text{(A.57)}
\end{aligned}
$$

Therefore, C_{22}, C_{23} and C_{33} are written as follows:

$$
\begin{aligned}
&C_{22}(M_1,M_2)\\
&\simeq C_{33}(M_1,M_2)\\
&=2\int_0^1dx\int_0^{1-x}dy\int\frac{d^Dq}{(2\pi)^D}\frac{x^2}{\left\{q^2-M_1^2(1-x-y)-(x+y)M_2^2\right\}^3}\\
&=\frac{i}{(4\pi)^2}\frac{11M_1^6-18M_1^4M_2^2+9M_1^2M_2^4-2M_2^6+6M_1^6\ln(M_2^2/M_1^2)}{18(M_1^2-M_2^2)^4}\\
&C_{23}(M_1,M_2)\\
&\simeq 2\int_0^1dx\int_0^{1-x}dy\int\frac{d^Dq}{(2\pi)^D}\frac{-xy}{\left\{q^2-M_1^2(1-x-y)-(x+y)M_2^2\right\}^3}\\
&=-\frac{i}{(4\pi)^2}\frac{11M_1^6-18M_1^4M_2^2+9M_1^2M_2^4-2M_2^6+6M_1^6\ln(M_2^2/M_1^2)}{36(M_1^2-M_2^2)^4}
\end{aligned}
\qquad\text{(A.58)}
$$

At last, we define C_0 as follows:

$$C_0(M_1, M_2) \tag{A.59}$$

$$= \int \frac{d^D \ell}{(2\pi)^D} \frac{1}{(\ell^2 - M_1^2)\{(\ell + p_2)^2 - M_2^2\}\{(p_3 - \ell)^2 - M_2^2\}} \tag{A.60}$$

$$= \frac{i}{(4\pi)^2} \frac{M_1^2 - M_2^2 - M_1^2 \ln(M_1^2/M_2^2)}{(M_1^2 - M_2^2)^2}. \tag{A.61}$$

A.1.5 The integral of the n-body phase space

In this section, we evaluate the integral over n-body phase space. The integral over 3-body phase space is written by 2-body phase space as follows:

$$d\Phi_3(P, p_1, p_2, p_3) \tag{A.62}$$

$$= \int \frac{d^3 p_1}{(2\pi)^3 2E_1} \frac{d^3 p_2}{(2\pi)^3 2E_2} \frac{d^3 p_3}{(2\pi)^3 2E_3} (2\pi)^4 \delta^4(P - p_1 - p_2 - p_3) \tag{A.63}$$

$$= \int \frac{d^3 p_3}{(2\pi)^3 2E_3} d^4 p_{12} \delta^4(p_{12} - p_1 - p_2)(2\pi)^4 \delta^4(P - p_{12} - p_3) \frac{d^3 p_1}{(2\pi)^3 2E_1} \frac{d^3 p_2}{(2\pi)^3 2E_2} \tag{A.64}$$

$$= \frac{1}{2\pi} \int_{(m_1+m_2)^2}^{(\sqrt{P^2}-m_3)^2} dm_{12}^2 d\Phi_2(P, p_{12}, p_3) d\Phi_2(p_{12}, p_1, p_2), \tag{A.65}$$

Here, 2-body phase space is written as follows:

$$\int d\Phi_2(p_1, p_2, p_3) \tag{A.66}$$

$$= \int (2\pi)^4 \delta^4(p_1 - p_2 - p_3) \frac{d^3 p_2}{(2\pi)^3 2E_2} \frac{d^3 p_3}{(2\pi)^3 2E_3} \tag{A.67}$$

$$= \frac{1}{(2\pi)^2} \int \frac{d^3 p_2}{4E_2 E_3} \delta\big(m_a - \sqrt{\mathbf{p_2}^2 + m_2^2} - \sqrt{\mathbf{p_2}^2 + m_3^2}\big) \tag{A.68}$$

$$= \frac{1}{2\pi} \int d|p_2| d\cos\theta \frac{\sqrt{m_a^4 - 2m_a^2(m_b^2 + m_c^2) + (m_b^2 - m_c^2)^2}}{8m_a^2} \times \delta\big(|p_2| - |p_{2\mathrm{zero}}|\big). \tag{A.69}$$

A.2 The two loop integral

In this section, we calculate 2-loop integral for Zee-Babu type diagrams. Our calculation refers to [220] and [221].

First, we define I_5 and rewrite it by other integrals: [34]

$$I_5(m_a, m_b, m_c, m_d, m_e) \tag{A.70}$$

$$\equiv(\tilde{\mathfrak{m}})^{-2\epsilon} \int \frac{d^Dp}{(2\pi)^D} \frac{d^Dq}{(2\pi)^D} \frac{1}{(p^2-m_a^2)(p^2-m_b^2)(q^2-m_c^2)(q^2-m_d^2)\{(p+q)^2-m_e^2\}} \tag{A.71}$$

$$=\frac{1}{(m_a^2-m_b^2)(m_c^2-m_d^2)} \tag{A.72}$$

$$\times (\tilde{\mathfrak{m}})^{-2\epsilon} \int \frac{d^Dp}{(2\pi)^D} \frac{d^Dq}{(2\pi)^D} \left(\frac{1}{p^2-m_a^2} - \frac{1}{p^2-m_b^2}\right)\left(\frac{1}{q^2-m_c^2} - \frac{1}{q^2-m_d^2}\right) \frac{1}{(p+q)^2-m_e^2} \tag{A.73}$$

$$=\frac{1}{(m_a^2-m_b^2)(m_c^2-m_d^2)}\big\{I_3(m_a,m_c,m_e) - I_3(m_a,m_d,m_e) - I_3(m_b,m_c,m_e) + I_3(m_b,m_d,m_e)\big\}. \tag{A.74}$$

Here, I_3 is defined as follows:

$$I_3(M_a, M_b, M_c) \tag{A.75}$$

$$\equiv(\tilde{\mathfrak{m}})^{-2\epsilon} \int \frac{d^Dp}{(2\pi)^D} \int \frac{d^Dq}{(2\pi)^D} \frac{1}{(p^2-M_a^2)(q^2-M_b^2)\{(p+q)^2-M_c^2\}}. \tag{A.76}$$

Next we define J_5 as follows:

$$J_5(m_a, m_b, m_c, m_d, m_e) \tag{A.77}$$

$$\equiv(\tilde{\mathfrak{m}})^{-2\epsilon} \int \frac{d^Dp}{(2\pi)^D} \frac{d^Dq}{(2\pi)^D} \frac{p\cdot q}{(p^2-m_a^2)(p^2-m_b^2)(q^2-m_c^2)(q^2-m_d^2)\{(p+q)^2-m_e^2\}} \tag{A.78}$$

$$=\frac{1}{2} I_2(m_a,m_b) I_2(m_c,m_d) + \frac{m_e^2}{2} I_5(m_a,m_b,m_c,m_d,m_e) \tag{A.79}$$

$$-\frac{1}{2}\frac{1}{m_a^2-m_b^2}\frac{1}{m_c^2-m_d^2} \tag{A.80}$$

$$\times\Big\{(m_a^2+m_c^2)I_3(m_a,m_c,m_e) - (m_a^2+m_d^2)I_3(m_a,m_d,m_e) \tag{A.81}$$

$$-(m_b^2+m_c^2)I_3(m_b,m_c,m_e) + (m_b^2+m_d^2)I_3(m_b,m_d,m_e)\Big\}. \tag{A.82}$$

Here, I_2 is defined as follows:

$$I_2(M_a, M_b) \equiv (\tilde{\mathfrak{m}})^{-\epsilon} \int \frac{d^Dp}{(2\pi)^D} \frac{1}{(p^2-M_a^2)(p^2-M_b^2)}. \tag{A.83}$$

[34] Here, $\tilde{\mathfrak{m}}$ is 't Hooft cale. Please see §A.3 for a detail. The physical values does not depend on this.

I_2 is divergent. Zee-Babu masses (i.e. $I_5(M_a, M_b, M_c, M_d, M_e)$ and $J_5(M_a, M_b, M_c, M_d, M_e) - J_5(M_a, M_b, M_c, M_d, M_f)$) will not depend on I_2.

Next we evaluate I_3:

$$I_3(M_a, M_b, M_c) \tag{A.84}$$

$$=(\tilde{\mathfrak{m}})^{-2\epsilon} \int \frac{d^D p}{(2\pi)^D} \int \frac{d^D q}{(2\pi)^D} \frac{1}{(p^2 - M_a^2)(q^2 - M_b^2)\{(p+q)^2 - M_c^2\}} \tag{A.85}$$

$$=(\tilde{\mathfrak{m}})^{-2\epsilon} \int \frac{d^D p}{(2\pi)^D} \int \frac{d^D q}{(2\pi)^D} \frac{\frac{1}{2D}\sum_{\mu=0}^{D-1}\left(\frac{\partial p_\mu}{\partial p_\mu} + \frac{\partial q_\mu}{\partial q_\mu}\right)}{(p^2 - M_a^2)(q^2 - M_b^2)\{(p+q)^2 - M_c^2\}} \tag{A.86}$$

$$=\frac{1}{D}(\tilde{\mathfrak{m}})^{-2\epsilon} \int \frac{d^D p}{(2\pi)^D} \int \frac{d^D q}{(2\pi)^D} \frac{1}{(p^2 - M_a^2)(q^2 - M_b^2)\{(p+q)^2 - M_c^2\}} \tag{A.87}$$

$$\times \left\{ \frac{p^2}{p^2 - M_a^2} + \frac{q^2}{q^2 - M_b^2} + \frac{(p+q)^2}{(p+q)^2 - M_c^2} \right\} \tag{A.88}$$

$$=\frac{3}{D} I_3(M_a, M_b, M_c) + \frac{1}{D}\{M_a^2 I_4(M_a, M_b, M_c) + M_b^2 I_4(M_b, M_c, M_a) + M_c^2 I_4(M_c, M_a, M_b)\}, \tag{A.89}$$

i.e.

$$I_3(M_a, M_b, M_c) \tag{A.90}$$

$$=\frac{1}{D-3}\{M_a^2 I_4(M_a, M_b, M_c) + M_b^2 I_4(M_b, M_c, M_a) + M_c^2 I_4(M_c, M_a, M_b)\}. \tag{A.91}$$

Here, I_4 is defined as follows:

$$I_4(M_a, M_b, M_c) \equiv (\tilde{\mathfrak{m}})^{-2\epsilon} \int \frac{d^D p}{(2\pi)^D} \int \frac{d^D q}{(2\pi)^D} \frac{1}{(p^2 - M_a^2)^2(q^2 - M_b^2)\{(p+q)^2 - M_c^2\}}. \tag{A.92}$$

Using the above results, $I_5(M_a, M_b, M_c, M_d, M_e)$ and
$J_5(M_a, M_b, M_c, M_d, M_e) - J_5(M_a, M_b, M_c, M_d, M_f)$ are written by I_4 (and I_2). I_4 is evaluated as follows:

$$\begin{aligned} & I_4(M_a, M_b, M_c) \\ =&(\tilde{\mathfrak{m}})^{-2\epsilon} \int \frac{d^D p}{(2\pi)^D} \int \frac{d^D q}{(2\pi)^D} \frac{1}{(p^2 - M_a^2)^2(q^2 - M_b^2)\{(p+q)^2 - M_c^2\}} \\ =&\frac{-\Gamma(4-D)(\tilde{\mathfrak{m}})^{-2\epsilon}}{(4\pi)^D M_a^{2(4-D)}} \int_0^1 dx \int_0^1 dy \frac{\{x(1-x)\}^{2-D/2} y^{1-D/2}(1-y)}{\{x(1-x)\}^{4-D}\{(1-y) + y\mu^2(x)\}^{4-D}}, \\ & \left(\mu^2(x) = \frac{x M_b^2 + (1-x) M_c^2}{x(1-x) M_a^2}\right). \end{aligned} \tag{A.93}$$

Here, integral over y are given as follows ($D = 4 + \epsilon\,(\epsilon < 0)$):

$$\int_0^1 dy \frac{y^{1-D/2}(1-y)}{\left\{(1-y)+y\mu^2(x)\right\}^{4-D}} \tag{A.94}$$

$$= -\frac{2}{\epsilon} - 1 + \left\{\frac{1}{2} - \mathrm{Li}_2(1-\mu^2) + \frac{\mu^2\ln(\mu^2)}{1-\mu^2}\right\}\epsilon + \mathcal{O}(\epsilon^2). \tag{A.95}$$

Therefore, I_4 is written by the divergent part I_{41} and the finite part I_{42}, shown as follows:

$$I_4(M_a, M_b, M_c) \tag{A.96}$$

$$= \frac{-\Gamma(4-D)(\tilde{\mathfrak{m}})^{-2\epsilon}}{(4\pi)^D M_a^{2(4-D)}} \int_0^1 dx \int_0^1 dy \frac{\left\{x(1-x)\right\}^{D/2-2} y^{1-D/2}(1-y)}{\left\{(1-y)+y\mu^2(x)\right\}^{4-D}} \tag{A.97}$$

$$= \frac{1}{(4\pi)^4}\left[-\frac{2}{\epsilon^2} + \frac{1-2\ln(M_a^2/\mathfrak{m}^2)}{\epsilon} - \frac{1}{2} - \frac{\pi^2}{12} + \ln(M_a^2/\mathfrak{m}^2) - \ln^2(M_a^2/\mathfrak{m}^2)\right] \tag{A.98}$$

$$+ \frac{1}{(4\pi)^4}\int_0^1 dx \left\{-\mathrm{Li}_2(1-\mu^2) + \frac{\mu^2\ln(\mu^2)}{1-\mu^2}\right\} + \mathcal{O}(\epsilon) \tag{A.99}$$

$$= I_{41}(M_a) + I_{42}(M_a, M_b, M_c). \tag{A.100}$$

Here, $\mathfrak{m} = (4\pi)^{1/2} e^{-\gamma_E/2}\tilde{\mathfrak{m}}$, and the I_{41} and I_{42} are defined by (A.98) and (A.99), respectively. Using the above results, $I_5(M_a, M_b, M_c, M_d, M_e)$ and $J_5(M_a, M_b, M_c, M_d, M_e) - J_5(M_a, M_b, M_c, M_d, M_f)$ are written by finite parts I_{42}, and infinite parts I_{41} and I_2 are canceled:

$$I_5(M_a, M_b, M_c, M_d, M_e) \tag{A.101}$$

$$= \frac{1}{(M_a^2 - M_b^2)(M_c^2 - M_d^2)} \tag{A.102}$$

$$\times \Big[M_a^2\big\{I_{42}(M_a, M_c, M_e) - I_{42}(M_a, M_d, M_e)\big\} - M_b^2\big\{I_{42}(M_b, M_c, M_e) - I_{42}(M_b, M_d, M_e)\big\}$$
$$+ M_c^2\big\{I_{42}(M_c, M_e, M_a) - I_{42}(M_c, M_e, M_b)\big\} - M_d^2\big\{I_{42}(M_d, M_e, M_a) - I_{42}(M_d, M_e, M_b)\big\}$$
$$+ M_e^2\big\{I_{42}(M_e, M_a, M_c) - I_{42}(M_e, M_a, M_d) - I_{42}(M_e, M_b, M_c) + I_{42}(M_e, M_b, M_d)\big\},\Big] \tag{A.103}$$

$$J_5(M_a, M_b, M_c, M_d, M_e) - J_5(M_a, M_b, M_c, M_d, M_f) \tag{A.104}$$

$$= -\frac{1}{2(M_a^2 - M_b^2)(M_c^2 - M_d^2)} \tag{A.105}$$

$$\Big\{ M_a^2(M_a^2 + M_c^2 - M_e^2) I_{42}(M_a, M_c, M_e) - M_a^2(M_a^2 + M_c^2 - M_f^2) I_{42}(M_a, M_c, M_f)$$
$$- M_a^2(M_a^2 + M_d^2 - M_e^2) I_{42}(M_a, M_d, M_e) + M_a^2(M_a^2 + M_d^2 - M_f^2) I_{42}(M_a, M_d, M_f)$$
$$- M_b^2(M_b^2 + M_c^2 - M_e^2) I_{42}(M_b, M_c, M_e) + M_b^2(M_b^2 + M_c^2 - M_f^2) I_{42}(M_b, M_c, M_f)$$
$$+ M_b^2(M_b^2 + M_d^2 - M_e^2) I_{42}(M_b, M_d, M_e) - M_b^2(M_b^2 + M_d^2 - M_f^2) I_{42}(M_b, M_d, M_f)$$
$$+ M_c^2(M_a^2 + M_c^2 - M_e^2) I_{42}(M_c, M_e, M_a) - M_c^2(M_b^2 + M_c^2 - M_e^2) I_{42}(M_c, M_e, M_b)$$
$$- M_c^2(M_a^2 + M_c^2 - M_f^2) I_{42}(M_c, M_f, M_a) + M_c^2(M_b^2 + M_c^2 - M_f^2) I_{42}(M_c, M_f, M_b)$$
$$- M_d^2(M_a^2 + M_d^2 - M_e^2) I_{42}(M_d, M_e, M_a) + M_d^2(M_b^2 + M_d^2 - M_e^2) I_{42}(M_d, M_e, M_b)$$
$$+ M_d^2(M_a^2 + M_d^2 - M_f^2) I_{42}(M_d, M_f, M_a) - M_d^2(M_b^2 + M_d^2 - M_f^2) I_{42}(M_d, M_f, M_b)$$
$$+ M_e^2(M_a^2 + M_c^2 - M_e^2) I_{42}(M_e, M_a, M_c) - M_e^2(M_a^2 + M_d^2 - M_e^2) I_{42}(M_e, M_a, M_d)$$
$$- M_e^2(M_b^2 + M_c^2 - M_e^2) I_{42}(M_e, M_b, M_c) + M_e^2(M_b^2 + M_d^2 - M_e^2) I_{42}(M_e, M_b, M_d)$$
$$- M_f^2(M_a^2 + M_c^2 - M_f^2) I_{42}(M_f, M_a, M_c) + M_f^2(M_a^2 + M_d^2 - M_f^2) I_{42}(M_f, M_a, M_d)$$
$$+ M_f^2(M_b^2 + M_c^2 - M_f^2) I_{42}(M_f, M_b, M_c) - M_f^2(M_b^2 + M_d^2 - M_f^2) I_{42}(M_f, M_b, M_d) \Big\}. \tag{A.106}$$

A.3 't Hooft scale

Under the dimensional regularization $D = 4 + \epsilon$, the mass dimensions of parameters are [35]

$$[\text{mass}] = 1 \tag{A.107}$$

$$[\text{boson field } \phi] = \frac{D-2}{2} \tag{A.108}$$

$$[\text{fermion field } \Psi] = \frac{D-1}{2} \tag{A.109}$$

$$\big[\phi^4\text{'s coefficient}\big] = -D + 4 = -\epsilon \tag{A.110}$$

$$\big[\phi\overline{\Psi}\Psi\text{'s coefficient}\big] = -\frac{D}{2} + 2 = -\frac{\epsilon}{2} \tag{A.111}$$

$$\big[\phi^3\text{'s coefficient}\big] = -\frac{D}{2} + 3 = 1 - \frac{\epsilon}{2}. \tag{A.112}$$

[35] We denote the mass dimension of A as $[A]$

After redefinition:

$$\text{Yukawa coupling } y \to\ y\tilde{\mathfrak{m}}^{-\epsilon/2} \tag{A.113}$$

$$(\text{scalar})^{3\prime}\text{s coupling } \mu \to\ \mu\tilde{\mathfrak{m}}^{-\epsilon/2} \tag{A.114}$$

$$(\text{scalar})^{4\prime}\text{s coupling } \lambda \to\ \lambda\tilde{\mathfrak{m}}^{-\epsilon} \tag{A.115}$$

$$\text{gauge coupling } g \to\ g\tilde{\mathfrak{m}}^{-\epsilon/2}, \tag{A.116}$$

the mass dimensions of couplings become as

$$[y] = 0,\ [\mu] = 1,\ [\lambda] = 0,\ [g] = 0. \tag{A.117}$$

It is convenient to define $\mathfrak{m}$ as

$$\mathfrak{m} =(4\pi)^{1/2}e^{-\gamma_E/2}\tilde{\mathfrak{m}}. \tag{A.118}$$

$\mathfrak{m}$ is known as 't Hooft scale.

A.4 The mass bound on H^{++}

In this subsection, we assume this Lagrangian:

$$\mathcal{L} =\frac{1}{2}H^{++}(2h_{Le}\overline{e_L^c}e_L + 2h_{Re}\overline{e_R^c}e_R) + H^{++}(2h_{L\mu\tau}\overline{\mu_L^c}\tau_L + 2h_{R\mu\tau}\overline{\mu_R^c}\tau_R) + \text{H.c.} \tag{A.119}$$

H^{++}'s decay widths are

$$\Gamma(H^{++} \to \overline{e_L}\,\overline{e_L}) =\frac{1}{2M_{H^{++}}}\frac{1}{2}\sum_{\text{spin}}\int \frac{d^3\mathbf{p}_1}{(2\pi)^3 2E_1}\frac{d^3\mathbf{p}_2}{(2\pi)^3 2E_2} \tag{A.120}$$

$$\times (2\pi)^4\delta^4(P - p_1 - p_2)|2h_{Le}|^2\left|\overline{u}(p_1)P_L v(p_2)\right|^2 \tag{A.121}$$

$$=\frac{|h_{Le}|^2 M_{H^{++}}}{8\pi} \tag{A.122}$$

$$\Gamma(H^{++} \to \overline{e_R}\,\overline{e_R}) =\frac{|h_{Re}|^2 M_{H^{++}}}{8\pi} \tag{A.123}$$

$$\Gamma(H^{++} \to \overline{\mu_L}\,\overline{\tau_L}) =\frac{|h_{L\mu\tau}|^2 M_{H^{++}}}{4\pi} \tag{A.124}$$

$$\Gamma(H^{++} \to \overline{\mu_R}\,\overline{\tau_R}) =\frac{|h_{R\mu\tau}|^2 M_{H^{++}}}{4\pi} \tag{A.125}$$

In the parameter setting in this thesis, $|h_{L,\,Re}|^2 \ll |h_{L,\,R\mu\tau}|^2$. [36] Therefore, $H^{++}_{11,2}$'s main decay mode is $H^{++}_{11,2} \to \mu_R\tau_R$. ATLAS and CMS search doubly-charged Higgs

[36] $|h_{L,\,R\mu\tau}|^2$ is large ($O(0.1-1)$), because Δa contains $h_{L,\,R\mu\tau}$. Furthermore, $h_{L,\,Re}$ is small ($O(10^{-2} - 10^{-3})$), because we assume normal hierarchy and $m_{\nu_1} = 0$. Using this smallness, we can avoid the experimental limit of $\tau \to ee\mu^c$.

boson in three or four lepton final states. The lepton final states in ATLAS's search are $\ell = e, \mu$ [222]. The ones in CMS consider final states are $\ell = e$, μ, τ [223]. We use limit for pair production ($H^{++}H^{--}$) in [223], because the main decay modes of $H^{++}_{11,2}$ contain τ.

The limit for double charged scalar mass is given as follows [37] [38]

$$M_{H^{++}} \gtrsim 537 \text{ GeV}. \tag{A.126}$$

B Appendix for Part III

B.1 $\chi \to \nu\nu$

We assume the following Lagrangian:

$$\begin{aligned}
\mathcal{L} =& -\frac{M_{N_i}}{2}\overline{N_i}N_i - \frac{f_i}{2\sqrt{2}}\Big(\phi\overline{N_i}N_i + i\chi\overline{N_i}\gamma_5 N_i\Big) && \text{(B.1)}\\
& - \Big(Y^{\nu}_{\alpha i}\overline{L_\alpha}\tilde{H}P_R N_i + \text{H.c.}\Big) && \text{(B.2)}\\
N_i =& \nu_{Ri} + \nu^c_{Ri},\ \Phi = \frac{1}{\sqrt{2}}(v_\phi + \phi + i\chi),\ M_i = \frac{f_{ij}v_\phi}{\sqrt{2}}. && \text{(B.3)}
\end{aligned}$$

Then, N gets Majorana masses, therefore, after integrating out N, we can explain neutrino oscillation. This χ is called as Majoron. Here, EOM of N_i are given as follows:

$$M_{N_i}N_i = -\frac{f_i}{\sqrt{2}}(\phi + i\chi\gamma_5)N_i - (Y^{\nu}_{ai}L^c_a\tilde{H} + Y^{\nu *}_{ai}\tilde{H}^\dagger L_a). \tag{B.4}$$

Using these equation,

$$\begin{aligned}
\mathcal{L}^{\text{eff}} =& \frac{M_{N_i}}{2}\overline{N_i}N_i + \frac{f_i}{2\sqrt{2}}\Big(\phi\overline{N_i}N_i + i\chi\overline{N_i}\gamma_5 N_i\Big) && \text{(B.5)}\\
& - \overline{N_i}\Big[M_{N_i}N_i + \frac{f_i}{\sqrt{2}}(\phi + i\chi\gamma_5)N_i + Y^{\nu}_{ai}L^c_a\tilde{H} + Y_{ai}\tilde{H}^\dagger L_a\Big] && \text{(B.6)}\\
\to& \frac{1}{2}\frac{Y^{\nu}_{ai}Y^{\nu}_{bi}v^2}{2M_{N_i}}\Big[1 + \frac{1}{v_\phi}(\phi + i\chi)\Big]\overline{\nu_{La}}\nu^c_{Lb} + \text{H.c.} && \text{(B.7)}\\
& + \text{dim 7 or higher},\ (H \to \langle H\rangle) && \text{(B.8)}\\
\supset& \frac{1}{2}\frac{im_{\nu_i}}{v_\phi}\chi\overline{\nu_i}(P_R - P_L)\nu_i = \frac{1}{2}\frac{im_{\nu_i}}{v_\phi}\chi\overline{\nu_i}\gamma_5\nu_i, && \text{(B.9)}\\
\nu_i =& \nu_{iL} + \nu^c_{iL}. && \text{(B.10)}
\end{aligned}$$

[37] Please see Table 6 in [223].

[38] This is not exact limit, because H^{++}_{11} and H^{++}_{2} are couple to $SU(2)$ gauge bosons in different ways.

Therefore, The amplitude of $\chi \to \nu_i \nu_i$ is:

$$i\mathcal{M}_{\chi(p_1)\to\nu_i(p_2)\nu_i(p_3)} = \overline{u}(p_2)\frac{-m_{\nu_i}}{v_\phi}\gamma_5 u(p_3), \tag{B.11}$$

$$\sum_{\text{d.o.f.}} |\mathcal{M}|^2 = \frac{m_{\nu_i}^2}{v_\phi^2}\text{Tr}(\not{p_2} + m_{\nu_i})\gamma_5(\not{p_3} + m_{\nu_i})(-\gamma_5) \tag{B.12}$$

$$= \frac{2m_{\nu_i}^2}{v_\phi^2}(m_\chi^2 - 4m_{\nu_i}^2). \tag{B.13}$$

Therefore, the decay rate of $\chi \to \nu_i \nu_i$ is given as follows:

$$\Gamma_{\chi\to\nu_i\nu_i} = \frac{1}{2m_\chi}\int d\Pi_2 d\Pi_3 (2\pi)^4 \delta^4(p_1 - p_2 - p_3)|\mathcal{M}_{\chi\to\nu_i\nu_i}|^2 \tag{B.14}$$

$$= \frac{m_\chi}{8\pi}\frac{m_{\nu_i}^2}{v_\phi^2}(1 - 4m_{\nu_i}^2/m_\chi^2)^{3/2}. \tag{B.15}$$

B.2 $\chi \to t\bar{t}$

In this section, we estimate the decay width of $\chi \to t\bar{t}$. First, the decay width is written by the amplitude:

$$\Gamma_{\chi\to t\bar{t}} = \frac{1}{2m_\chi}\int \frac{d^3p_2}{(2\pi)^3 2E_2}\int \frac{d^3p_3}{(2\pi)^3 2E_3}(2\pi)^4\delta(m_\chi - E_2 - E_3) \tag{B.16}$$

$$\times \delta^3(\mathbf{p}_2 + \mathbf{p}_3) \times \sum_{\text{fin}} \left|i\mathcal{M}_{\chi\to t\bar{t}}\right|^2. \tag{B.17}$$

Here, the amplitude is evaluated as follows

$$
\begin{aligned}
i\mathcal{M}_{\chi\to t\bar{t}} =&\delta_{\mathbf{3}}^{ab}\times\frac{ie}{c_W s_W}\overline{u(p_2)}\gamma^\mu\left[\frac{1}{2}P_L-\frac{2}{3}s_W^2\right]v(p_3)\times\frac{i\Big(-\eta_{\mu\nu}+\frac{p_{1\mu}p_{1\nu}}{M_Z^2}\Big)}{{p_1}^2-M_Z^2}\\
&\times(-1)\times\int\frac{d^D\ell}{(2\pi)^D}\mathrm{Tr}\frac{i\not{\ell}}{\ell^2}\frac{-iY^\nu_{\alpha i}v}{\sqrt{2}}P_R\frac{i(\not{\ell}+M_{N_i})}{\ell^2-M_{N_i}^2}\frac{f_i}{\sqrt{2}}\gamma_5\\
&\times\frac{i\big\{\cancel{(\ell-p_1)}+M_{N_i}\big\}}{(\ell^2-p_1)^2-M_{N_i}^2}\frac{-iY^{\nu*}_{\alpha i}v}{\sqrt{2}}P_L\frac{i\cancel{(\ell-p_1)}}{(\ell-p_1)^2}\frac{i}{2}\frac{e}{c_W s_W}\gamma^\nu P_L &\text{(B.18)}\\
=&-\frac{i}{4\sqrt{2}}\delta_{\mathbf{3}}^{ab}\frac{e^2}{c_W^2 s_W^2}|Y^\nu_{\alpha i}|^2v^2f_i\overline{u(p_2)}\gamma^\mu\left[\frac{1}{2}P_L-\frac{2}{3}s_W^2\right]v(p_3) &\text{(B.19)}\\
&\times\frac{\Big(-\eta_{\mu\nu}+\frac{p_{1\mu}p_{1\nu}}{M_Z^2}\Big)}{M_\chi^2-M_Z^2} &\text{(B.20)}\\
&\times\int\frac{d^D\ell}{(2\pi)^D}\frac{1}{\ell^2(\ell^2-M_{N_i}^2)\big\{(\ell-p_1)^2-M_{N_i}^2\big\}(\ell-p_1)^2} &\text{(B.21)}\\
&\times\mathrm{Tr}\not{\ell}P_R(\not{\ell}+M_{N_i})\gamma_5\big\{\cancel{(\ell-p_1)}+M_{N_i}\big\}P_L\cancel{(\ell-p_1)}\gamma^\nu P_L. &\text{(B.22)}
\end{aligned}
$$

Here, the loop integral can be evaluated as follows

$$
\begin{aligned}
&\int\frac{d^D\ell}{(2\pi)^D}\frac{f(\ell)}{\ell^2(\ell^2-M_{N_i}^2)\big\{(\ell-p_1)^2-M_{N_i}^2\big\}(\ell-p_1)^2} &\text{(B.23)}\\
=&3!\int_0^1dx\int_0^{1-x}dy\int_0^{1-x-y}dz\int\frac{d^D\ell}{(2\pi)^D}\frac{f(\ell)}{\big[\sum_i x_i\Delta_i\big]^4} &\text{(B.24)}\\
\sum_i x_i\Delta_i =&(1-x-y-z)\ell^2+x(\ell^2-M_{N_i}^2)+y(\ell-p_1)^2+z\big\{(\ell-p_1)^2-M_{N_i}^2\big\} &\text{(B.25)}\\
=&q^2+(y+z)(1-y-z)M_\chi^2-(x+z)M_{N_i}^2, &\text{(B.26)}\\
&\Big(q=\ell-(y+z)p_1\Big). &\text{(B.27)}
\end{aligned}
$$

Furthemore, the trace of gamma matrices is

$$
\begin{aligned}
&\mathrm{Tr}\not{\ell}P_R(\not{\ell}+M_{N_i})\gamma_5\big\{\cancel{(\ell-p_1)}+M_{N_i}\big\}P_L\cancel{(\ell-p_1)}\gamma^\nu P_L &\text{(B.28)}\\
\simeq&M_{N_i}q^2p_1^\nu. &\text{(B.29)}
\end{aligned}
$$

Finally, the loop integral can be evaluated as

$$\int \frac{d^D\ell}{(2\pi)^D}\frac{1}{\ell^2(\ell^2-M_{N_i}^2)\big\{(\ell-p_1)^2-M_{N_i}^2\big\}(\ell-p_1)^2} \tag{B.30}$$

$$\times \mathrm{Tr}\not{\ell}P_R(\not{\ell}-M_{N_i})\gamma_5\big\{\cancel{(\ell-p_1)}-M_{N_i}\big\}P_L\cancel{(\ell-p_1)}\gamma^\nu P_L \tag{B.31}$$

$$\simeq 3!\int_0^1 dx\int_0^{1-x}dy\int_0^{1-x-y}dz\int\frac{d^Dq}{(2\pi)^D}\frac{-M_{N_i}q^2p_1^\nu}{(q^2-\Delta)^4} \tag{B.32}$$

$$\simeq \frac{iM_{N_i}p_1^\nu}{8\pi^2}\times\frac{1}{2M_{N_i}^2}\quad (M_\chi \ll M_{N_i}). \tag{B.33}$$

Combining the above results, the amplitude is given as follows:

$$i\mathcal{M}_{\chi\to t\bar{t}} = -\frac{i}{4\sqrt{2}}\delta_{\mathbf{3}}^{ab}\frac{e^2}{c_W^2s_W^2}|Y_{\alpha i}^\nu|^2v^2f_i\overline{u(p_2)}\gamma^\mu\left[\frac{1}{2}P_L-\frac{2}{3}s_W^2\right]v(p_3) \tag{B.34}$$

$$\times\frac{\left(-\eta_{\mu\nu}+\frac{p_{1\mu}p_{1\nu}}{M_Z^2}\right)}{M_\chi^2-M_Z^2}\times\frac{iM_{N_i}p_1^\nu}{8\pi^2}\frac{1}{2M_{N_i}^2} \tag{B.35}$$

$$=\frac{1}{4\sqrt{2}}\delta_{\mathbf{3}}^{ab}\frac{e^2}{c_W^2s_W^2}|Y_{\alpha i}^\nu|^2v^2f_i\frac{1}{2M_{N_i}^2}\times\frac{M_{N_i}}{8\pi^2}\frac{1}{M_Z^2} \tag{B.36}$$

$$\times\frac{-M_t}{2}\overline{u(p_2)}\gamma_5v(p_3). \tag{B.37}$$

The squared amplitude is

$$\sum_{\text{fin}}|i\mathcal{M}_{\chi\to t\bar{t}}|^2 \tag{B.38}$$

$$\simeq\frac{3}{32}\frac{1}{(8\pi^2)^2}\frac{e^4v^4}{c_W^4s_W^4M_Z^4}\Big[\sum_{i,\,\alpha}|Y_{\alpha i}^\nu|^2f_i\frac{1}{2M_{N_i}^2}M_{N_i}\Big]^2 \tag{B.39}$$

$$\times\frac{M_t^2}{4}\mathrm{Tr}(\cancel{p_2}+M_t)\gamma_5(\cancel{p_3}+M_t)(-\gamma_5) \tag{B.40}$$

$$\simeq\frac{3}{32}\frac{1}{4}\frac{1}{(8\pi^2)^2}\frac{e^4v^4}{c_W^4s_W^4M_Z^4}\Big[\sum_{i,\,\alpha}|Y_{\alpha i}^\nu|^2f_iM_{N_i}^{-1}\Big]^2\cdot\frac{M_t^2M_\chi^2}{2}\,(M_t\ll M_\chi). \tag{B.41}$$

Finally, the decay width can be evaluated as follows

$$\Gamma_{\chi\to t\bar{t}} = \frac{1}{2m_\chi}\int\frac{d^3p_2}{(2\pi)^3 2E_2}\int\frac{d^3p_3}{(2\pi)^3 2E_3}(2\pi)^4\delta(m_\chi-E_2-E_3) \tag{B.42}$$

$$\times\delta^3(\mathbf{p}_2+\mathbf{p}_3)\times\sum_{\text{fin}}\left|i\mathcal{M}_{\chi\to t\bar{t}}\right|^2 \tag{B.43}$$

$$\simeq\frac{3M_\chi}{4096\pi^3}\frac{\alpha_W^2(v/\sqrt{2})^4M_t^2}{M_W^4}\Big[\sum_{i,\,\alpha}|Y_{\alpha i}^\nu|^2f_iM_{N_i}^{-1}\Big]^2. \tag{B.44}$$

B.3 The Casas Ibarra Parametrization

First, neutrino Majorana mass and PMNS matrix are [39]

$$\mathcal{L} \supset -\frac{1}{2}(M_\nu)_{ab}\overline{\nu}_{La}\nu^c_{Lb} + \text{H.c.}, \tag{B.45}$$

$$\nu_{La} = (U_{\text{PMNS}})_{ai}\nu_{Li} \ (\nu_{Li}: \text{ mass engenstate}), \tag{B.46}$$

$$U_{\text{PMNS}} = \begin{pmatrix} 1 & & \\ & c_{23} & s_{23} \\ & -s_{23} & c_{23} \end{pmatrix} \begin{pmatrix} c_{13} & & s_{13}e^{-i\delta_{\text{CP}}} \\ & 1 & \\ -s_{13}e^{+i\delta_{\text{CP}}} & & c_{13} \end{pmatrix} \tag{B.47}$$

$$\times \begin{pmatrix} c_{12} & s_{12} & \\ -s_{12} & c_{12} & \\ & & 1 \end{pmatrix} \begin{pmatrix} e^{+i\eta_1} & & \\ & e^{+i\eta_2} & \\ & & 1 \end{pmatrix}, \tag{B.48}$$

$$m_\nu^{\text{diag}} = U^\dagger_{\text{PMNS}} M_\nu U^*_{\text{PMNS}} \tag{B.49}$$

In our model, neutrino Yukawa and N_R's mass are shown as follows:

$$\mathcal{L} \supset -y_{ai}\overline{\ell_{La}}N_{Ri}(i\sigma_2)H^* - \frac{1}{2}N_{N_i}\overline{N^c_{R_i}}N_{R_i} + \text{H.c.} \tag{B.50}$$

$$\to -y_{ai}\overline{\ell_{La}}N_{Ri}\begin{pmatrix} & 1 \\ -1 & \end{pmatrix}\begin{pmatrix} 0 \\ v_{\text{EW}}/\sqrt{2} \end{pmatrix} - \frac{1}{2}N_{N_i}\overline{N^c_{R_i}}N_{R_i} + \text{H.c.} \tag{B.51}$$

$$= -\frac{y_{ai}v_{\text{EW}}}{\sqrt{2}}\overline{\nu_{La}}N_{Ri} - \frac{1}{2}M_{N_i}\overline{N^c_{R_i}}N_{R_i} + \text{H.c.}. \tag{B.52}$$

the equation of motion (EOM) for N_{Ri} (without kinetic term) is

$$N_{Ri} = -\frac{1}{M_{N_i}}\frac{y_{ai}v_{\text{EW}}}{\sqrt{2}}\nu^c_{La}. \tag{B.53}$$

Therefore,

$$\mathcal{L} \supset +\frac{y_{ai}y_{bi}v^2_{\text{EW}}}{2M_{N_i}}\overline{\nu_{La}}\nu^c_{Lb} - \frac{y_{ai}y_{bi}v^2_{\text{EW}}}{4M_{N_i}}\overline{\nu_{La}}\nu^c_{Lb} + \text{H.c.} \tag{B.54}$$

$$= +\frac{y_{ai}y_{bi}v^2_{\text{EW}}}{4M_{N_i}}\overline{\nu_{La}}\nu^c_{Lb} + \text{H.c.} \tag{B.55}$$

$$= -\frac{1}{2}(M_\nu)_{ab}\overline{\nu_{La}}\nu^c_{Lb} + \text{H.c.}, \tag{B.56}$$

$$(M_\nu)_{ab} = -\frac{y_{ai}y_{bi}v^2_{\text{EW}}}{2M_{N_i}} = (U_{\text{PMNS}})_{ai}m_{\nu_i}(U_{\text{PMNS}})_{bi}. \tag{B.57}$$

Therefore, y_{ai} can be written as follows (Casas Ibarra parametrization):

$$y = \frac{\sqrt{2}i}{v_{\text{EW}}}U_{\text{PMNS}}\sqrt{m_\nu^{\text{diag}}}O\sqrt{M_N}, \ (OO^{\text{T}} = I). \tag{B.58}$$

[39] $\langle H\rangle = (0, v_{\text{EW}}/\sqrt{2})^{\text{T}}$.

B.4 Energy density, number density, entropy density

Energy density, numeber density, pressure are given as follows:

$$n = \frac{g}{(2\pi)^3}\int f(\mathbf{p})d^3p,\ \rho = \frac{g}{(2\pi)^3}\int E(\mathbf{p})f(\mathbf{p})d^3p, \tag{B.59}$$

$$p = \frac{g}{(2\pi)^3}\int \frac{|p|^2}{3E(\mathbf{p})}f(\mathbf{p})d^3p,\ f(\mathbf{p}) = \frac{1}{\exp\left[\beta(E-\mu)\right]\pm 1},\ (+:\text{ Fermi}, -:\text{ Bose}). \tag{B.60}$$

When $\mu \ll T$, entropy density is given as:

$$s = \frac{\rho - n\mu + p}{T} \simeq \frac{\rho + p}{T}. \tag{B.61}$$

In relativistic limit $T \gg m$ and $\mu \ll T$,

$$\rho = \begin{cases} \frac{\pi^2}{30}gT^4,\ \text{(Bose)} \\ \frac{7}{8}\frac{\pi^2}{30}gT^4,\ \text{(Fermi)} \end{cases},\ n = \begin{cases} \frac{\zeta(3)}{\pi^2}gT^3,\ \text{(Bose)} \\ \frac{3}{4}\frac{\zeta(3)}{\pi^2}gT^3,\ \text{(Fermi)} \end{cases},\ p = \frac{\rho}{3}. \tag{B.62}$$

Then total energy density and total entropy density is given as follows:

$$\rho_{\text{tot}} = \frac{\pi^2}{30}g_*T^4,\ g_* = \sum_{\text{boson}} g_i\Big(\frac{T_i}{T}\Big)^4 + \sum_{\text{fermion}} \frac{7}{8}g_i\Big(\frac{T_i}{T}\Big)^4, \tag{B.63}$$

$$s = \frac{2\pi^2}{45}g_{*S}T^3,\ g_{*S} = \sum_{\text{boson}} g_i\Big(\frac{T_i}{T}\Big)^3 + \sum_{\text{fermion}} \frac{7}{8}g_i\Big(\frac{T_i}{T}\Big)^3. \tag{B.64}$$

When using Maxwell-Boltzmann distribution with $\mu \ll T$, number density is given as below (this is useful for solving Boltzmann equation):

$$n^{\text{eq}} = \frac{4\pi g}{(2\pi)^3}\int_m^\infty dE\cdot E^2\sqrt{E^2-m^2}e^{-E/T} = \frac{gm^2TK_2(m/T)}{2\pi^2}, \tag{B.65}$$

$$Y^{\text{eq}} = \frac{n}{s} = \frac{nm^3}{s(m)T^3} = \frac{gm^5T^{-2}K_2(m/T)}{2\pi^2 s(m)} = \frac{gm^3x^2K_2(x)}{2\pi^2 s(m)},\ (x = m/T). \tag{B.66}$$

B.5 The Boltzmann equation

Boltzmann equation is ($x = m_\psi/T$):

$$\frac{dY}{dx} = -\frac{x^4}{H(m_\psi)s(m_\psi)}\int d\Pi_\psi d\Pi_a\cdots d\Pi_b d\Pi_c\cdots \tag{B.67}$$

$$\times (2\pi)^4\delta^4(p_\psi + p_a + \cdots - p_b - p_c - \cdots) \tag{B.68}$$

$$\times \left[|\mathcal{M}_{\psi+a+\cdots\to b+c+\cdots}|^2 f_\psi f_a\cdots(1\pm f_b)(1\pm f_c)\cdots\right. \tag{B.69}$$

$$\left. - |\mathcal{M}_{b+c+\cdots\to\psi+a\cdots}|^2 f_b f_c\cdots(1\pm f_\psi)(1\pm f_a)\cdots\right]. \tag{B.70}$$

Here, $|\mathcal{M}|$ is "summed" over freedom of the initial and final states [40], Y is defined as $Y = n/s$.

We define an interaction density γ as below:

$$\gamma^{\psi a\cdots}{}_{bc\cdots} \equiv \gamma(\psi + a + \cdots \to b + c + \cdots) \tag{B.71}$$

$$= \int d\Pi_\psi d\Pi_a \cdots d\Pi_b d\Pi_c \left|\mathcal{M}(X + a + \cdots \to b + c + \cdots)\right|^2 \tag{B.72}$$

$$\times (2\pi)^4 \delta^4(p_\psi + p_a + \cdots - p_b - p_c - \cdots) f_\psi^{\rm EQ} f_a^{\rm EQ} \cdots . \tag{B.73}$$

When $1 \pm f \simeq f$ and $f_x \simeq f_x^{\rm EQ} \frac{Y_x}{Y_x^{\rm eq}}$,

$$\frac{H(m_\psi)s(m_\psi)}{x^4}\frac{dY}{dx} = -\left(y^\psi y^a \cdots \gamma^{\psi a\cdots}{}_{bc\cdots} - y^b y^c \cdots \gamma^{bc\cdots}{}_{\psi a\cdots}\right) \tag{B.74}$$

$$= -\left[\psi a \cdots \leftrightarrow b + c \cdots\right], \tag{B.75}$$

$$\left[\psi a \cdots \leftrightarrow b + c \cdots\right] \equiv y^\psi y^a \cdots \gamma^{\psi a\cdots}{}_{bc\cdots} - y^b y^c \cdots \gamma^{bc\cdots}{}_{\psi a\cdots},\ y_x = \frac{Y_x}{Y_x^{\rm EQ}}. \tag{B.76}$$

B.6 The integrals of (thermal-averaged) phase spaces

In this section, we evaluate the integrals of (thermal-averaged) phase spaces. These are used in Boltzmann equations. First, we evaluate the integral of 2-body phase space, which used in the integral over phase space of final states. The evaluation is shown as follows:

$$\int d\Pi_1 d\Pi_2 (2\pi)^4 \delta^4(k - p_1 - p_2) \tag{B.77}$$

$$= \theta\left[s - (m_1 + m_2)^2\right] \frac{1}{2^4\pi}\sqrt{\lambda(1, m_1^2/s, m_2^2/s)} \int d(\cos\theta),\ (\lambda(a,b,c) = (a-b-c)^2 - 4bc). \tag{B.78}$$

Next, we evaluate the integral of thermal averaged (2-body) phase space, which used in the integral over phase space of initial states. The evaluation is shown as follows:

$$\int d\Pi_1 d\Pi_2 e^{-\beta(E_1+E_2)} f(s) \tag{B.79}$$

$$= \frac{1}{2^6\pi^4}\int_{s'>(m_1+m_2)^2} ds' \frac{s^{1/2} K_1(\beta\sqrt{s'}) f(s')}{\beta}\sqrt{\lambda(1, m_1^2/s, m_2^2/s)}. \tag{B.80}$$

[40] It depends on the definition of $d\Pi_i$. In my notation, $d\Pi_i = \frac{1}{(2\pi)^3}\frac{dp_i^3}{2E}$.

B.7 $\sigma^{ab}{}_{cd}(s)$

In this subsections, we evaluate the cross section of $ab \to cd$ ($\sigma^{ab}{}_{cd}(s)$). It is written as follows: [41]

$$\sigma^{ab}{}_{cd}(s) = \frac{1}{g_a g_b S_f!} \frac{1}{4\sqrt{(p_a p_b)^2 - m_a^2 m_b^2}} \int d\Pi_a d\Pi_b (2\pi)^4 \delta^4(p_a + p_b - p_c - p_d) |\mathcal{M}(s,\, \cos\theta)|^2 \tag{B.81}$$

$$= \frac{1}{g_a g_b S_f!} \frac{1}{2^5 \pi s} \sqrt{\frac{\lambda(1, m_c^2/s, m_d^2/s)}{\lambda(1,\, m_a^2/s,\, m_b^2/s)}} \theta\big[s - (m_c + m_d)^2\big] \tag{B.82}$$

$$\times \int d(\cos\theta) |\mathcal{M}(s,\, \cos\theta)|^2. \tag{B.83}$$

B.8 The evaluation of $\gamma^{a}{}_{bc}$ and $\gamma^{ab}{}_{cd}$

In this section, we evaluate $\gamma^{a}{}_{bc}$ and $\gamma^{ab}{}_{cd}$. These are used in Boltzmann equations. First, $\gamma^{a}{}_{bc}$ is evaluated as follows: [42]

$$\gamma^{a}{}_{bc} = \int d\Pi_a d\Pi_b d\Pi_c (2\pi)^4 \delta^4(p_a - p_b - p_c) |\mathcal{M}_{a\to bc}|^2 e^{-\beta E_a} \tag{B.84}$$

$$= \frac{g_a m_a^3 \Gamma_{a\to bc}}{2\pi^2} x_a^{-1} K_1(x_a),\ (x_a = m_a/T). \tag{B.85}$$

Next, we evaluate $\gamma^{ab}{}_{cd}$ as follows [43]:

$$\gamma^{ab}{}_{cd} = \frac{1}{S_i! S_f!} \int d\Pi_{p_a} d\Pi_{p_b} d\Pi_{p_c} d\Pi_{p_d} (2\pi)^4 \delta(p_a + p_b - p_c - p_d) e^{-\beta(E_a + E_b)} \left|\mathcal{M}^{ab}_{cd}\right|^2 \tag{B.86}$$

$$= \frac{g_a g_b}{2^5 \pi^4 S_i!} \int_{s > \max\left[(m_a+m_b)^2,\, (m_c+m_d)^2\right]} ds \frac{s^{3/2} K_1(\beta s^{1/2})}{\beta} \lambda(1,\, m_a^2/s,\, m_b^2/s) \sigma_{ab\to cd}(s), \tag{B.87}$$

$$\big(\lambda(a,\, b,\, c) = (a - b - c) - 4bc\big).$$

B.9 The narrow width approximation

In this section, we approximate $\gamma^{ab\cdots}{}_{cd\cdots}$ by narrow width approximation. We assume that the process $ab\cdots \to cd\cdots$ contains the intermediate state B as $ab\cdots \to B \to cd\cdots$.

[41] S_f is the symmetric factor of final state phase space. g_a, g_b are the degrees of freedom of a and b, respectively.

[42] Here, we use the formulas in §inttheravephasespsec.

[43] S_i, S_f is the number of identical particles.

Through out this section, $|\mathcal{M}|^2$ is "summed" over d.o.f of the initial and final states. First, we evaluate the following integral by narrow width approximation: [44] [45]

$$\int d\Pi_c d\Pi_d \cdots (2\pi)^4 \delta^4(p_B - p_c - p_d - \cdots) \left|\mathcal{M}_{ab\cdots\to cd\cdots}\right|^2 \tag{B.90}$$

$$= g_B^{-1} \int d\Pi_c d\Pi_d \cdots \left|\mathcal{M}_{ab\cdots\to B}\right|^2 (2\pi)^4 \delta^4(p_B - p_c - p_d - \cdots) \tag{B.91}$$

$$\times \left|\frac{i}{s - M^2 + iM\Gamma_{\text{tot}}}\right|^2 \left|\mathcal{M}_{B\to cd\cdots}\right|^2 \tag{B.92}$$

$$\simeq \left|\mathcal{M}_{ab\cdots\to B}\right|^2 \frac{2M\Gamma_{B\to cd\cdots}}{(s-M^2)^2 + (M\Gamma_{\text{tot}})^2} \quad \left(\text{When } p_B^2 = s \sim M^2 \text{ (on-shell)}\right) \tag{B.93}$$

$$= \left|\mathcal{M}_{ab\cdots\to B}\right|^2 2\pi\delta(s - M^2) \times \frac{\Gamma_{B\to cd\cdots}}{\Gamma_{\text{tot}}} \quad \left(|s - M^2| \gg M\Gamma\right). \tag{B.94}$$

Here, Γ_{tot} is the total decay width of the intermediate state B. Then, $\gamma^{ab\cdots}{}_{cd\cdots}$ is approximated as follows:

$$\gamma^{ab\cdots}{}_{cd\cdots} = \int d\Pi_a d\Pi_b \cdots d\Pi_c d\Pi_d \cdots (2\pi)^4 \delta^4(p_a + p_b + \cdots - p_c - p_d) \tag{B.95}$$

$$\times \left|\mathcal{M}_{ab\cdots\to cd\cdots}\right|^2 e^{-\beta(E_a + E_b + \cdots)} \tag{B.96}$$

$$\simeq \int d\Pi_a d\Pi_b \cdots \left|\mathcal{M}_{ab\cdots\to B}\right|^2 \tag{B.97}$$

$$\times (2\pi)\delta(s - M^2) e^{-\beta(E_a + E_b + \cdots)} \times \text{Br}_{B\to cd\cdots} \tag{B.98}$$

$$= \gamma^{ab\cdots}{}_B \text{Br}_{B\to cd\cdots}. \tag{B.99}$$

Here, $\text{Br}_{B\to cd\cdots}$ is the branching ratio of the process $B \to cd\cdots$.

[44] $\delta(x) = \frac{1}{2\pi i}\left(\frac{1}{x - i\epsilon} - \frac{1}{x + i\epsilon}\right) = \frac{1}{\pi}\frac{\epsilon}{x^2 + \epsilon^2}$.

[45] When B have nonzero spins or inertial degree of freedom, we need sum over B's degree of freedom. (cf. $\sum_s u_s \overline{u_s} = \not{p} - m$, $\sum_\lambda \epsilon^*_{\mu\lambda}\epsilon_{\nu\lambda} = -(\eta_{\mu\nu} - k_\mu k_\nu/m^2)$.) Therefore,

$$\left|\mathcal{M}_{ab\cdots\to cd\cdots}\right|^2 = \left|\sum_{B\text{'s degree of freedom}} \mathcal{M}_{ab\cdots\to B} \frac{i}{s - M^2 + iM\Gamma_{\text{tot}}} \mathcal{M}_{B\to cd\cdots}\right|^2 \tag{B.88}$$

$$\simeq \frac{1}{g_B}\left(\sum_{B\text{'s d.o.f}} \left|\mathcal{M}_{ab\cdots\to B}\right|^2\right) \left|\frac{i}{s - M^2 + iM\Gamma_{\text{tot}}}\right|^2 \left(\sum_{B\text{'s d.o.f}} \left|\mathcal{M}_{B\to cd\cdots}\right|^2\right). \tag{B.89}$$

Here, we ignore the coherences of B's different state in (B.89). Overline means average over spin.

C Appendix for Part IV

C.1 Fujikawa Method

First, we assume the following Lagrangian:

$$\mathcal{L} = \overline{\Psi_L}(i\not{D})\Psi_L - \frac{1}{4}\big(F^a_{\mu\nu}\big)^2. \tag{C.1}$$

Here, we assume that the gauge anomaly of Ψ is cancelled with other contributions of the gauge anomaly.

Under the local transformation: $\Psi_L \to \Psi'_L = e^{+i\alpha(x)}\Psi_L = e^{-i\alpha(x)\gamma^5}\Psi_L$, the Lagrangian is transformed as follows:

$$\delta\mathcal{L}_{\rm cl} = \partial_\mu\alpha(x)\overline{\Psi_L}\gamma^\mu\gamma^5\Psi_L. \tag{C.2}$$

Next, we evaluate the measure of path integral: [46]

$$\mathcal{D}\overline{\Psi_L}\mathcal{D}\Psi_L \to \mathcal{D}\big(\overline{\Psi_L}e^{-i\alpha(x)\gamma^5}\big)\mathcal{D}\big(e^{-i\alpha(x)\gamma^5}\Psi_L\big) \tag{C.3}$$

$$= (\det{}_L J)^{-1}(\det{}_R J)^{-1}\mathcal{D}\overline{\Psi_L}\mathcal{D}\Psi_L. \tag{C.4}$$

Here, Jacobian J is given as follows:

$$J(x,y) = \delta(x-y)e^{-i\alpha(x)\gamma^5} = \sum_n \frac{1}{n!}\big(-i\alpha(x)1_{xy}\gamma^5\big)^n = \exp\big(-i\alpha(x)1_{xy}\gamma^5\big) \tag{C.5}$$

Using this definition, we can evaluate $(\det_L J)(\det_R J)$:

$$(\det{}_L J)(\det{}_R J) = \exp\left[\int dx \mathrm{Tr}\big\{-i\alpha(x)\delta(x-x)\gamma^5 P_L\big\}\right] \tag{C.6}$$

$$\times \exp\left[\int dx \mathrm{Tr}\big\{-i\alpha(x)\delta(x-x)\gamma^5 P_R\big\}\right] \tag{C.7}$$

$$= \exp\left[\int dx \mathrm{Tr}\big\{-i\alpha(x)\delta(x-x)\gamma^5\big\}\right]. \tag{C.8}$$

Though $\mathrm{Tr}\gamma_5 = 0$ and $\delta(x-x) = \infty$, we can evaluate by Fujikawa method. First, we replace delta function as follows: [47]

$$\delta(x-y) \to e^{(i\not{D}_x)^2/M^2}\delta(x-y) = \int \frac{d^4k}{(2\pi)^4} e^{(i\not{D}_x)^2/M^2} e^{ik(x-y)} \tag{C.9}$$

$$= \int \frac{d^4k}{(2\pi)^4} e^{ik(x-y)} e^{-(\not{D}_x + i\not{k})^2/M^2}. \tag{C.10}$$

[46] Naively, $\ln\big[\prod_x e^{-i\alpha(x)}e^{+i\alpha(x)}\big] = -i\int_x \mathrm{Tr}\gamma_5 = 0$. However, $\int_x 1 = \infty$, therefore, $\int_x \mathrm{Tr}\gamma_5$ can have non-zero values.

[47] $\partial e^{ikx} = e^{ikx}(\partial + ik)$, $\partial^n e^{ikx} = \partial^{n-1}e^{ikx}(\partial + ik) = e^{ikx}(\partial + ik)^n$, therefore, $f(\partial)e^{ikx} = e^{ikx}f(\partial + ik)$.

Here,

$$(\not{D} + i\not{k})^2 = \not{D}^2 - k^2 + i\{\not{D}, \not{k}\} \tag{C.11}$$

$$= D^2 - gF_{\mu\nu}\sigma^{\mu\nu}/2 - k^2 + 2ik \cdot D. \tag{C.12}$$

Therefore, the trace of $\delta(x-x)\gamma^5$ is evaluated as follows:

$$\mathrm{Tr}\big[\delta(x-x)\gamma^5\big] = \int \frac{d^4k}{(2\pi)^4} \mathrm{Tr} e^{-\left[D^2 - gF_{\mu\nu}\sigma^{\mu\nu}/2 - k^2 + 2ik\cdot D\right]/M^2}\gamma^5 \tag{C.13}$$

$$= M^4 \int \frac{d^4\kappa}{(2\pi)^4} \mathrm{Tr} e^{-\left[M^{-2}D^2 - gM^{-2}F_{\mu\nu}\sigma^{\mu\nu}/2 - \kappa^2 + 2iM^{-1}\kappa\cdot D\right]}\gamma^5, \ (k = M\kappa) \tag{C.14}$$

$$= M^4 \int \frac{d^4\kappa}{(2\pi)^4} e^{\kappa^2}\left[\frac{g^2}{2\cdot 2^2 M^4}\mathrm{Tr}F_{\mu\nu}F_{\rho\sigma}\mathrm{Tr}\sigma^{\mu\nu}\sigma^{\rho\sigma}\gamma^5 + O(M^{-5})\right] \tag{C.15}$$

$$= -\frac{g^2}{16\pi^2}\mathrm{Tr}F_{\mu\nu}\tilde{F}^{\mu\nu}. \tag{C.16}$$

Then, the determinant of Jacobian is written by field strength, as follows:

$$(\det_L J)^{-1}(\det_R J)^{-1} = \exp\left[-\int dx \mathrm{Tr}\big\{-i\alpha(x)\delta(x-x)\gamma^5\big\}\right] \tag{C.17}$$

$$= \exp\left[-i\frac{g^2}{16\pi^2}\int dx\alpha(x)\mathrm{Tr}F\tilde{F}\right]. \tag{C.18}$$

Therefore, path integral is written as follows:

$$Z = \int \mathcal{D}\overline{\Psi_L}\mathcal{D}\Psi_L e^{iS(\Psi)} = \int \mathcal{D}\overline{\Psi'_L}\mathcal{D}\Psi'_L e^{iS(\Psi')} \tag{C.19}$$

$$= \int \mathcal{D}\overline{\Psi_L}\mathcal{D}\Psi_L \exp\Big\{i\big[S + \delta S\big]\Big\} \tag{C.20}$$

$$\delta\mathcal{L} = (\partial_\mu\alpha)\overline{\Psi_L}\gamma^\mu\gamma^5\Psi_L - \frac{g^2\alpha}{16\pi^2}\mathrm{Tr}F\tilde{F}. \tag{C.21}$$

When assuming the following right-handed Lagrangian:

$$\mathcal{L} = \overline{\Psi_R}(i\not{D})\Psi_R - \frac{1}{4}\big(F^a_{\mu\nu}\big)^2, \tag{C.22}$$

and the local transformation: $\Psi_R \to e^{-i\alpha(x)}\Psi_R = e^{-i\alpha(x)\gamma^5}\Psi_R$, the path integral is written

as follows

$$Z = \int \mathcal{D}\overline{\Psi_R}\mathcal{D}\Psi_R e^{iS(\Psi)} = \int \mathcal{D}\overline{\Psi'_R}\mathcal{D}\Psi'_R e^{iS(\Psi')} \tag{C.23}$$

$$= \int \mathcal{D}\overline{\Psi_R}\mathcal{D}\Psi_R \exp\Big\{i\big[S+\delta S\big]\Big\} \tag{C.24}$$

$$\delta\mathcal{L} = (\partial_\mu\alpha)\overline{\Psi_R}\gamma^\mu\gamma^5\Psi_R - \frac{g^2\alpha}{16\pi^2}\mathrm{Tr}F\tilde{F}. \tag{C.25}$$

C.2 The couplings in the QCD axion models and the chiral Lagrangian

This subsection is based on [157, 158].

C.2.1 PQWW axon model or DFSZ axion model

In this section, we assume the following axion effective Lagrangian ($q = (u,\, d)^{\mathrm{T}}$, $c_q^0 = \mathrm{diag}(c_u^0,\, c_d^0)$, $M_q = \mathrm{diag}(m_u,\, m_d)$):

$$\mathcal{L} \supset \frac{1}{2}(\partial a)^2 - \frac{a}{f_a}\frac{g_s^2}{16\pi^2}\mathrm{Tr}G\tilde{G} + \frac{1}{4}g^0_{a\gamma}aF\tilde{F} + \frac{\partial_\mu a}{2f_a}\overline{q}c_q^0\gamma^\mu\gamma^5 q - \overline{q}M_q q. \tag{C.26}$$

When q is transformed as $q \to e^{i\gamma_5\frac{a}{2f_a}Q_a}q$ (Q_a: Hermite, q is the first generation), $\mathcal{L}$ is transformed as $\mathcal{L} \to \mathcal{L} + \delta\mathcal{L}$:

$$\delta\mathcal{L} = -\frac{\partial a}{2f_a}\overline{q}\gamma^\mu\gamma^5 Q_a q + \frac{g_s^2}{8\pi^2}\frac{a}{2f_a}\mathrm{Tr}Q_a\mathrm{Tr}G\tilde{G} \tag{C.27}$$

$$+ \frac{e^2}{8\pi^2}\cdot N_c\frac{a}{2f_a}\mathrm{Tr}Q_aQ^2F\tilde{F} - \overline{q}e^{i\gamma_5\frac{a}{2f_a}Q_a}M_q e^{i\gamma_5\frac{a}{2f_a}Q_a}q. \tag{C.28}$$

When choosing $\mathrm{Tr}Q_a = 1$, $a\mathrm{Tr}G\tilde{G}$ is canceled:

$$\mathcal{L} \supset \frac{1}{2}(\partial a)^2 + \frac{1}{4}g_{a\gamma}aF\tilde{F} + \frac{\partial_\mu a}{2f_a}\overline{q}c_q\gamma^\mu\gamma^5 q - \overline{q}M_a q, \tag{C.29}$$

$$g_{a\gamma} = g^0_{a\gamma} + \frac{e^2}{4\pi^2 f_a}N_c\mathrm{Tr}Q^2Q_a,\; c_q = c_q^0 - Q_a, \tag{C.30}$$

$$M_a = e^{i\gamma_5\frac{a}{2f_a}Q_a}M_q e^{i\gamma_5\frac{a}{2f_a}Q_a}. \tag{C.31}$$

In order to choose Q_a, we consider the following effective Lagrangian:

$$\mathcal{L} = \mathcal{L}_{\mathrm{kin}} + \mathcal{L}_{\mathrm{mass}} \tag{C.32}$$

$$= \frac{f_\pi^2}{4}\Big[\mathrm{Tr}(DU)^\dagger(DU) + 2B_0\mathrm{Tr}(UM_a^\dagger + M_aU^\dagger)\Big], \tag{C.33}$$

$$U = \exp\big[i(\pi^a\sigma^a + \eta)/f_\pi\big],\; M_a = e^{iaQ_a/(2f_a)}M_q e^{iaQ_a/(2f_a)},\; M_q = \mathrm{diag}(m_u,\, m_d). \tag{C.34}$$

Here, $\mathcal{L}_{\rm mass}$ is expanded as follows:

$$\mathcal{L}_{\rm mass} \supset \frac{f_\pi^2}{4}(2B_0){\rm Tr}(UM_a^\dagger + M_aU^\dagger) \tag{C.35}$$

$$= \frac{f_\pi^2}{4}(2B_0)\Big\{(m_u+m_d)\big[2 - f_\pi^{-2}(\pi^{a2}+\eta^2)\big] - 2(m_u-m_d)f_\pi^{-2}\pi^3\eta\Big] \tag{C.36}$$

$$- \frac{ia}{2f_a}{\rm Tr}\big[U\{Q_a,\, M_q\} - {\rm H.c.}\big] - \frac{a^2}{f_a^2}{\rm Tr}[M_qQ_a^2]\Big\} + \text{higher order} \tag{C.37}$$

$$= -\frac{m_\pi^2}{2}(\pi^{a2}+\eta^2) - m_\pi^2\frac{m_u-m_d}{m_u+m_d}\pi^3\eta - \frac{\overline{m}_a^2}{2}a^2 + \text{higher order}. \tag{C.38}$$

Here, we choose Q_a as $Q_a = M_q^{-1}/{\rm Tr}(M_q^{-1})$ so that the term $a{\rm Tr}\big[U\{Q_a,\, M_q\} - {\rm H.c.}\big]$ is canceled. c_q, $g_{a\gamma}$ are written by this Q_a.

Next, we consider the mass term of η and a from anomaly. $\mathcal{L}_{\rm kin}$ has the symmetry: $SU(2)_L \otimes SU(2)_R$ $U \to RUL^\dagger$ ($q_L \to Lq_L$, $q_R \to Rq_R$). When $L = e^{+i\eta/(2f_\pi)}$ and $R = e^{-i\eta/(2f_\pi)}$ (i.e $q \to e^{-i\eta\gamma^5 1_{2\times2}/(2f_\pi)}q$), $\mathcal{L}$ is transformed as $\mathcal{L} \to \mathcal{L} + \delta\mathcal{L}$, $\delta\mathcal{L} \supset \frac{g_s^2}{8\pi^2}\frac{\eta}{2f_\pi}{\rm Tr}1_{2\times2}{\rm Tr}G\tilde{G} = \frac{g_s^2}{16\pi^2}\frac{2\eta}{f_\pi}{\rm Tr}G\tilde{G}$. Therefore, η and a get the following mass terms from anomaly:

$$\mathcal{L}_{\rm anomaly} = -\frac{m_{\eta 0}^2}{2}\big[\eta + af_\pi/(2f_a)\big]^2. \tag{C.39}$$

On the other hands, axion-neucleon coupling $\mathcal{L} \supset \frac{C_{af}}{2f_a}\partial_\mu a\overline{f}\gamma^\mu\gamma^5 f$ is given as follows: [224]

$$C_{ap} = -0.47(3) + 0.88(3)c_u^0 - 0.39(2)c_d^0 - C_{a,\,\rm sea}, \tag{C.40}$$

$$C_{an} = -0.02(3) + 0.88(3)c_d^0 - 0.39(2)c_u^0 - C_{a,\,\rm sea}, \tag{C.41}$$

$$C_{a,\,\rm sea} = 0.038(5)c_s^0 + 0.012(5)c_c^0 + 0.009(2)c_b^0 + 0.0035(4)c_t^0. \tag{C.42}$$

C.2.2 KSVZ axion model

In this section, we assume the following axion effective Lagrangian ($q = (u,\, d)^{\rm T}$, $c_q^0 = {\rm diag}(c_u^0,\, c_d^0)$, $M_q = {\rm diag}(m_u,\, m_d)$):

$$\mathcal{L} \supset \frac{1}{2}(\partial a)^2 - \frac{a}{f_a}\frac{g_s^2}{16\pi^2}{\rm Tr}G\tilde{G} + \frac{1}{4}g_{a\gamma}^0 aF\tilde{F} - \overline{q}M_qq. \tag{C.43}$$

η and a get the following mass terms from anomaly:

$$\mathcal{L}_{\rm anomaly} = -\frac{m_{\eta 0}^2}{2}\big[\eta + af_\pi/(2f_a)\big]^2. \tag{C.44}$$

Axion-neucleon coupling $\mathcal{L} \supset \frac{C_{af}}{2f_a}\partial_\mu a\overline{f}\gamma^\mu\gamma^5 f$ is given as follows: [224]

$$C_{ap} = -0.47(3),\ C_{an} = -0.02(3). \tag{C.45}$$

References

[1] Nabarun Chakrabarty, Cheng-Wei Chiang, Takahiro Ohata, and Koji Tsumura. Charged scalars confronting neutrino mass and muon $g-2$ anomaly. JHEP, 12:104, 2018.

[2] Yoshihiko Abe, Yu Hamada, Takahiro Ohata, Kenta Suzuki, and Koichi Yoshioka. TeV-scale Majorogenesis. JHEP, 07(07):105, 2020.

[3] Ernest Ma, Takahiro Ohata, and Koji Tsumura. Majoron as the QCD axion in a radiative seesaw model. Phys. Rev. D, 96(7):075039, 2017.

[4] Ziro Maki, Masami Nakagawa, and Shoichi Sakata. Remarks on the unified model of elementary particles. Prog. Theor. Phys., 28:870–880, 1962.

[5] B. Pontecorvo. Neutrino Experiments and the Problem of Conservation of Leptonic Charge. Sov. Phys. JETP, 26:984–988, 1968.

[6] Ivan Esteban, M.C. Gonzalez-Garcia, Michele Maltoni, Thomas Schwetz, and Albert Zhou. The fate of hints: updated global analysis of three-flavor neutrino oscillations. JHEP, 09:178, 2020. http://www.nu-fit.org/?q=node/228.

[7] B.T. Cleveland, Timothy Daily, Jr. Davis, Raymond, James R. Distel, Kenneth Lande, C.K. Lee, Paul S. Wildenhain, and Jack Ullman. Measurement of the solar electron neutrino flux with the Homestake chlorine detector. Astrophys. J., 496:505–526, 1998.

[8] F. Kaether, W. Hampel, G. Heusser, J. Kiko, and T. Kirsten. Reanalysis of the GALLEX solar neutrino flux and source experiments. Phys. Lett. B, 685:47–54, 2010.

[9] J.N. Abdurashitov et al. Measurement of the solar neutrino capture rate with gallium metal. III: Results for the 2002–2007 data-taking period. Phys. Rev. C, 80:015807, 2009.

[10] J. Hosaka et al. Solar neutrino measurements in super-Kamiokande-I. Phys. Rev. D, 73:112001, 2006.

[11] J.P. Cravens et al. Solar neutrino measurements in Super-Kamiokande-II. Phys. Rev. D, 78:032002, 2008.

[12] K. Abe et al. Solar neutrino results in Super-Kamiokande-III. Phys. Rev. D, 83:052010, 2011.

[13] Y. Nakajima. "SuperKamiokande" Talk given at the XXIX International Conference on Neutrino Physics and Astrophysics, Chicago, USA, June 22–July 2, 2020 (online conference).

[14] B. Aharmim et al. Combined Analysis of all Three Phases of Solar Neutrino Data from the Sudbury Neutrino Observatory. Phys. Rev. C, 88:025501, 2013.

[15] G. Bellini et al. Measurement of the solar 8B neutrino rate with a liquid scintillator target and 3 MeV energy threshold in the Borexino detector. Phys. Rev. D, 82:033006, 2010.

[16] G. Bellini et al. Precision measurement of the 7Be solar neutrino interaction rate in Borexino. Phys. Rev. Lett., 107:141302, 2011.

[17] G. Bellini et al. Neutrinos from the primary proton–proton fusion process in the Sun. Nature, 512(7515):383–386, 2014.

[18] Núria Vinyoles, Aldo M. Serenelli, Francesco L. Villante, Sarbani Basu, Johannes Bergström, M.C. Gonzalez-Garcia, Michele Maltoni, Carlos Peña Garay, and Ningqiang Song. A new Generation of Standard Solar Models. Astrophys. J., 835(2):202, 2017.

[19] M. G. Aartsen et al. Determining neutrino oscillation parameters from atmospheric muon neutrino disappearance with three years of IceCube DeepCore data. Phys. Rev. D, 91(7):072004, 2015.

[20] J. P. Yanez et al. IceCube Oscillations: 3 years muon neutrino disappearance data. https://icecube.wisc.edu/science/data/nu_osc.

[21] K. Abe et al. Atmospheric neutrino oscillation analysis with external constraints in Super-Kamiokande I-IV. Phys. Rev. D, 97(7):072001, 2018. (data release: http://www-sk.icrr.u-tokyo.ac.jp/sk/publications/result-e.html#atmosci2018).

[22] M. Honda, M. Sajjad Athar, T. Kajita, K. Kasahara, and S. Midorikawa. Atmospheric neutrino flux calculation using the NRLMSISE-00 atmospheric model. Phys. Rev. D, 92(2):023004, 2015.

[23] A. Gando et al. Reactor On-Off Antineutrino Measurement with KamLAND. Phys. Rev. D, 88(3):033001, 2013.

[24] Feng Peng An et al. Improved Measurement of the Reactor Antineutrino Flux and Spectrum at Daya Bay. Chin. Phys. C, 41(1):013002, 2017.

[25] H. de Kerret et al. Double Chooz θ_{13} measurement via total neutron capture detection. Nature Phys., 16(5):558–564, 2020.

[26] T. Bezerra. "New Results from the Double Chooz Experiment." Talk given at the XXIX International Conference on Neutrino Physics and Astrophysics, Chicago, USA, June 22–July 2, 2020 (online conference).

[27] D. Adey et al. Measurement of the Electron Antineutrino Oscillation with 1958 Days of Operation at Daya Bay. Phys. Rev. Lett., 121(24):241805, 2018.

[28] G. Bak et al. Measurement of Reactor Antineutrino Oscillation Amplitude and Frequency at RENO. Phys. Rev. Lett., 121(20):201801, 2018.

[29] J. Yoo. "RENO." Talk given at the XXIX International Conference on Neutrino Physics and Astrophysics, Chicago, USA, June 22–July 2, 2020 (online conference).

[30] P. Adamson et al. Electron neutrino and antineutrino appearance in the full MINOS data sample. Phys. Rev. Lett., 110(17):171801, 2013.

[31] P. Adamson et al. Measurement of Neutrino and Antineutrino Oscillations Using Beam and Atmospheric Data in MINOS. Phys. Rev. Lett., 110(25):251801, 2013.

[32] K. Abe et al. Constraint on the matter–antimatter symmetry-violating phase in neutrino oscillations. Nature, 580(7803):339–344, 2020. [Erratum: Nature 583, E16 (2020)].

[33] P. Dunne. "Latest Neutrino Oscillation Results from T2K." Talk given at the XXIX International Conference on Neutrino Physics and Astrophysics, Chicago, USA, June 22–July 2, 2020 (online conference).

[34] M.A. Acero et al. First Measurement of Neutrino Oscillation Parameters using Neutrinos and Antineutrinos by NOvA. Phys. Rev. Lett., 123(15):151803, 2019.

[35] A. Himmel. "New Oscillation Results from the NOvA Experiment." Talk given at the XXIX International Conference on Neutrino Physics and Astrophysics, Chicago, USA, June 22–July 2, 2020 (online conference).

[36] Peter Minkowski. $\mu \to e\gamma$ at a Rate of One Out of 10^9 Muon Decays? Phys. Lett. B, 67:421–428, 1977.

[37] Tsutomu Yanagida. Horizontal gauge symmetry and masses of neutrinos. Conf. Proc. C, 7902131:95–99, 1979.

[38] Murray Gell-Mann, Pierre Ramond, and Richard Slansky. Complex Spinors and Unified Theories. Conf. Proc. C, 790927:315–321, 1979.

[39] S.L. Glashow. The Future of Elementary Particle Physics. NATO Sci. Ser. B, 61:687, 1980.

[40] Rabindra N. Mohapatra and Goran Senjanovic. Neutrino Mass and Spontaneous Parity Nonconservation. Phys. Rev. Lett., 44:912, 1980.

[41] J. Schechter and J.W.F. Valle. Neutrino Masses in SU(2) x U(1) Theories. Phys. Rev. D, 22:2227, 1980.

[42] M. Magg and C. Wetterich. Neutrino Mass Problem and Gauge Hierarchy. Phys. Lett. B, 94:61–64, 1980.

[43] George Lazarides, Q. Shafi, and C. Wetterich. Proton Lifetime and Fermion Masses in an SO(10) Model. Nucl. Phys. B, 181:287–300, 1981.

[44] Robert Foot, H. Lew, X.G. He, and Girish C. Joshi. Seesaw Neutrino Masses Induced by a Triplet of Leptons. Z. Phys. C, 44:441, 1989.

[45] A. Zee. A Theory of Lepton Number Violation, Neutrino Majorana Mass, and Oscillation. Phys. Lett. B, 93:389, 1980. [Erratum: Phys.Lett.B 95, 461 (1980)].

[46] Lincoln Wolfenstein. A Theoretical Pattern for Neutrino Oscillations. Nucl. Phys. B, 175:93–96, 1980.

[47] A. Zee. Quantum Numbers of Majorana Neutrino Masses. Nucl. Phys. B, 264:99–110, 1986.

[48] K.S. Babu. Model of 'Calculable' Majorana Neutrino Masses. Phys. Lett. B, 203:132–136, 1988.

[49] Lawrence M. Krauss, Salah Nasri, and Mark Trodden. A Model for neutrino masses and dark matter. Phys. Rev. D, 67:085002, 2003.

[50] Ernest Ma. Verifiable radiative seesaw mechanism of neutrino mass and dark matter. Phys. Rev. D, 73:077301, 2006.

[51] Y. Chikashige, Rabindra N. Mohapatra, and R.D. Peccei. Are There Real Goldstone Bosons Associated with Broken Lepton Number? Phys. Lett. B, 98:265–268, 1981.

[52] J. Schechter and J.W.F. Valle. Neutrino Decay and Spontaneous Violation of Lepton Number. Phys. Rev. D, 25:774, 1982.

[53] Takeshi Fukuyama, Hiroaki Sugiyama, and Koji Tsumura. Constraints from muon g-2 and LFV processes in the Higgs Triplet Model. JHEP, 03:044, 2010.

[54] T. Aoyama et al. The anomalous magnetic moment of the muon in the Standard Model. 6 2020.

[55] G.W. Bennett et al. Final Report of the Muon E821 Anomalous Magnetic Moment Measurement at BNL. Phys. Rev. D, 73:072003, 2006.

[56] Peter J. Mohr, David B. Newell, and Barry N. Taylor. CODATA Recommended Values of the Fundamental Physical Constants: 2014. Rev. Mod. Phys., 88(3):035009, 2016.

[57] Tatsumi Aoyama, Masashi Hayakawa, Toichiro Kinoshita, and Makiko Nio. Complete Tenth-Order QED Contribution to the Muon g-2. Phys. Rev. Lett., 109:111808, 2012.

[58] Tatsumi Aoyama, Toichiro Kinoshita, and Makiko Nio. Theory of the Anomalous Magnetic Moment of the Electron. Atoms, 7(1):28, 2019.

[59] Andrzej Czarnecki, William J. Marciano, and Arkady Vainshtein. Refinements in electroweak contributions to the muon anomalous magnetic moment. Phys. Rev. D, 67:073006, 2003. [Erratum: Phys.Rev.D 73, 119901 (2006)].

[60] C. Gnendiger, D. Stöckinger, and H. Stöckinger-Kim. The electroweak contributions to $(g-2)_\mu$ after the Higgs boson mass measurement. Phys. Rev. D, 88:053005, 2013.

[61] Michel Davier, Andreas Hoecker, Bogdan Malaescu, and Zhiqing Zhang. Reevaluation of the hadronic vacuum polarisation contributions to the Standard Model predictions of the muon $g-2$ and $\alpha(m_Z^2)$ using newest hadronic cross-section data. Eur. Phys. J. C, 77(12):827, 2017.

[62] Alexander Keshavarzi, Daisuke Nomura, and Thomas Teubner. Muon $g-2$ and $\alpha(M_Z^2)$: a new data-based analysis. Phys. Rev. D, 97(11):114025, 2018.

[63] Gilberto Colangelo, Martin Hoferichter, and Peter Stoffer. Two-pion contribution to hadronic vacuum polarization. JHEP, 02:006, 2019.

[64] Martin Hoferichter, Bai-Long Hoid, and Bastian Kubis. Three-pion contribution to hadronic vacuum polarization. JHEP, 08:137, 2019.

[65] M. Davier, A. Hoecker, B. Malaescu, and Z. Zhang. A new evaluation of the hadronic vacuum polarisation contributions to the muon anomalous magnetic moment and to $\boldsymbol{\alpha(\mathbf{m_Z^2})}$. Eur. Phys. J. C, 80(3):241, 2020. [Erratum: Eur.Phys.J.C 80, 410 (2020)].

[66] Alexander Keshavarzi, Daisuke Nomura, and Thomas Teubner. $g-2$ of charged leptons, $\alpha(M_Z^2)$, and the hyperfine splitting of muonium. Phys. Rev. D, 101(1):014029, 2020.

[67] Alexander Kurz, Tao Liu, Peter Marquard, and Matthias Steinhauser. Hadronic contribution to the muon anomalous magnetic moment to next-to-next-to-leading order. Phys. Lett. B, 734:144–147, 2014.

[68] B. Chakraborty et al. Strong-Isospin-Breaking Correction to the Muon Anomalous Magnetic Moment from Lattice QCD at the Physical Point. Phys. Rev. Lett., 120(15):152001, 2018.

[69] Sz. Borsanyi et al. Hadronic vacuum polarization contribution to the anomalous magnetic moments of leptons from first principles. Phys. Rev. Lett., 121(2):022002, 2018.

[70] T. Blum, P.A. Boyle, V. Gülpers, T. Izubuchi, L. Jin, C. Jung, A. Jüttner, C. Lehner, A. Portelli, and J.T. Tsang. Calculation of the hadronic vacuum polarization contribution to the muon anomalous magnetic moment. Phys. Rev. Lett., 121(2):022003, 2018.

[71] D. Giusti, V. Lubicz, G. Martinelli, F. Sanfilippo, and S. Simula. Electromagnetic and strong isospin-breaking corrections to the muon $g-2$ from Lattice QCD+QED. Phys. Rev. D, 99(11):114502, 2019.

[72] Eigo Shintani and Yoshinobu Kuramashi. Hadronic vacuum polarization contribution to the muon $g-2$ with 2+1 flavor lattice QCD on a larger than (10 fm)^4 lattice at the physical point. Phys. Rev. D, 100(3):034517, 2019.

[73] C.T.H. Davies et al. Hadronic-vacuum-polarization contribution to the muon's anomalous magnetic moment from four-flavor lattice QCD. Phys. Rev. D, 101(3):034512, 2020.

[74] Antoine Gérardin, Marco Cè, Georg von Hippel, Ben Hörz, Harvey B. Meyer, Daniel Mohler, Konstantin Ottnad, Jonas Wilhelm, and Hartmut Wittig. The leading hadronic contribution to $(g-2)_\mu$ from lattice QCD with $N_\mathrm{f} = 2+1$ flavours of O(a) improved Wilson quarks. Phys. Rev. D, 100(1):014510, 2019.

[75] Christopher Aubin, Thomas Blum, Cheng Tu, Maarten Golterman, Chulwoo Jung, and Santiago Peris. Light quark vacuum polarization at the physical point and contribution to the muon $g-2$. Phys. Rev. D, 101(1):014503, 2020.

[76] D. Giusti and S. Simula. Lepton anomalous magnetic moments in Lattice QCD+QED. PoS, LATTICE2019:104, 2019.

[77] Sz. Borsanyi et al. Leading-order hadronic vacuum polarization contribution to the muon magnetic momentfrom lattice QCD. 2 2020.

[78] Kirill Melnikov and Arkady Vainshtein. Hadronic light-by-light scattering contribution to the muon anomalous magnetic moment revisited. Phys. Rev. D, 70:113006, 2004.

[79] Pere Masjuan and Pablo Sanchez-Puertas. Pseudoscalar-pole contribution to the $(g_\mu - 2)$: a rational approach. Phys. Rev. D, 95(5):054026, 2017.

[80] Gilberto Colangelo, Martin Hoferichter, Massimiliano Procura, and Peter Stoffer. Dispersion relation for hadronic light-by-light scattering: two-pion contributions. JHEP, 04:161, 2017.

[81] Martin Hoferichter, Bai-Long Hoid, Bastian Kubis, Stefan Leupold, and Sebastian P. Schneider. Dispersion relation for hadronic light-by-light scattering: pion pole. JHEP, 10:141, 2018.

[82] Antoine Gérardin, Harvey B. Meyer, and Andreas Nyffeler. Lattice calculation of the pion transition form factor with $N_f = 2 + 1$ Wilson quarks. Phys. Rev. D, 100(3):034520, 2019.

[83] Johan Bijnens, Nils Hermansson-Truedsson, and Antonio Rodríguez-Sánchez. Short-distance constraints for the HLbL contribution to the muon anomalous magnetic moment. Phys. Lett. B, 798:134994, 2019.

[84] Gilberto Colangelo, Franziska Hagelstein, Martin Hoferichter, Laetitia Laub, and Peter Stoffer. Longitudinal short-distance constraints for the hadronic light-by-light contribution to $(g-2)_\mu$ with large-N_c Regge models. JHEP, 03:101, 2020.

[85] Vladyslav Pauk and Marc Vanderhaeghen. Single meson contributions to the muon‘s anomalous magnetic moment. Eur. Phys. J. C, 74(8):3008, 2014.

[86] Igor Danilkin and Marc Vanderhaeghen. Light-by-light scattering sum rules in light of new data. Phys. Rev. D, 95(1):014019, 2017.

[87] Friedrich Jegerlehner. The $g-2$ experiments. In The Anomalous Magnetic Moment of the Muon, pages 571–607. Springer, 2017.

[88] M. Knecht, S. Narison, A. Rabemananjara, and D. Rabetiarivony. Scalar meson contributions to a μ from hadronic light-by-light scattering. Phys. Lett. B, 787:111–123, 2018.

[89] Gernot Eichmann, Christian S. Fischer, and Richard Williams. Kaon-box contribution to the anomalous magnetic moment of the muon. Phys. Rev. D, 101(5):054015, 2020.

[90] Pablo Roig and Pablo Sanchez-Puertas. Axial-vector exchange contribution to the hadronic light-by-light piece of the muon anomalous magnetic moment. Phys. Rev. D, 101(7):074019, 2020.

[91] Gilberto Colangelo, Martin Hoferichter, Andreas Nyffeler, Massimo Passera, and Peter Stoffer. Remarks on higher-order hadronic corrections to the muon g−2. Phys. Lett. B, 735:90–91, 2014.

[92] Thomas Blum, Norman Christ, Masashi Hayakawa, Taku Izubuchi, Luchang Jin, Chulwoo Jung, and Christoph Lehner. Hadronic Light-by-Light Scattering Contribution to the Muon Anomalous Magnetic Moment from Lattice QCD. Phys. Rev. Lett., 124(13):132002, 2020.

[93] Robert Foot, X.G. He, H. Lew, and R.R. Volkas. Model for a light Z-prime boson. Phys. Rev. D, 50:4571–4580, 1994.

[94] S.N. Gninenko and N.V. Krasnikov. The Muon anomalous magnetic moment and a new light gauge boson. Phys. Lett. B, 513:119, 2001.

[95] Seungwon Baek, N.G. Deshpande, X.G. He, and P. Ko. Muon anomalous g-2 and gauged L(muon) - L(tau) models. Phys. Rev. D, 64:055006, 2001.

[96] Brandon Murakami. The Impact of lepton flavor violating Z-prime bosons on muon g-2 and other muon observables. Phys. Rev. D, 65:055003, 2002.

[97] Ernest Ma, D.P. Roy, and Sourov Roy. Gauged L(mu) - L(tau) with large muon anomalous magnetic moment and the bimaximal mixing of neutrinos. Phys. Lett. B, 525:101–106, 2002.

[98] Maxim Pospelov. Secluded U(1) below the weak scale. Phys. Rev. D, 80:095002, 2009.

[99] Julian Heeck and Werner Rodejohann. Gauged $L_\mu - L_\tau$ Symmetry at the Electroweak Scale. Phys. Rev. D, 84:075007, 2011.

[100] Hooman Davoudiasl, Hye-Sung Lee, and William J. Marciano. Dark Side of Higgs Diphoton Decays and Muon g-2. Phys. Rev. D, 86:095009, 2012.

[101] Christopher D. Carone. Flavor-Nonuniversal Dark Gauge Bosons and the Muon g-2. Phys. Lett. B, 721:118–122, 2013.

[102] Keisuke Harigaya, Takafumi Igari, Mihoko M. Nojiri, Michihisa Takeuchi, and Kazuhiro Tobe. Muon g-2 and LHC phenomenology in the $L_\mu - L_\tau$ gauge symmetric model. JHEP, 03:105, 2014.

[103] Wolfgang Altmannshofer, Stefania Gori, Maxim Pospelov, and Itay Yavin. Quark flavor transitions in $L_\mu - L_\tau$ models. Phys. Rev. D, 89:095033, 2014.

[104] Wolfgang Altmannshofer, Stefania Gori, Maxim Pospelov, and Itay Yavin. Neutrino Trident Production: A Powerful Probe of New Physics with Neutrino Beams. Phys. Rev. Lett., 113:091801, 2014.

[105] Hye-Sung Lee. Muon g$-$2 anomaly and dark leptonic gauge boson. Phys. Rev. D, 90(9):091702, 2014.

[106] Andreas Crivellin, Lars Hofer, Joaquim Matias, Ulrich Nierste, Stefan Pokorski, and Janusz Rosiek. Lepton-flavour violating B decays in generic Z' models. Phys. Rev. D, 92(5):054013, 2015.

[107] Ben Allanach, Farinaldo S. Queiroz, Alessandro Strumia, and Sichun Sun. $Z2$ models for the LHCb and $g-2$ muon anomalies. Phys. Rev. D, 93(5):055045, 2016. [Erratum: Phys.Rev.D 95, 119902 (2017)].

[108] Julian Heeck. Lepton flavor violation with light vector bosons. Phys. Lett. B, 758:101–105, 2016.

[109] Sudhanwa Patra, Soumya Rao, Nirakar Sahoo, and Narendra Sahu. Gauged $U(1)_{L_\mu - L_\tau}$ model in light of muon $g-2$ anomaly, neutrino mass and dark matter phenomenology. Nucl. Phys. B, 917:317–336, 2017.

[110] Wolfgang Altmannshofer, Chien-Yi Chen, P.S. Bhupal Dev, and Amarjit Soni. Lepton flavor violating Z' explanation of the muon anomalous magnetic moment. Phys. Lett. B, 762:389–398, 2016.

[111] Darwin Chang, We-Fu Chang, Chung-Hsien Chou, and Wai-Yee Keung. Large two loop contributions to g-2 from a generic pseudoscalar boson. Phys. Rev. D, 63:091301, 2001.

[112] Athanasios Dedes and Howard E. Haber. Can the Higgs sector contribute significantly to the muon anomalous magnetic moment? JHEP, 05:006, 2001.

[113] King-man Cheung, Chung-Hsien Chou, and Otto C.W. Kong. Muon anomalous magnetic moment, two Higgs doublet model, and supersymmetry. Phys. Rev. D, 64:111301, 2001.

[114] Kingman Cheung and Otto C.W. Kong. Can the two Higgs doublet model survive the constraint from the muon anomalous magnetic moment as suggested? Phys. Rev. D, 68:053003, 2003.

[115] Junjie Cao, Peihua Wan, Lei Wu, and Jin Min Yang. Lepton-Specific Two-Higgs Doublet Model: Experimental Constraints and Implication on Higgs Phenomenology. Phys. Rev. D, 80:071701, 2009.

[116] Alessandro Broggio, Eung Jin Chun, Massimo Passera, Ketan M. Patel, and Sudhir K. Vempati. Limiting two-Higgs-doublet models. JHEP, 11:058, 2014.

[117] Lei Wang and Xiao-Fang Han. A light pseudoscalar of 2HDM confronted with muon g-2 and experimental constraints. JHEP, 05:039, 2015.

[118] Yuji Omura, Eibun Senaha, and Kazuhiro Tobe. Lepton-flavor-violating Higgs decay $h \to \mu\tau$ and muon anomalous magnetic moment in a general two Higgs doublet model. JHEP, 05:028, 2015.

[119] Tomohiro Abe, Ryosuke Sato, and Kei Yagyu. Lepton-specific two Higgs doublet model as a solution of muon g $-$ 2 anomaly. JHEP, 07:064, 2015.

[120] P.A. Zyla et al. Review of Particle Physics, 10. Electroweak Model and Constraints on New Physics. PTEP, 2020(8):083C01, 2020.

[121] Pei-Hong Gu, Ernest Ma, and Utpal Sarkar. Pseudo-Majoron as Dark Matter. Phys. Lett. B, 690:145–148, 2010.

[122] Michele Frigerio, Thomas Hambye, and Eduard Masso. Sub-GeV dark matter as pseudo-Goldstone from the seesaw scale. Phys. Rev. X, 1:021026, 2011.

[123] Evgeny K. Akhmedov, Z.G. Berezhiani, R.N. Mohapatra, and G. Senjanovic. Planck scale effects on the majoron. Phys. Lett. B, 299:90–93, 1993.

[124] I.Z. Rothstein, K.S. Babu, and D. Seckel. Planck scale symmetry breaking and majoron physics. Nucl. Phys. B, 403:725–748, 1993.

[125] Rodrigo Alonso and Alfredo Urbano. Wormholes and masses for Goldstone bosons. JHEP, 02:136, 2019.

[126] V. Berezinsky and J.W.F. Valle. The KeV majoron as a dark matter particle. Phys. Lett. B, 318:360–366, 1993.

[127] M. Lattanzi and J.W. F. Valle. Decaying warm dark matter and neutrino masses. Phys. Rev. Lett., 99:121301, 2007.

[128] Federica Bazzocchi, Massimiliano Lattanzi, Signe Riemer-Sørensen, and Jose W.F. Valle. X-ray photons from late-decaying majoron dark matter. JCAP, 08:013, 2008.

[129] Massimiliano Lattanzi, Signe Riemer-Sorensen, Mariam Tortola, and Jose W. F. Valle. Updated CMB and x- and γ-ray constraints on Majoron dark matter. Phys. Rev. D, 88(6):063528, 2013.

[130] Farinaldo S. Queiroz and Kuver Sinha. The Poker Face of the Majoron Dark Matter Model: LUX to keV Line. Phys. Lett. B, 735:69–74, 2014.

[131] Weijian Wang and Zhi-Long Han. Global $U(1)_L$ Breaking in Neutrinophilic 2HDM: From LHC Signatures to X-Ray Line. Phys. Rev. D, 94(5):053015, 2016.

[132] Camilo Garcia-Cely and Julian Heeck. Neutrino Lines from Majoron Dark Matter. JHEP, 05:102, 2017.

[133] Julian Heeck and Hiren H. Patel. Majoron at two loops. Phys. Rev. D, 100(9):095015, 2019.

[134] Lawrence J. Hall, Karsten Jedamzik, John March-Russell, and Stephen M. West. Freeze-In Production of FIMP Dark Matter. JHEP, 03:080, 2010.

[135] P.A. Zyla et al. Review of Particle Physics, 30 Cosmic Rays. PTEP, 2020(8):083C01, 2020.

[136] M. Aguilar et al. Towards Understanding the Origin of Cosmic-Ray Electrons. Phys. Rev. Lett., 122(10):101101, 2019.

[137] R. Cowsik, B. Burch, and T. Madziwa-Nussinov. The origin of the spectral intensities of cosmic-ray positrons. Astrophys. J., 786:124, 2014.

[138] L. Accardo et al. High Statistics Measurement of the Positron Fraction in Primary Cosmic Rays of 0.5–500 GeV with the Alpha Magnetic Spectrometer on the International Space Station. Phys. Rev. Lett., 113:121101, 2014.

[139] J.J. Beatty et al. New measurement of the cosmic-ray positron fraction from 5 to 15-GeV. Phys. Rev. Lett., 93:241102, 2004.

[140] O. Adriani et al. A new measurement of the antiproton-to-proton flux ratio up to 100 GeV in the cosmic radiation. Phys. Rev. Lett., 102:051101, 2009.

[141] Oscar Adriani et al. An anomalous positron abundance in cosmic rays with energies 1.5-100 GeV. Nature, 458:607–609, 2009.

[142] I.V. Moskalenko and A.W. Strong. Production and propagation of cosmic ray positrons and electrons. Astrophys. J., 493:694–707, 1998.

[143] Alejandro Ibarra, David Tran, and Christoph Weniger. Indirect Searches for Decaying Dark Matter. Int. J. Mod. Phys. A, 28:1330040, 2013.

[144] Daniele Gaggero, Luca Maccione, Giuseppe Di Bernardo, Carmelo Evoli, and Dario Grasso. Three-Dimensional Model of Cosmic-Ray Lepton Propagation Reproduces Data from the Alpha Magnetic Spectrometer on the International Space Station. Phys. Rev. Lett., 111:021102, 2013.

[145] Peng-Fei Yin, Zhao-Huan Yu, Qiang Yuan, and Xiao-Jun Bi. Pulsar interpretation for the AMS-02 result. Phys. Rev. D, 88(2):023001, 2013.

[146] R. Abbasi et al. Search for dark matter from the Galactic halo with the IceCube Neutrino Telescope. Phys. Rev. D, 84:022004, 2011.

[147] M.G. Aartsen et al. Search for neutrinos from decaying dark matter with IceCube. Eur. Phys. J. C, 78(10):831, 2018.

[148] Marco Cirelli, Gennaro Corcella, Andi Hektor, Gert Hutsi, Mario Kadastik, Paolo Panci, Martti Raidal, Filippo Sala, and Alessandro Strumia. PPPC 4 DM ID: A Poor Particle Physicist Cookbook for Dark Matter Indirect Detection. JCAP, 03:051, 2011. [Erratum: JCAP 10, E01 (2012)].

[149] Jatan Buch, Marco Cirelli, Gaëlle Giesen, and Marco Taoso. PPPC 4 DM secondary: A Poor Particle Physicist Cookbook for secondary radiation from Dark Matter. JCAP, 09:037, 2015.

[150] Edward A. Baltz and Joakim Edsjo. Positron propagation and fluxes from neutralino annihilation in the halo. Phys. Rev. D, 59:023511, 1998.

[151] M. Aguilar et al. Antiproton Flux, Antiproton-to-Proton Flux Ratio, and Properties of Elementary Particle Fluxes in Primary Cosmic Rays Measured with the Alpha Magnetic Spectrometer on the International Space Station. Phys. Rev. Lett., 117(9):091103, 2016.

[152] Rohan Iwashima (Kyoto University). The master thesis 「重いマヨロンダークマターの崩壊とその宇宙線による間接探索」.

[153] Rohan Iwashima Koichi Yoshioka, Masato Yamanaka. to appear.

[154] Ming-Yang Cui, Qiang Yuan, Yue-Lin Sming Tsai, and Yi-Zhong Fan. Possible dark matter annihilation signal in the AMS-02 antiproton data. Phys. Rev. Lett., 118(19):191101, 2017.

[155] Fatemeh Elahi, Christopher Kolda, and James Unwin. UltraViolet Freeze-in. JHEP, 03:048, 2015.

[156] J.A. Casas and A. Ibarra. Oscillating neutrinos and $\mu \to e, \gamma$. Nucl. Phys. B, 618:171–204, 2001.

[157] Luca Di Luzio, Maurizio Giannotti, Enrico Nardi, and Luca Visinelli. The landscape of QCD axion models. Phys. Rept., 870:1–117, 2020.

[158] R.D. Peccei. The Strong CP problem and axions. Lect. Notes Phys., 741:3–17, 2008.

[159] Maxim Pospelov and Adam Ritz. Theta vacua, QCD sum rules, and the neutron electric dipole moment. Nucl. Phys. B, 573:177–200, 2000.

[160] Varouzhan Baluni. CP Violating Effects in QCD. Phys. Rev. D, 19:2227–2230, 1979.

[161] R.J. Crewther, P. Di Vecchia, G. Veneziano, and Edward Witten. Chiral Estimate of the Electric Dipole Moment of the Neutron in Quantum Chromodynamics. Phys. Lett. B, 88:123, 1979. [Erratum: Phys.Lett.B 91, 487 (1980)].

[162] Antonio Pich and Eduardo de Rafael. Strong CP violation in an effective chiral Lagrangian approach. Nucl. Phys. B, 367:313–333, 1991.

[163] Lorenzo Bartolini, Francesco Bigazzi, Stefano Bolognesi, Aldo L. Cotrone, and Andrea Manenti. Neutron electric dipole moment from gauge/string duality. Phys. Rev. Lett., 118(9):091601, 2017.

[164] M. Abramczyk, S. Aoki, T. Blum, T. Izubuchi, H. Ohki, and S. Syritsyn. Lattice calculation of electric dipole moments and form factors of the nucleon. Phys. Rev. D, 96(1):014501, 2017.

[165] Jack Dragos, Thomas Luu, Andrea Shindler, Jordy de Vries, and Ahmed Yousif. Confirming the Existence of the strong CP Problem in Lattice QCD with the Gradient Flow. 2 2019.

[166] C. Abel et al. Measurement of the permanent electric dipole moment of the neutron. Phys. Rev. Lett., 124(8):081803, 2020.

[167] R.D. Peccei and Helen R. Quinn. CP Conservation in the Presence of Instantons. Phys. Rev. Lett., 38:1440–1443, 1977.

[168] R.D. Peccei and Helen R. Quinn. Constraints Imposed by CP Conservation in the Presence of Instantons. Phys. Rev. D, 16:1791–1797, 1977.

[169] Steven Weinberg. A New Light Boson? Phys. Rev. Lett., 40:223–226, 1978.

[170] Frank Wilczek. Problem of Strong P and T Invariance in the Presence of Instantons. Phys. Rev. Lett., 40:279–282, 1978.

[171] Jihn E. Kim. Weak Interaction Singlet and Strong CP Invariance. Phys. Rev. Lett., 43:103, 1979.

[172] Mikhail A. Shifman, A.I. Vainshtein, and Valentin I. Zakharov. Can Confinement Ensure Natural CP Invariance of Strong Interactions? Nucl. Phys. B, 166:493–506, 1980.

[173] Michael Dine, Willy Fischler, and Mark Srednicki. A Simple Solution to the Strong CP Problem with a Harmless Axion. Phys. Lett. B, 104:199–202, 1981.

[174] A.R. Zhitnitsky. On Possible Suppression of the Axion Hadron Interactions. (In Russian). Sov. J. Nucl. Phys., 31:260, 1980.

[175] V. Anastassopoulos et al. New CAST Limit on the Axion-Photon Interaction. Nature Phys., 13:584–590, 2017.

[176] S.J. Asztalos et al. A SQUID-based microwave cavity search for dark-matter axions. Phys. Rev. Lett., 104:041301, 2010.

[177] N. Du et al. A Search for Invisible Axion Dark Matter with the Axion Dark Matter Experiment. Phys. Rev. Lett., 120(15):151301, 2018.

[178] T. Braine et al. Extended Search for the Invisible Axion with the Axion Dark Matter Experiment. Phys. Rev. Lett., 124(10):101303, 2020.

[179] Adrian Ayala, Inma Domínguez, Maurizio Giannotti, Alessandro Mirizzi, and Oscar Straniero. Revisiting the bound on axion-photon coupling from Globular Clusters. Phys. Rev. Lett., 113(19):191302, 2014.

[180] Oscar Straniero, Adrian Ayala, Maurizio Giannotti, Alessandro Mirizzi, and Inma Dominguez. Axion-Photon Coupling: Astrophysical Constraints. In 11th Patras Workshop on Axions, WIMPs and WISPs, pages 77–81, 2015.

[181] P.A. Zyla et al. Review of Particle Physics, 91. Axions and Other Similar Particles. PTEP, 2020(8):083C01, 2020.

[182] Mikhail V. Beznogov, Ermal Rrapaj, Dany Page, and Sanjay Reddy. Constraints on Axion-like Particles and Nucleon Pairing in Dense Matter from the Hot Neutron Star in HESS J1731-347. Phys. Rev. C, 98(3):035802, 2018.

[183] Koichi Hamaguchi, Natsumi Nagata, Keisuke Yanagi, and Jiaming Zheng. Limit on the Axion Decay Constant from the Cooling Neutron Star in Cassiopeia A. Phys. Rev. D, 98(10):103015, 2018.

[184] Nicolás Viaux, Márcio Catelan, Peter B. Stetson, Georg Raffelt, Javier Redondo, Aldo A. R. Valcarce, and Achim Weiss. Neutrino and axion bounds from the globular cluster M5 (NGC 5904). Phys. Rev. Lett., 111:231301, 2013.

[185] Marcelo M. Miller Bertolami, Brenda E. Melendez, Leandro G. Althaus, and Jordi Isern. Revisiting the axion bounds from the Galactic white dwarf luminosity function. JCAP, 10:069, 2014.

[186] Guillermo Ballesteros, Javier Redondo, Andreas Ringwald, and Carlos Tamarit. Standard Model—axion—seesaw—Higgs portal inflation. Five problems of particle physics and cosmology solved in one stroke. JCAP, 08:001, 2017.

[187] Michael Shin. Light Neutrino Masses and Strong {CP} Problem. Phys. Rev. Lett., 59:2515, 1987. [Erratum: Phys.Rev.Lett. 60, 383 (1988)].

[188] Z.G. Berezhiani. Horizontal Symmetry and Quark - Lepton Mass Spectrum: The SU(5) x SU(3)-h Model. Phys. Lett. B, 150:177–181, 1985.

[189] Jihn E. Kim. Reason for SU(6) Grand Unification. Phys. Lett. B, 107:69–72, 1981.

[190] Rabindra N. Mohapatra and Goran Senjanovic. The Superlight Axion and Neutrino Masses. Z. Phys. C, 17:53–56, 1983.

[191] Q. Shafi and F.W. Stecker. Implications of a Class of Grand Unified Theories for Large Scale Structure in the Universe. Phys. Rev. Lett., 53:1292, 1984.

[192] A.G. Dias, A.C.B. Machado, C.C. Nishi, A. Ringwald, and P. Vaudrevange. The Quest for an Intermediate-Scale Accidental Axion and Further ALPs. JHEP, 06:037, 2014.

[193] Guillermo Ballesteros, Javier Redondo, Andreas Ringwald, and Carlos Tamarit. Unifying inflation with the axion, dark matter, baryogenesis and the seesaw mechanism. Phys. Rev. Lett., 118(7):071802, 2017.

[194] Guillermo Ballesteros, Javier Redondo, Andreas Ringwald, and Carlos Tamarit. Several Problems in Particle Physics and Cosmology Solved in One SMASH. Front. Astron. Space Sci., 6:55, 2019.

[195] P. Langacker, R.D. Peccei, and T. Yanagida. Invisible Axions and Light Neutrinos: Are They Connected? Mod. Phys. Lett. A, 1:541, 1986.

[196] X.G. He and R.R. Volkas. Models Featuring Spontaneous {CP} Violation: An Invisible Axion and Light Neutrino Masses. Phys. Lett. B, 208:261, 1988. [Erratum: Phys.Lett.B 218, 508 (1989)].

[197] Alex G. Dias and V. Pleitez. The Invisible axion and neutrino masses. Phys. Rev. D, 73:017701, 2006.

[198] Alberto Salvio. A Simple Motivated Completion of the Standard Model below the Planck Scale: Axions and Right-Handed Neutrinos. Phys. Lett. B, 743:428–434, 2015.

[199] Jackson D. Clarke and Raymond R. Volkas. Technically natural nonsupersymmetric model of neutrino masses, baryogenesis, the strong CP problem, and dark matter. Phys. Rev. D, 93(3):035001, 2016.

[200] Ernest Ma. Making neutrinos massive with an axion in supersymmetry. Phys. Lett. B, 514:330–334, 2001.

[201] S. Bertolini and A. Santamaria. The Strong CP problem and the solar neutrino puzzle: Are they related? Nucl. Phys. B, 357:222–240, 1991.

[202] H. Arason, Pierre Ramond, and B.D. Wright. A Standard model extension with neutrino masses and an invisible axion. Phys. Rev. D, 43:2337–2350, 1991.

[203] Stefano Bertolini, Luca Di Luzio, Helena Kolešová, and Michal Malinský. Massive neutrinos and invisible axion minimally connected. Phys. Rev. D, 91(5):055014, 2015.

[204] Y.H. Ahn and Eung Jin Chun. Minimal Models for Axion and Neutrino. Phys. Lett. B, 752:333–337, 2016.

[205] Stefano Bertolini, Luca Di Luzio, Helena Kolešová, Michal Malinský, and Juan Carlos Vasquez. Neutrino-axion-dilaton interconnection. Phys. Rev. D, 93(1):015009, 2016.

[206] Basudeb Dasgupta, Ernest Ma, and Koji Tsumura. Weakly interacting massive particle dark matter and radiative neutrino mass from Peccei-Quinn symmetry. Phys. Rev. D, 89(4):041702, 2014.

[207] Ernest Ma, Diego Restrepo, and Óscar Zapata. Anomalous leptonic U(1) symmetry: Syndetic origin of the QCD axion, weak-scale dark matter, and radiative neutrino mass. Mod. Phys. Lett. A, 33:1850024, 2018.

[208] Chian-Shu Chen and Lu-Hsing Tsai. Peccei-Quinn symmetry as the origin of Dirac Neutrino Masses. Phys. Rev. D, 88(5):055015, 2013.

[209] Pei-Hong Gu. Peccei-Quinn symmetry for Dirac seesaw and leptogenesis. JCAP, 07:004, 2016.

[210] Cristian D.R. Carvajal and Óscar Zapata. One-loop Dirac neutrino mass and mixed axion-WIMP dark matter. Phys. Rev. D, 99(7):075009, 2019.

[211] Eduardo Peinado, Mario Reig, Rahul Srivastava, and Jose W.F. Valle. Dirac neutrinos from Peccei–Quinn symmetry: A fresh look at the axion. Mod. Phys. Lett. A, 35(21):2050176, 2020.

[212] Pavel Fileviez Perez and Mark B. Wise. On the Origin of Neutrino Masses. Phys. Rev. D, 80:053006, 2009.

[213] Jose F. Nieves. Baryon and Lepton Number Nonconserving Processes and Intermediate Mass Scales. Nucl. Phys. B, 189:182–204, 1981.

[214] Chun-Khiang Chua, Xiao-Gang He, and W-Y.P. Hwang. Neutrino mass induced radiatively by supersymmetric leptoquarks. Phys. Lett. B, 479:224–229, 2000.

[215] Uma Mahanta. Neutrino masses and mixing angles from leptoquark interactions. Phys. Rev. D, 62:073009, 2000.

[216] D. Aristizabal Sierra, M. Hirsch, and S.G. Kovalenko. Leptoquarks: Neutrino masses and accelerator phenomenology. Phys. Rev. D, 77:055011, 2008.

[217] Paul W. Angel, Yi Cai, Nicholas L. Rodd, Michael A. Schmidt, and Raymond R. Volkas. Testable two-loop radiative neutrino mass model based on an $LLQd^cQd^c$ effective operator. JHEP, 10:118, 2013. [Erratum: JHEP 11, 092 (2014)].

[218] Yi Cai, Juan Herrero-García, Michael A. Schmidt, Avelino Vicente, and Raymond R. Volkas. From the trees to the forest: a review of radiative neutrino mass models. Front. in Phys., 5:63, 2017.

[219] Durmus A. Demir and Ernest Ma. Relaxation of the dynamical gluino phase and unambiguous electric dipole moments. Phys. Rev. D, 62:111901, 2000.

[220] Kristian L. McDonald and B.H.J. McKellar. Evaluating the two loop diagram responsible for neutrino mass in Babu's model. 9 2003.

[221] J. van der Bij and M.J.G. Veltman. Two Loop Large Higgs Mass Correction to the rho Parameter. Nucl. Phys. B, 231:205–234, 1984.

[222] Morad Aaboud et al. Search for doubly charged Higgs boson production in multi-lepton final states with the ATLAS detector using proton–proton collisions at $\sqrt{s} = 13\,\text{TeV}$. Eur. Phys. J. C, 78(3):199, 2018.

[223] A search for doubly-charged Higgs boson production in three and four lepton final states at $\sqrt{s} = 13$ TeV. 1 2017.

[224] Giovanni Grilli di Cortona, Edward Hardy, Javier Pardo Vega, and Giovanni Villadoro. The QCD axion, precisely. JHEP, 01:034, 2016.